THE AMIDINIUM-CARBOXYLATE SALT BRIDGE AND ELECTRON TRANSFER REACTIONS

By

James Patrick Kirby

A DISSERTATION

Submitted to

Michigan State University

in partial fulfillment of the requirements

for the degree of

DOCTOR OF PHILOSOPHY

Department of Chemistry

1997

ABSTRACT

THE AMIDINIUM–CARBOXLYATE SALT BRIDGE AND ELECTRON TRANSFER REACTIONS

By

James Patrick Kirby

Salt bridges occur in a variety of natural structural motifs including proteins, protein-protein complexes, protein-substrate complexes, and protein-DNA or protein–RNA assemblies. In addition to their role as natural structural building blocks, salt bridges also control reaction chemistry by modulating redox activity at the protein active site. One way this occurs is when salt bridges mediate redox processes, as in sulfite and nitrite reductases (SiRs and NiRs). Salt bridges are also proposed pathways for electron transfer in cytochrome *c* oxidase. We are interested in examining the affect of proton motion or the proton position within a salt bridge on fixed distance electron transfer (ET) rates. There are an array of chromophore/quencher complexes where an electron donor is held at some fixed distance relative to an electron acceptor. Upon excitation of either the donor or acceptor, depending on the design of the particular molecule, it is possible to time the electron as it makes its journey from one point to another, that is to measure the rate of photoinduced ET at some fixed distance. This strategy has been employed to characterize the distance dependence of ET reactions, and also assess the role of solvation in fixed distance ET reactions. Alternatively, pulse radiolysis experiments have been employed to measure the rates of electron transfer at fixed distances. From these classical experiments the existence of the Marcus inverted region has been established experimentally, nearly 30 years after it was proposed by theory. In the inverted region for ET, increasing the

exergisity of an ET reaction results in a decrease in the reaction rate, in sharp contrast to the prediction of classical chemical reaction theory.

Presented here is a series of donor/acceptor complexes assembled via the non–covalent amidinium-carboxylate salt bridge. A series of donor/acceptor complexes have been chemically modified with the amidine functional group. It is shown that the amidine group is readily transformed into a 1:1 amidinium-carboxylate salt bridge with concomitant protonation by a carboxylic acid. This salt bridge structural motif parallels Asp-Arg salt bridges occurring in proteins, yet has the advantage of having only one specific two hydrogen bond binding mode, where the guanidine group of arginine has multiple binding modes. The synthetic details of preparing and characterizing amidines and their salt bridge complexes are described. The association constants for various amidinium-carboxylate salt bridge complexes have been determined by either titration or dilution ^{1}H NMR methods. The synthesis and characterization of 1:1 amidinium-carboxylate salt bridge complexes and kinetics measurements aimed at exploring proton-coupled electron transfer are presented for inorganic, bioinorganic and organic complexes.

To my parents, Jeannine and James, grandparents, Katherine and James Wood, and my brothers and sisters, Anita, Keith, Linda, Marcy, and Johnn.

ACKNOWLEDGEMENTS

Traveling the long and winding road towards completing the research and writing of this thesis I was fortunate to meet and work with many talented individuals. Much of their insight made the research for this thesis possible. Dan Nocera saw me through the highs and lows of graduate school, always teaching me to keep things in perspective, and to look at the "big picture". I am grateful to him for his guidance and support. Many thanks go to my guidance committee, Professor C. K. Chang, who served as my second reader, Gerry Babcock and Ned Jackson. John Miller provided me with a unique experience at Argonne National Laboratory mid-way through my graduate career. These individuals have acted as my mentors, and have demonstrated to me how to think in excruciating detail about scientific problems.

I would like to thank my friends and group members, past and present, including Mark Torgerson, Jim Roberts, Dimitri Popostakis, Rich Marassas, Dan Engebretson, Sara Helvoight, Einhard Schmidt, Adrian Ponce, Ying Liang, Carolyn Hsu, Zoe Pikramenou, Yongqi Deng, Dean Lantero, Doug Motry, Carl Iverson, Ann MacIntosh, Al Barney, Linda Kraus and Eric Saari for providing me with many entertaining moments, and for making my graduate experience a lot of fun. These individuals (and the ones I forgot to list) have made my life a little easier over the last few years. Finally, I would to thank God and the St. Johns student parish for providing me with shelter and a spiritual outlet during the many good times here, but also for the few times when my troubles and worries tried to get the best of me.

TABLE OF CONTENTS

LIST OF FIGURES

LIST OF TABLES

LIST OF ABBREVIATIONS

*	excited state
A	acceptor
Ac	acetyl
ACN	acetonitrile
Aib	α-aminoisobutyric acid
Ala	alanine
Am	amidinium
Am:Ca	amidinium-carboxylate
AQ	anthraquinone
Arg	arginine
Asp	aspartate
BPh_4	tetraphenylborate
bpy	2,2'-bipyridine
BQ	benzoquinone
Ca	carboxylate
cyt *c*	cytochrome *c*
D	donor
d	doublet
DCM	dichloromethane
decb	4,4'-di(ethylcarboxy)-2,2-bipyridine
DMAB	N,N-dimethylaminobenzene
DMSO	dimethylsulfoxide

DNA	deoxyribonucleic acid
DNB	dinitrobenzene
ET	electron transfer
Et	ethyl
FCWD	Franck-Condon weighted density of states
G	guanidinium
GC	guanine-cytosine
Gln	glycine
His	histidine
NBu_4	tetrabutylammonium
NMR	nuclear magnetic resonance
NMP	N-methylpyrrolidone
NQ	1,4-naphthaquinone
P	protein
p	pentet
PCET	proton-coupled electron transfer
ppm	parts per million
Pyr	pyrene
PZT	phenothiazene
q	quartet
RNA	ribonucleic acid
S	sulphonate
s	singlet
t	triplet
THF	tetrahydrofuran
tmbpy	4,4',5,5'-tetramethyl-2,2-bipyridine
TMDAB	N,N,N'N'-tetramethyl-p-diaminobenzene

Tyr	tyrosine
ZnP	zinc(II)porphyrin

Chapter 1

PERSPECTIVES ON SALT BRIDGES AND ELECTRON TRANSFER

A. Salt Bridges

1. Introduction

Hydrogen bonds are ubiquitous in nature, biomimetic and synthetic systems forming the basis for biological and chemical supramolecular assemblies as described by Lehn.[1] A particular type of hydrogen bonding interaction is the salt bridge, where the components of the hydrogen bond consist of a positively charged proton donor and a negatively charged proton acceptor. A complementary two point salt bridge hydrogen bonding interaction occurs between 1,3 spaced charged pairs such as the one shown schematically on the left side of Eq. 1.1. This and other salt bridge structural motifs are present throughout biological systems and are involved in essential biological transformations. In bioenergetics for instance, the coupling of proton motion to the motion of the electron is evident where salt bridges are present. However, the role that salt bridges play in such schemes has yet to be clearly defined.

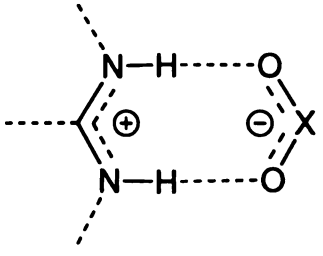

primary

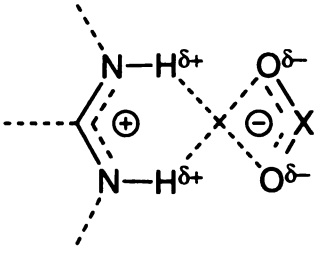

secondary

(1.1)

The stabilizing forces that result in the formation of a salt bridge are a combination of hydrogen bonding interactions and electrostatic interactions, which stem from the charged nature of the individual components of the salt bridge. First, there exists a strong primary electrostatic interaction associated with the attraction between positively charged adjacent N–H protons and negatively charged oxygen atoms. This is in part symbolized by the dashed lines connecting H with O in the left side of Eq. 1.1. But there exists another electrostatic force acting to stabilize the salt bridge, a secondary electrostatic interaction (SEI).[2] This SEI is due to the attraction between the diagonal arrangement of partially positive charged N-H protons and the partially negative charged oxygen atoms. On the right side of Eq. 1.1, this important contribution to the overall stabilization of the salt bridge moiety is symbolized by diagonal dashed lines.

Due to the ionic nature of the salt bridge, there is a pronounced electrostatic interaction with the medium surrounding the salt bridge. In solution, the strength of the salt bridge bond is inversely proportional to the dielectric constant (ε_S) of the surrounding solvent molecules as described by Coulomb energy, Eq. 1.2, where ΔE_C is the electrostatic energy stabilizing the salt bridge within a solvent of some ε_S, q_1 and q_2 are the respective charges of the salt bridge proton donor and proton acceptor, and r_{12} is the distance separating q_1 and q_2. Therefore, in solvents with low ε_S's, the salt bridge interactions are expected to be strong; conversely in solvents with high ε_S's, the salt bridge interactions are expected to be weak.

$$\Delta E_C = \frac{(q_1 \cdot q_2)}{(r_{12} \cdot \varepsilon_S)} \tag{1.2}$$

Within this context, salt bridges located in the interior of proteins display unique behavior, inasmuch as that the ε_S for the interior of proteins is dependent on the structure of the local or surrounding protein side chain groups.[3] The magnitude of the electrostatic

attraction in the salt bridge within the interior of a protein is effectively on a sliding scale, because ΔE_C is a function of the ε_S of the surrounding protein side chain groups versus the bulk dielectric of the solvent, water. This characteristic of salt bridges in biological systems may be especially important in bioenergetic cycles based on charge transport.

2. Examples of Salt Bridges

Examples of salt bridge interactions are found in diverse areas or research ranging from crystal engineering to biochemistry. A class of salt bridges important to this thesis are ones formed from anion complexation with protonated positively charge guanidine, ariginine and amidine groups, depicted schematically in Figure 1. The molecular basis for each of the three groups listed here determines the overall specificity and pattern of salt bridge hydrogen bonding. For the guanidinium ion there exists a three fold symmetry axis, and salt bridge interactions can occur through one, two or three sets of two-point hydrogen bonds as shown in Figure 1 (a). Close inspection of the structure of the protein side chain group, arginine, shows that it is in fact structurally rooted to guanidine group through a covalent link from one of the three guanidinium nitrogen atoms to the polypeptide backbone. For the arginine group there exists lower symmetry giving rise to salt bridge hydrogen bonding interactions though one or two sets of two-point hydrogen bonds as shown in Figure 1 (b). The diverse structural motifs germane to the arginine group are extensively employed in an array of biological functions in nature. Arginine based salt bridge hydrogen bonds are essential in protein recognition and activation of DNA, RNA as well as in catalysis in biological systems. Finally, the amidinium group displays only one mode of specific two point hydrogen bonding as shown by Figure 1 (c).

a. Guanidine Based Salt Bridges

A series of crystalline salt bridge complexes structures have been investigated by Etter and Ward based on the interaction of guanidinium with a variety of different sulfonate groups.[4] One of the most notable systems is the recently reported guanidinium-sulfonate

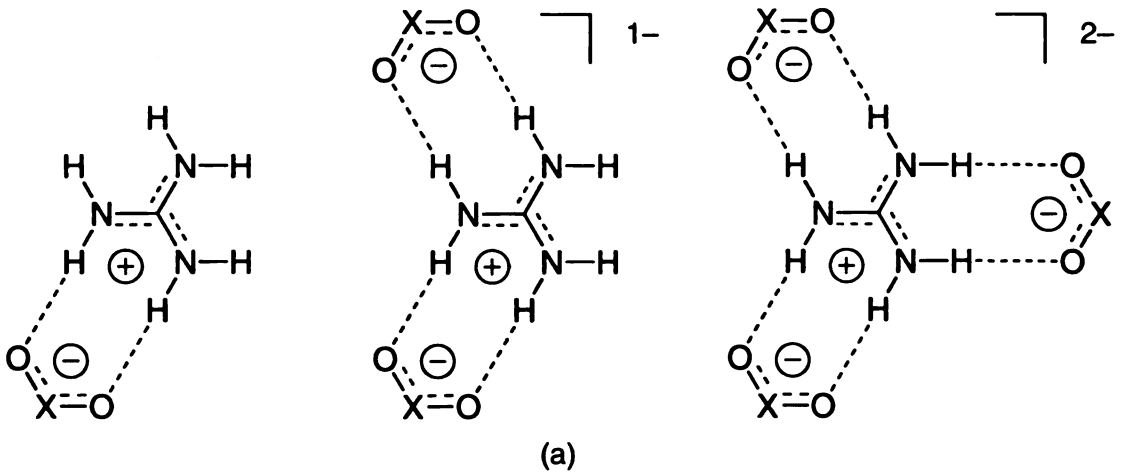

(a)

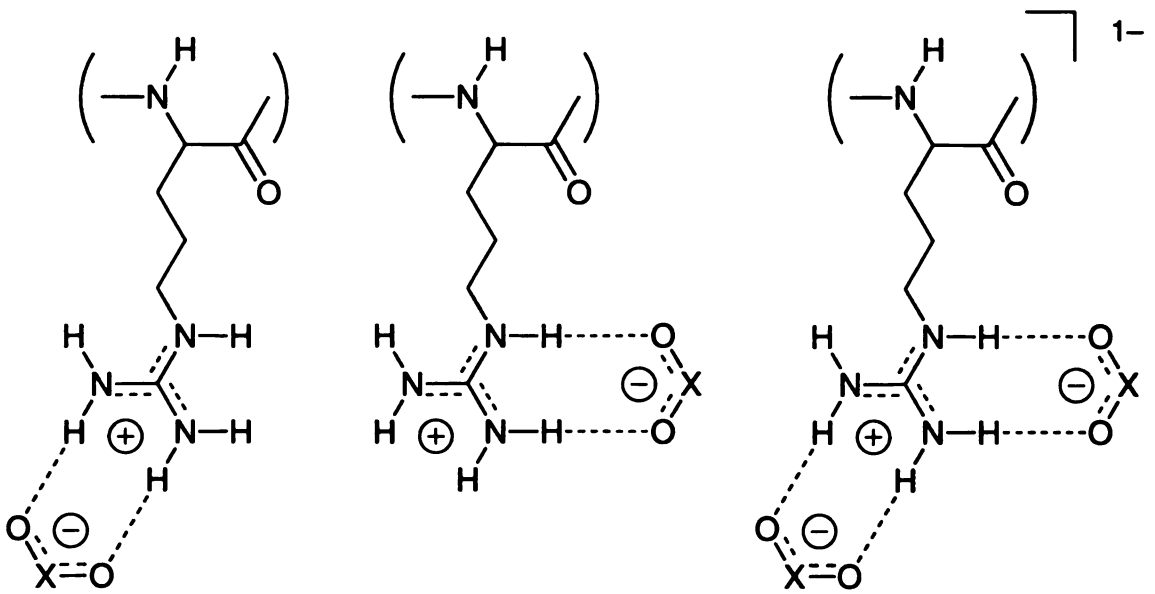

(b)

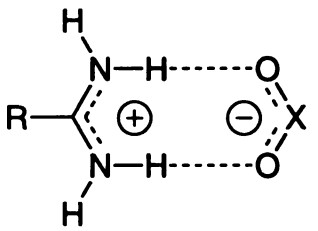

(c)

Figure 1. Salt bridges composed of (a) guanidine (b) arginine and (c) amidine. X may be SO-R', C-R', $P(O\text{-}R')_2$, SO^{1-}, and PO_2^{2-}.

salt sheet structure shown in Figure 2 (a). The basic building block shown there forms from the packing of three guanidinium groups with three sulfonate groups yielding a pseudo hexagonal packing motif. Represented in Figure 2 (b) is formation of pillared bilayer sheets, upon co-crystallization of the two equivalents of guanidinium with one equivalent of biphenyl-4,4'-disulfonate. In this structure, layered sheets pack together in the crystal lattice. The biphenyl groups extend out from the sulphonates to form pillars between the two dimensional sheets of salt bridge hydrogen bonds. This pillaring effect of the biphenyl spacers creates large channels between the salt bridge layers. These open channels have been structurally characterized by x-ray crystallography with the channels occupied by methanol or host molecules such as styrene, as represented in Figure 2 (c). These remarkable systems represent a pivotal achievement in the field of crystal engineering inasmuch as they point the way towards the design of host lattices.

b. Arginine Based Salt Bridges.

Arginine salt bridges are prevalent in nature. They are especially prominent in zinc finger protein-DNA complexes. Crystallographic studies on this class of proteins reveals the formation of protein-DNA assemblies, which are stabilized by buttressed salt-bridge interactions between aspartate (Asp) and arginine (Arg) within the protein main chain forming two hydrogen bonds to a guanine-cytosine (GC) base pair in the major groove of DNA, Figure 3 (a).[5] A similar structural motif has been revealed for a class of proteins, which interact in a likewise fashion forming protein-RNA complexes as revealed by solution NMR structural studies, Figure 3 (b).[6] RNA stem loops form a similar recognition complex with arginamide, which exhibits buttressed phosphodiester salt bridge interaction in place of the carboxylate interaction the DNA complex. These studies reveal that salt-bridges are the key to the assembly of protein/DNA or RNA complexes.

Arginine salt-bridges also figure prominently in biological transformations. The conversion of chorismate ion to prephenate ion, Eq. 1.3, is a rare example in nature of the

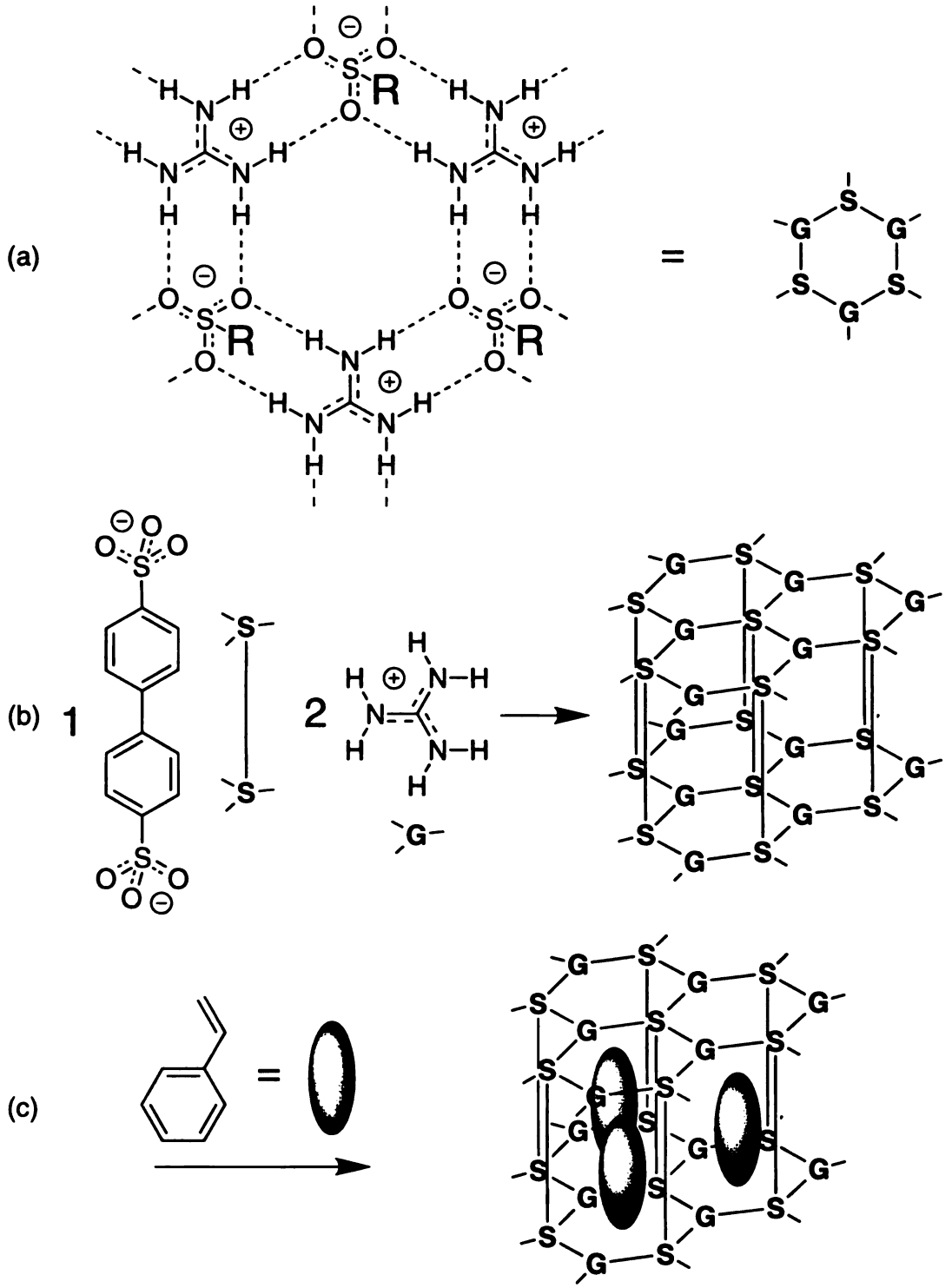

Figure 2. Solid state materials based on the pseudo planar hexagonal salt bridge interactions of guanidinium (G) with organic sulfonate (S) as shown schematically in (a); A three dimensional pillared bilayer structural motif results from the interaction of 4,4'-biphenyldisulfonate with guanidinium (b) which has been shown to accommodate small organic molecules such as styrene (c).

Claisen rearrangement (pericylic reaction) and is present in the biochemical synthetic pathway of the essential amino acid phenyl alanine. Chorismate mutase from *Escherichia coli* accelerates the transformation by more than 6 orders of magnitude. The x-ray crystal structure of two chorismate mutase proteins have been solved with an inhibitor bound to the active site, Figure 4.[7,8]

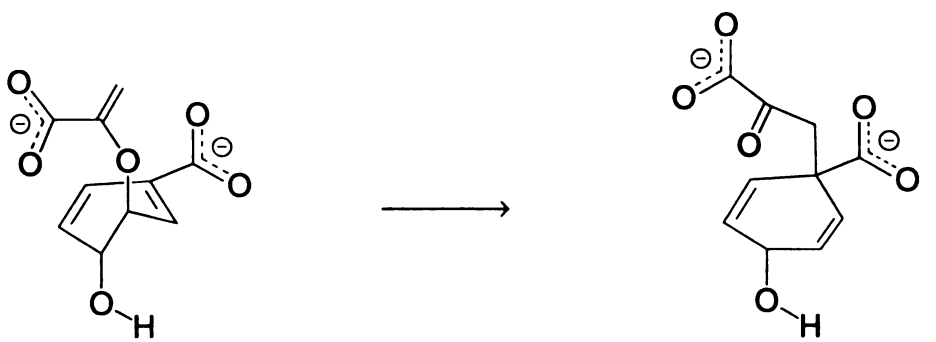

chorismate ion prephenate ion (1.3)

A synthetic peptide sequence containing a pair of aspartates (Asp) spaced at an interval of i + 3 along the peptide main chain is shown to recognize a synthetic bis-guanidinium receptor in water.[9] The proposed solution structure involves two salt bridges between the bis-guanidinium (arginine like) receptor and the two carboxylates from the i + 3 spaced Asp peptides along the α-helix, as shown schematically in Figure 5.

c. Amidine Based Salt Bridges

A model system for the action of phosphodiesterase is presented in Figure 6.[10] Here the primary hydrogen bonding interactions formed by the amidinium group to a phosphodiester salt bridge is employed to withdraw electron density from the phosphodiester, which then undergoes an intramolecular trans-phosphodiesterification reaction. This reaction pathway is at the heart of the action for phosphodiesteraces, which are involved in the transformation of phosphodiesters such as those located in the backbone linkages of DNA and RNA. This enzyme catalyses the overall transformation by more than

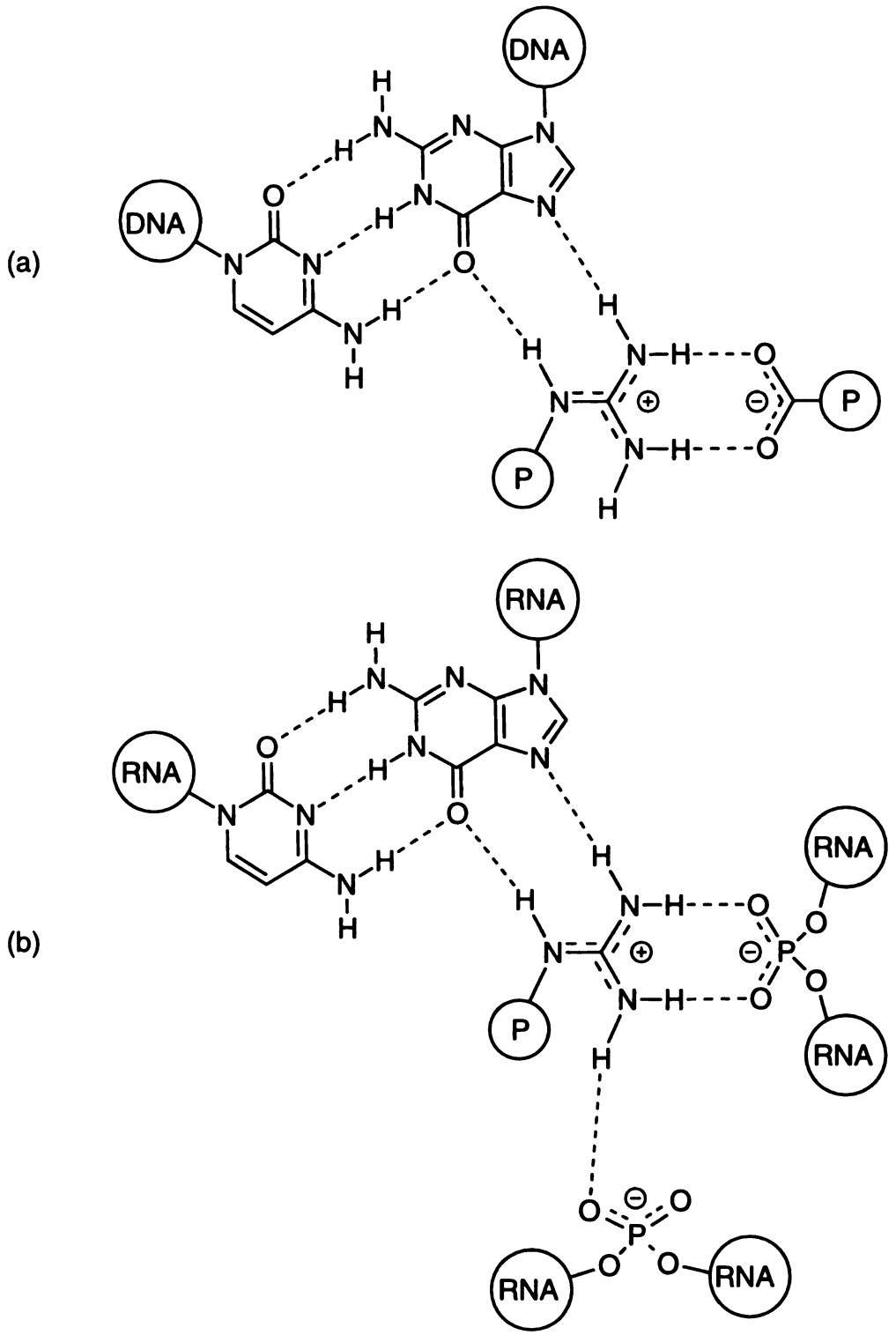

Figure 3. Biological examples of DNA-Protein recognition (a) and RNA-Protein recognition (b).

(a)

(b)

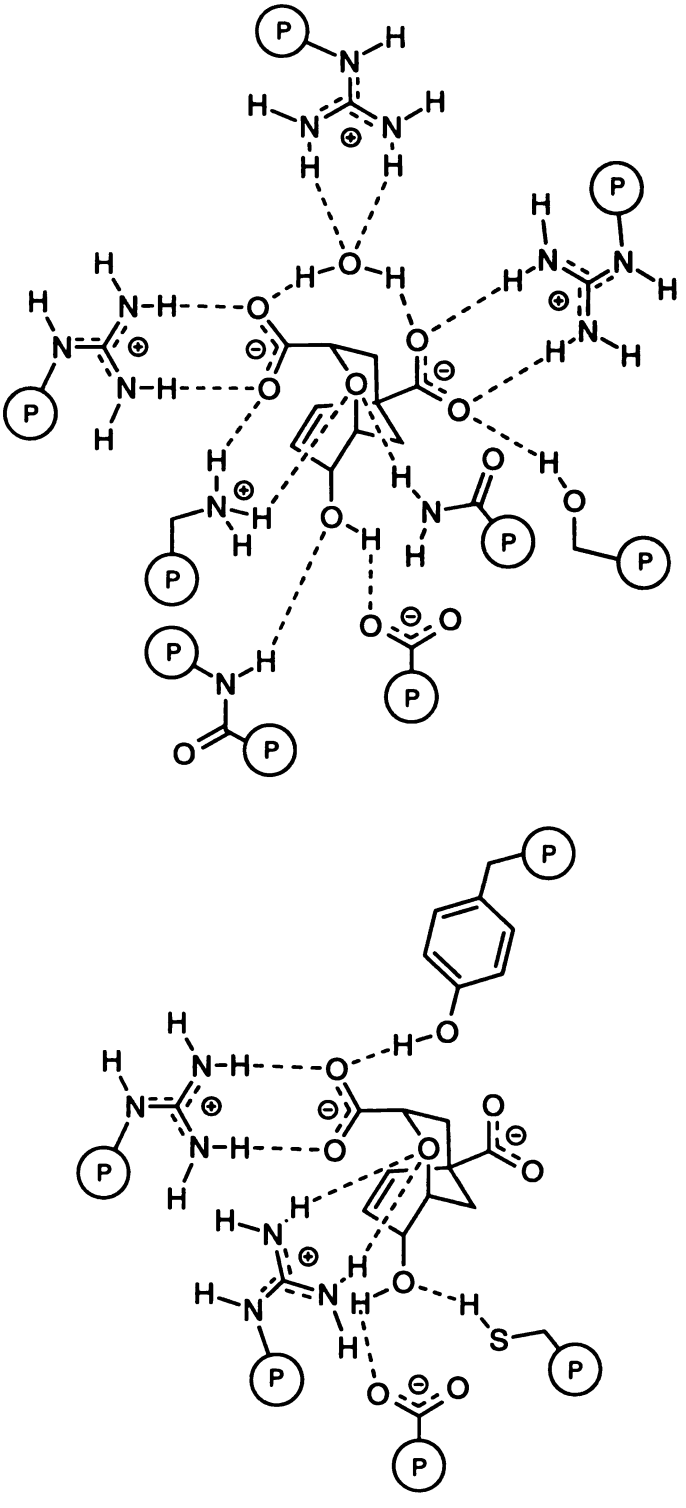

Figure 4. Stick structure representation of the active site of two chorismate mutase enzymes-inhibitor bound complexes from *Bacillus subtilis* (a) and *Saccharomysce cerevisia* (b).

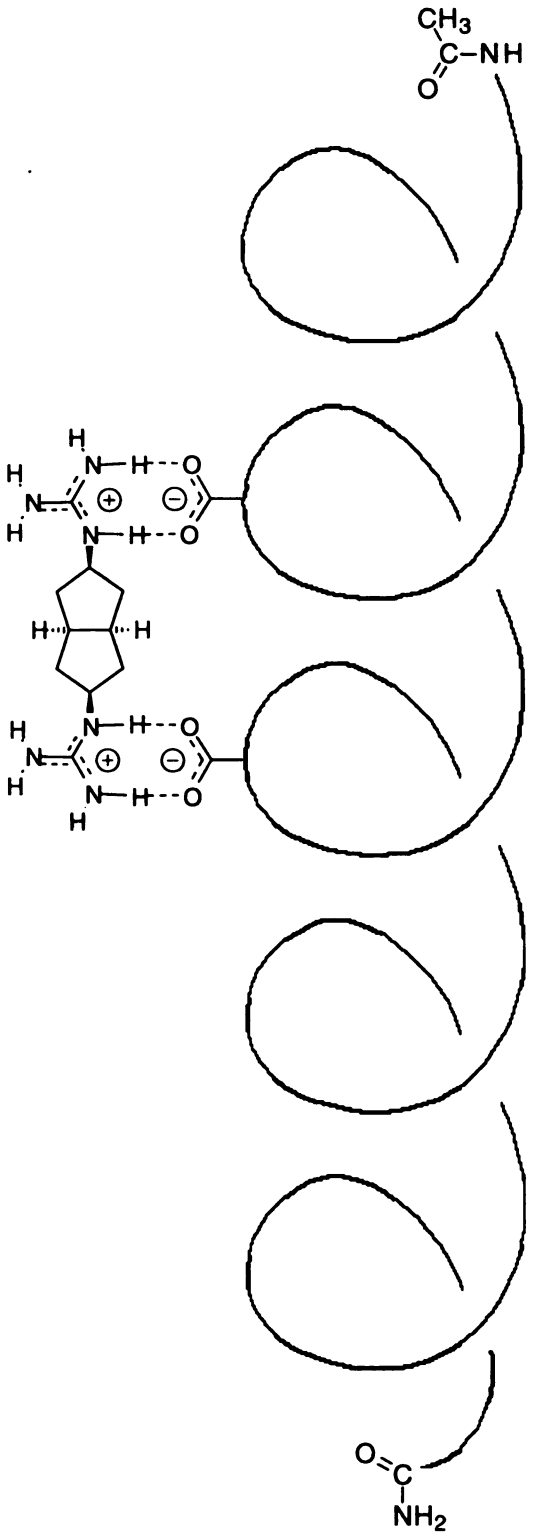

Figure 5. Schematic representation of a salt bridge complex formed between an α-helical polypeptide, Ac-Ala-Ala-Gln-**Asp**-Ala-Ala-**Asp**-Ala-Ala-Ala-Ala-Ala-Gln-Ala-Ala-Tyr-$CONH_2$, and a bis-guanidinium receptor molecule in water.

twelve orders of magnitude. Salt bridge interactions are important in the active site of this enzyme. Systems aimed at modeling the active site of the protein contain amidinium linked to an ethanol pendant group of an aromatic. This protein mimic reacts efficiently with model phosphodiesters and displays Michaelis-Menten type reaction kinetics, which is consistent with an enzyme substrate complex from which an irreversible reaction occurs. The crystal structure of the product of this reaction shows strong hydrogen bonding between the phosphodiester group of the product and the amidinium group of the template. The kinetics were assessed against control molecules and Michaelis-Menten parameters k_{cat} and K_m could be determined and a 9000-fold rate enhancement was calculated. This model system is an elegant example of how salt bridge interactions can be employed in a synthetic setting to influence reaction chemistry.

Amidinium-carboxylate salt bridges are the key recognition component for a self-replicating chemical system, Figure 7.[11] In this pseudo-living system, a complementary pair of reactive molecules were prepared where one molecule contains the carboxylate and aldehyde groups while a second molecule contains the amidinium and amine groups. In the first step of the sequence, a molecule of each are brought into contact by two complementary salt bridge interactions. In the reaction scheme described in Figure 8, Kiedrowski shows how a self-replicating system reacts to form templates of the original molecule and water. The next step allows for the reaction of the localized aldehyde group with the amine group to yield an imine linkage and water. At this stage the molecule is transformed into a template dimer, which is then free to exchange into free template as governed by the equilibrium characteristic of the salt bridge. The net concentration of the template doubles and each can then go on to form two more copies of the template, in a numerical progression. In a very simplistic sense, the autocatalysis described is analogous to one circuit of the polymerase chain reaction (PCR) technique employed by molecular biologist for gene amplification, which is a special case of autocatalysis.

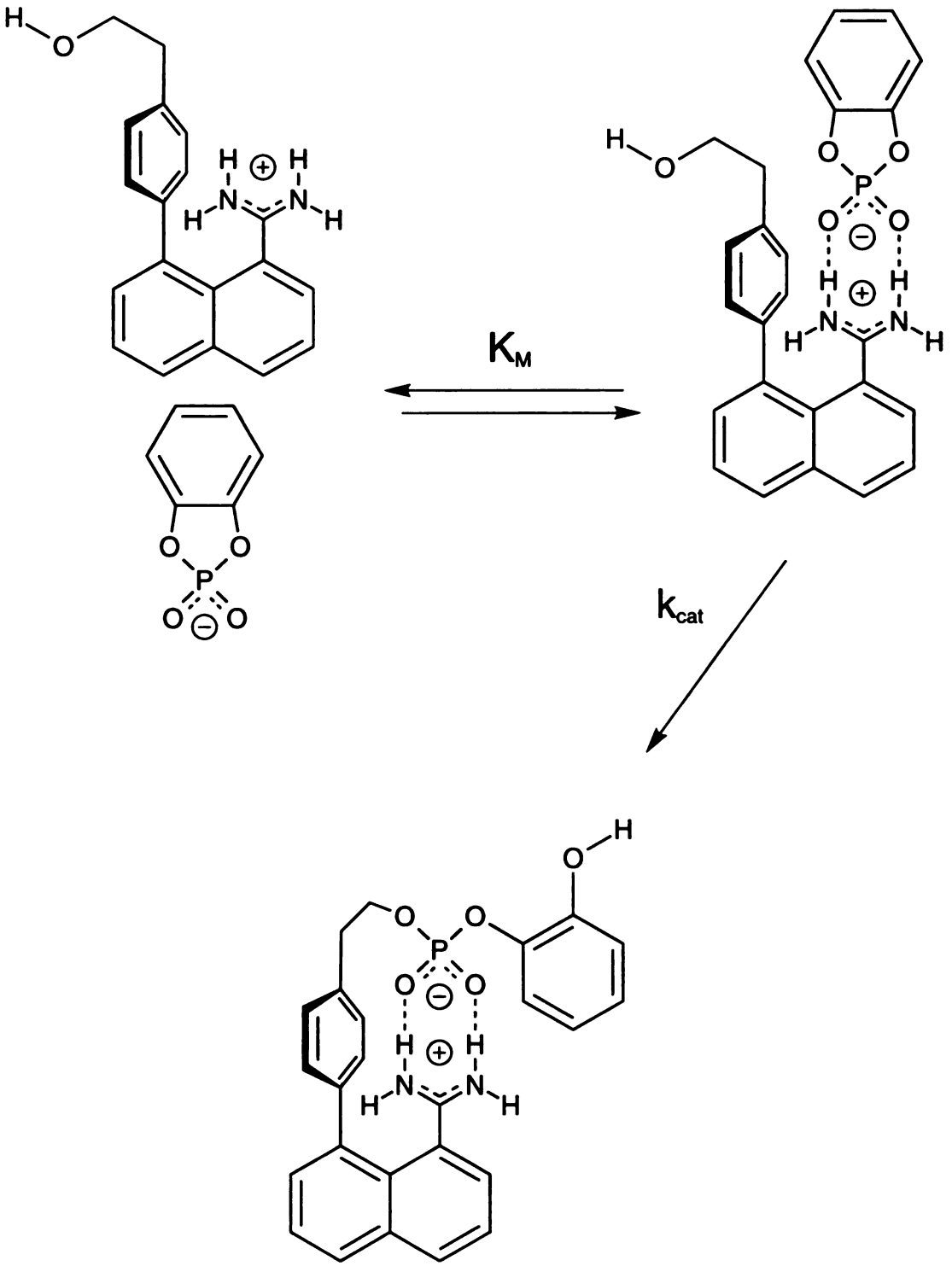

Figure 6. An amidinium complex to model the action of phosphodiesterase.

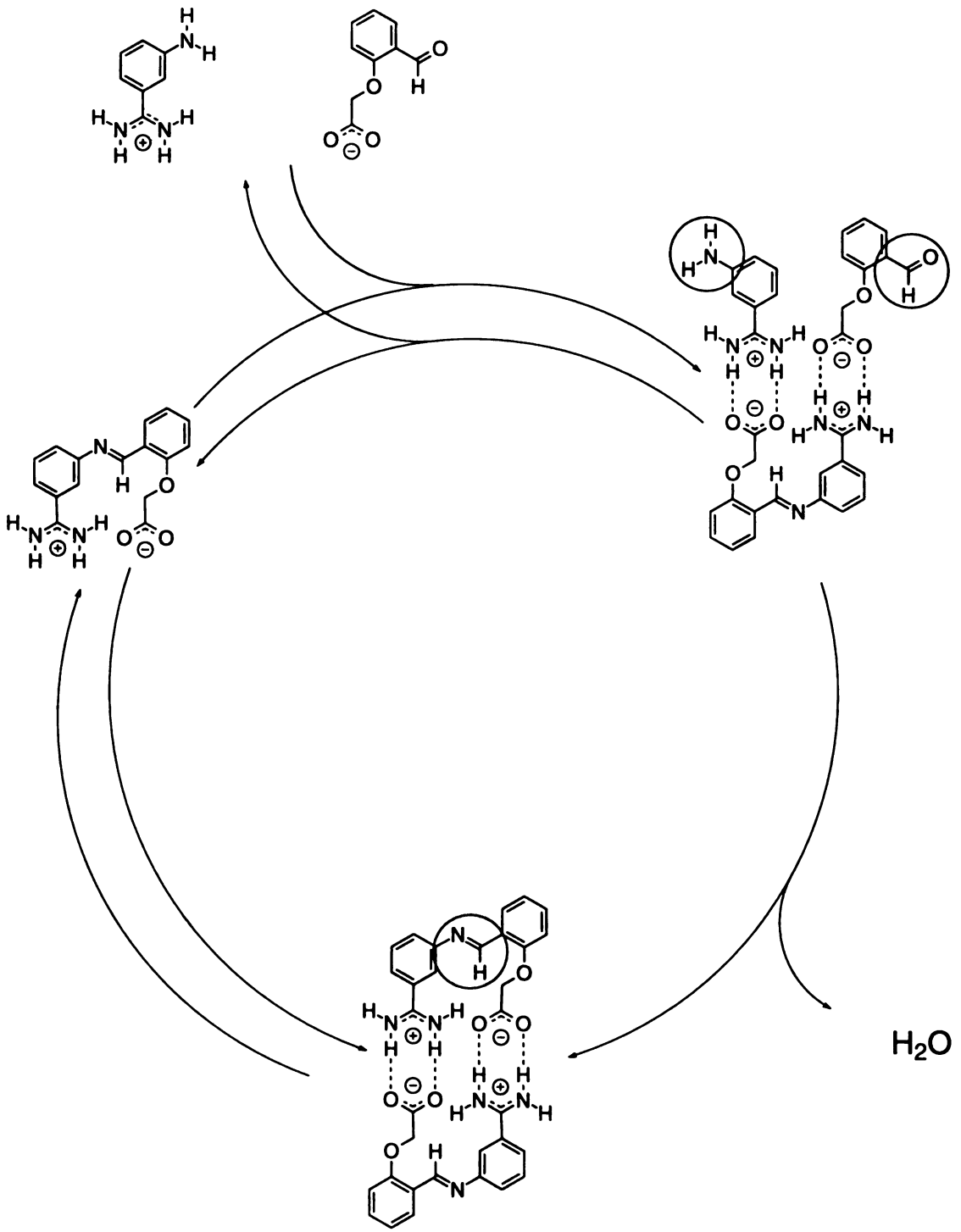

Figure 7. A self-replicating amidinium-carboxylate system to model natural replication.

B. Electron Transfer

1. Introduction

Electron transfer (ET) reactions have been characterized for a variety of model systems though few have involved salt bridge interactions. More generally an electron donors (D) and electron acceptors (A) are separated at some fixed distance defined by a rigid spacer group. Systems of this type have been investigated as models of the early events in photosynthesis, where natural D/A moieties are held at fixed distances and orientations as governed by the supporting protein matrix. Experiments to measure the rates for ET reactions in D/A model systems invoke the use of time resolved spectroscopy. Absorption of photons in the form of visible pulsed laser light can yield excited states (D* or A*) in molecular ensembles, which can subsequently undergo charge separation ET reactions via a reductive mechanism as described by Eq. 1.4 or by an oxidative mechanism as described by Eq. 1.5, relative to the excited state. Whether charge separation proceeds through the reductive or oxidative pathway depends on thermodynamics of the particular D/A system to model ET reaction rates. The kinetics for the subsequent ET events can be monitored by transient absorption spectroscopy techniques or by times resolved emission lifetime measurements for which specific examples will be described in a later section of this chapter.

$$D^*\text{–spacer–}A \longrightarrow D^{\bullet+1}\text{–spacer–}A^{\bullet-1} \quad (1.4)$$

$$D\text{–spacer–}A^* \longrightarrow D^{\bullet+1}\text{–spacer–}A^{\bullet-1} \quad (1.5)$$

In simple dyad D/A systems, the light absorbing chromophore is either the ultimate D or A. This basic design has been elaborated in recent years to include triads, tetrads and pentads. In the simplest extension to triads, the reductive and oxidative components are constructed about the light-absorbing chromophore. The ET events originate from the

chromophore excited state (chromophore*) for which charge separation events involving both oxidation and reduction are summarized by Eq. 1.6.

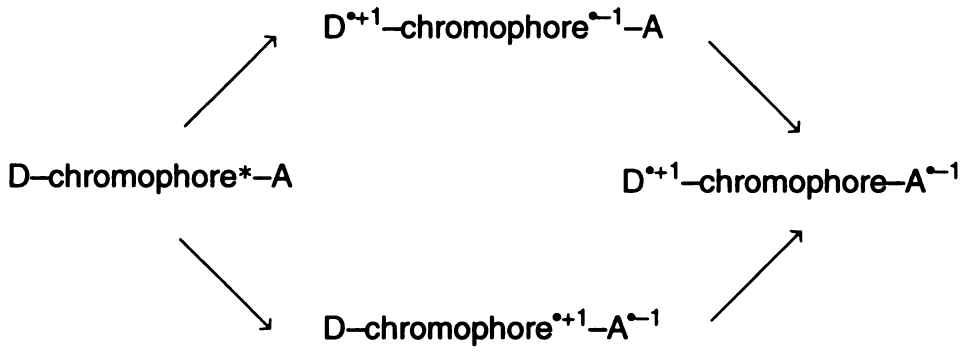

(1.6)

Photons are not a prerequisite for triggering ET reactions. Irradiation with high energy pulsed electrons can produce reactive charged radical anions ($D^{\bullet -1}$) or radical cations, depending on the chemical conditions of the pulse radiolysis experiment. As depicted in Eq. 1.7, measurement of ET rates in systems of this type have been studied and have provided a wealth of insight into the physical description and understanding of ET.

$$D^{\bullet -1}\text{–spacer–A} \longrightarrow \text{D–spacer–}A^{\bullet -1} \qquad (1.7)$$

2. Theory to Describe Electron Transfer Rates

a. Classical Chemical Reaction Rate Theory

The foundations of ET theory are rooted in the Fermi equation or golden rule equation, Eq. 1.8, which states that the reaction rate for electron transfer, k_{ET},, is a product of an electronic term and the nuclear coordinates. For instance, with respect to fixed

$$k_{ET} = \frac{2\pi}{\hbar}|H_{DA}|^2 \, FCWD \qquad (1.8)$$

distance ET in the pulse radiolysis experiment, the electronic term is quantified by the electronic coupling matrix element, H_{DA}, and is obtained by solving the time dependent Schrödinger equation for the of mixing of the two wave functions at the intersection of the

reactant and product potential energy surfaces corresponding to the molecules depicted on the left side of Eq. 1.7, and the right side of Eq. 1.7. This intersection point, or crossing point, is where the nuclear coordinates are presumed to be frozen in some transition state geometry, according to the Born-Oppenheimer approximation. Restated, in the transition state, at the curve-crossing, the nuclear coordinates of the reactant surface are equal to the nuclear coordinates on the product surface. The nuclear coordinates of the system form the Franck-Condon-weighted density of states (FCWD). This theory is operative in the non-adiabatic limit where the electronic coupling matrix element, H_{DA}, is much smaller than the thermal energy, k_BT ($H_{DA} << k_BT$, where k_B is Boltzmann's constant, and T is the absolute temperature of the system).[12]

b. Marcus Theory

The classical Marcus expression describing k_{ET} is obtained when the FCWD term in Eq. 1.17 is substituted with the expression shown in Eq. 1.9 for parabolic reactant and

$$\text{FCWD} = \left(4\pi\lambda_s k_B T\right)^{-1/2} \exp\left(-\frac{\left\{(\lambda_s + \Delta G^\circ)^2\right\}}{\left(4\pi\lambda_s k_B T\right)}\right) \tag{1.9}$$

product potential energy surface. The displacement of the wells or potential energy surfaces describing the nuclear coordinates of the product surface and reactant surface is λ_S as described by Marcus in Eq. 1.10. The definition of λ_S as put forth by Marcus is the energy

$$\lambda_S = e^2\left[\left(2r_D\right)^{-1} + \left(2r_A\right)^{-1} - \left(R_{DA}\right)^{-1}\right]\left(\varepsilon_S^{-1} + \varepsilon_{op}^{-1}\right) \tag{1.10}$$

required to change the solvation geometry in the solvent shell surrounding the system, in going from the reactant potential energy surface to the product potential energy surface. This energy is essentially a Coulomb energy for an ellipsoid as calculated by approximating the size of the solvent shell of system by a radius for the donor and acceptor portions to the

system or molecule as r_D and r_A which are separated by some distance R_{DA} and the dielectric of the solvent and the optical dielectric constant ε_{op}.

c. Semiclassical Marcus Theory

The semiclassical Marcus expression as put in its final form by Jortner, Eq. 1.11, includes the electron-phonon coupling term S which is the ratio of the inner sphere reorganizational energy, λ_v, and a high frequency molecular vibrational mode, hν, Eq. 1.12. The summation of this quantum mechanical vibrational progression is employed in describing k_{ET} and is obtained by substituting the FCWD of Eq. 1.8, with the expressions shown in Eq. 1.11 and 1.12.

$$\text{FCWD} = \left(4\pi\lambda_s k_B T\right)^{-1/2} \sum_{\omega=0}^{\infty} \exp(-S)\frac{S^{\omega}}{\omega!} \exp\left(-\frac{\left\{(\lambda_s + \Delta G^{\circ} + \omega h\nu)^2\right\}}{\left(4\pi\lambda_s k_B T\right)}\right) \tag{1.11}$$

$$S = \lambda_v / h\nu \tag{1.12}$$

3. Observation of and Implications of the Marcus Inverted Region

a. Free Energy Effects on k_{ET}

The pulse radiolysis technique is a powerful experimental tool for studying fixed distance intramolecular ET reactions. In the pulse radiolysis experiment short pulses of high energy electrons generate negative ions, which are strong reductants, such as the biphenyl radical anion, which can go on to reduce a neighboring electron acceptor group. The reaction proceeds with a unimolecular rate constant for the ET event, k_{ET}, as shown schematically in Eq. 1.13. Applying this technique to the study of ET reactions, Miller and Closs have provided the first unequivocal experimental evidence for the existence of the Marcus inverted region, where it is demonstrated that increasing the ET reaction driving force ($-\Delta G^{\circ}$) beyond the solvent reorganization energy (λ_S) results in a decrease in k_{ET}, as

described by Eq. 1.11.[13] A plot of the observed ET rate constant, k_{ET}, versus $-\Delta G°$ in the shown in Figure 8. Also shown is the fit to the theory shown above, Eq. 1.11. The agreement is excellent between the fit and the experimentally observed k_{ET}, with the use of four adjustable parameters in the fit, $\Delta G°$, λ_S, λ_V and hν. This result is in stark contrast to classical theories developed to describe reaction chemistry and bears out Marcus' elegant prediction of the inverted region more than 30 years prior to the experiments of Miller and Closs.

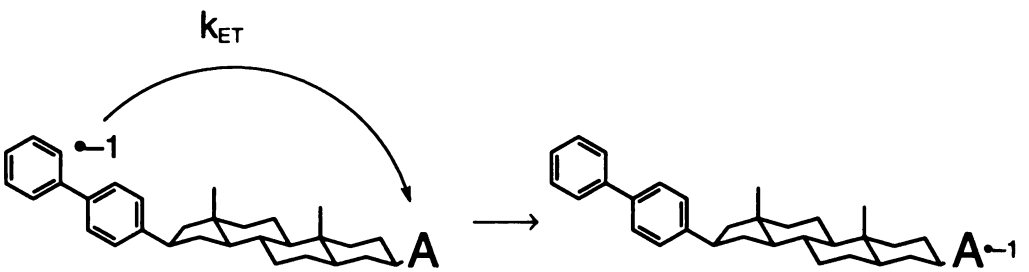

(1.13)

b. Effects of Temperature on k_{ET} in the Marcus Inverted Region

Semiclassical Marcus expressions are revealed in temperature dependence studies on k_{ET} in the normal and inverted regions.[14] Temperature studies on normal region ET are predicted by the classical Marcus expression Eq. 1.9 due to the fact that quantum mechanical effects in the normal region are minimal; restated, in the normal region most ET occurs primarily to the lowest vibrational level or when w is 0, Eq. 1.11 reduces to Eq. 9. However, little or no temperature dependence on k_{ET} in the inverted region. This confirms the validity of the quantum mechanical treatment of the FCWD described in Eq. 1.11.

c. Structural and Solvent Perturbations and the Effects on k_{ET}

Other studies aimed at emphasizing the importance of the semi-classical Marcus expression have shown the effects on k_{ET} by perturbing λ_S by altering the molecular structure of the D portion of the dyad system. In a molecule where a rigid fluorene D group is substituted for the biphenyl D group, λ_S is changes by 0.15 eV. This translates to an increase in k_{ET} in the normal region, where A is 2-naphthalene, by factor of 8 and a

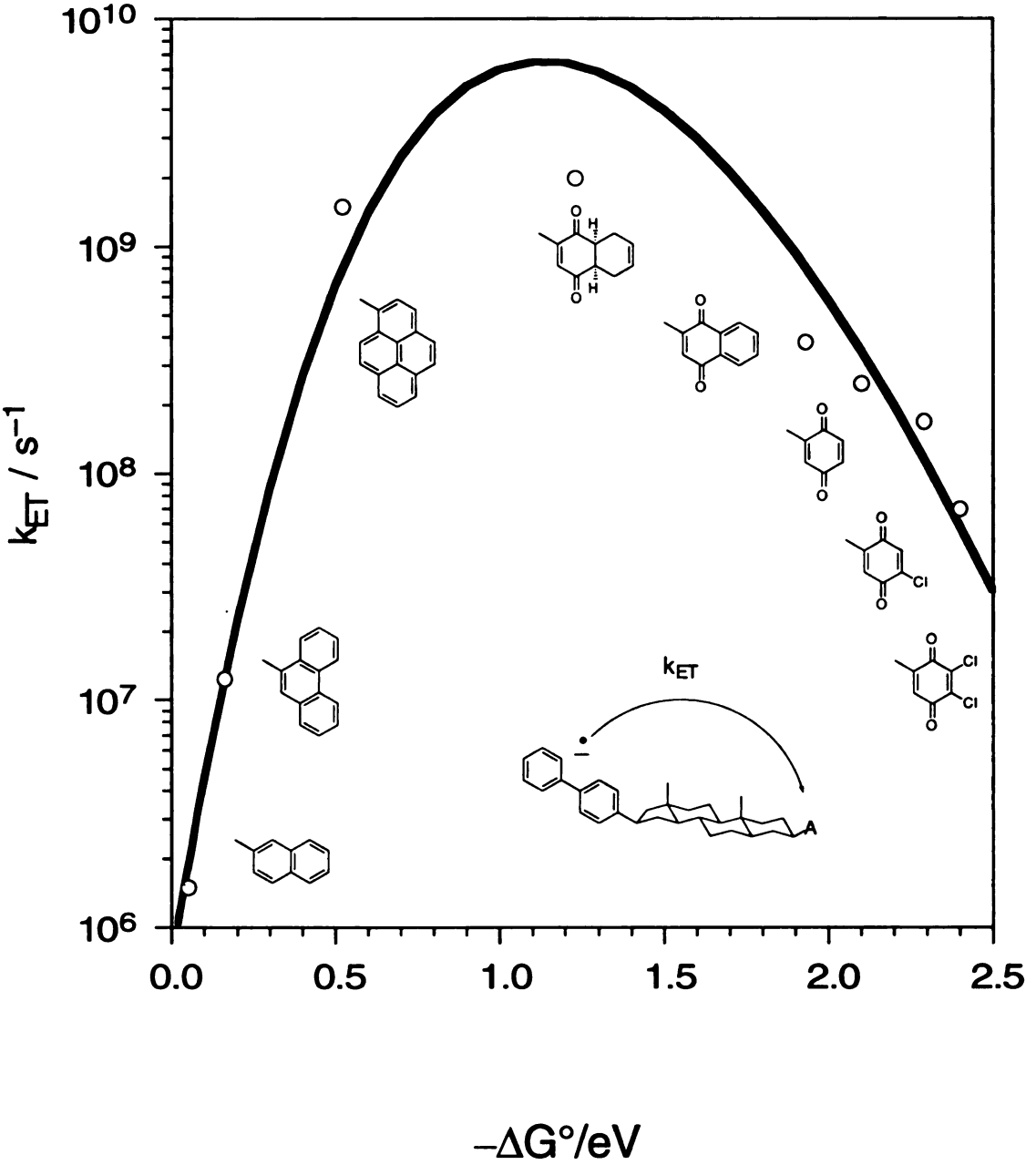

Figure 8. Log of the rate constant for intramolecular ET reactions, k_{ET}, versus reaction exergonicity, $\Delta G°$, observed in eight molecules (O) and fit to theory (solid line) as discussed in the text.

decrease in k_{ET} in the inverted, where A is benzoquinone region by a factor of 2.5, Eq. 1.14.[15]

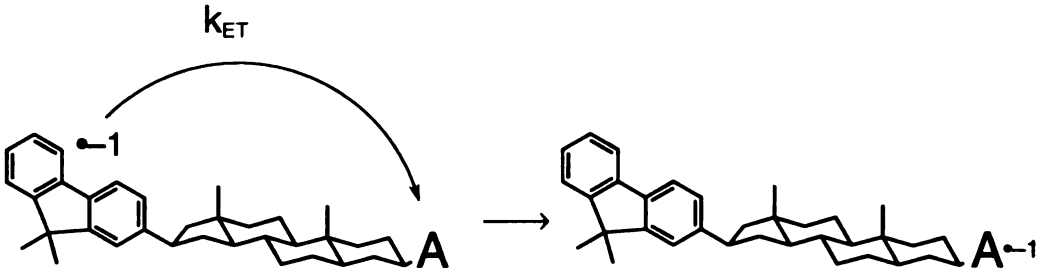

(1.14)

4. Photoinitiated ET in Covalent Dyad and Triad Systems

a. ET in Porphyrin-Quinone D/A Dyad

Wasliewski has prepared and studied a wide range of molecules based on reducing excited state of metalloporphyrins such as the complex shown in Figure 9 (a).[16] The ZnP* in this particular system is in proximity to an electron deficient electron acceptor, naphthaquinone (NQ). Photoexcitation produces an ET reaction in 25 picoseconds, yielding a charge separated state represented schematically by Eq 1.16. The charge separated species decays in 370 picoseconds back to the ground state via a thermal ET reaction. The progress of the reaction is monitored by time resolved transient absorption spectroscopy incorporating an optical delay line, which allows for time increments on the order of a few picoseconds to be assessed in kinetic measurements.

$$ZnP^*\text{–}NQ \longrightarrow ZnP^{\bullet+1}\text{–}NQ^{\bullet-1} \qquad (1.16)$$

b. ET in D-Chromophore-A Triads

To extend the lifetime of this charge separated state, as is the case in photosynthesis in biology, a sequence of oxidation and reductive steps are employed to extend the overall charge separation out over an even greater distance. This process is summarized in Eq 1.17 for the triad complex shown Figure 9 (b).[17] This is essentially a two step ET process. The process combines ET to the NQ in one direction and a hole transfer (a form of ET) in the

(a)

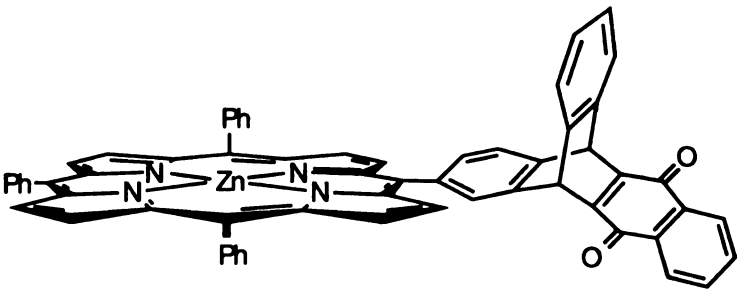

ZnP–NQ

(b)

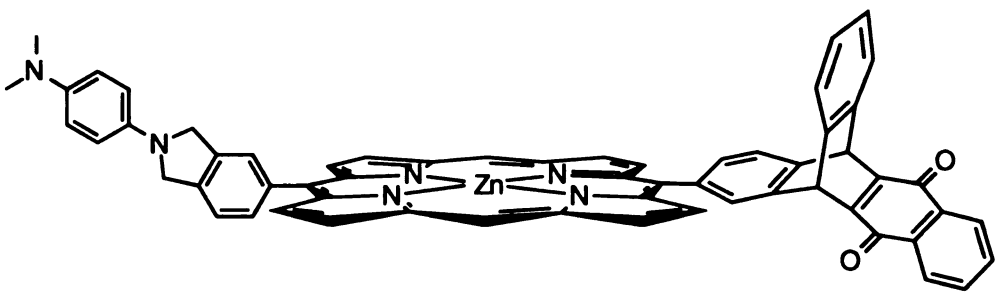

TMDAB–ZnP–NQ

(c)

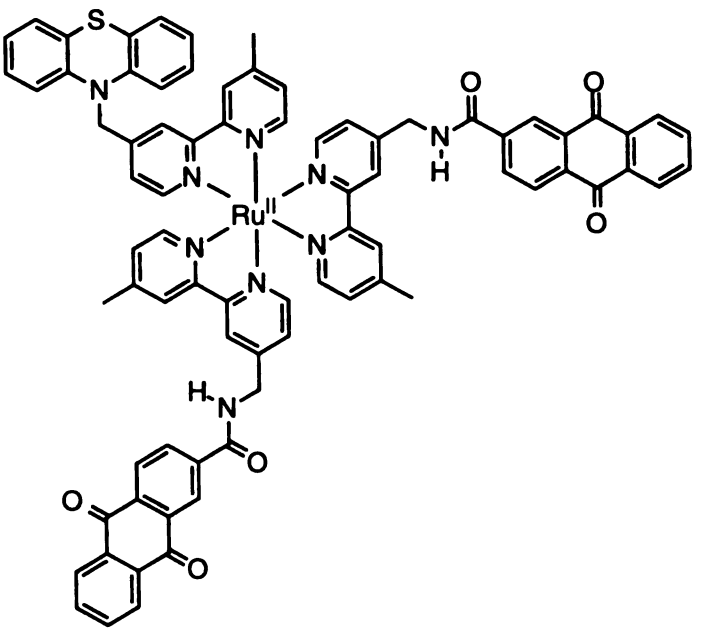

PZT–Ru(dmb)$_3$–AQ

Figure 9. Photoinitiated electron transfer reactions yielding charge separation in a porphyrin based dyad ZnP–NQ (a), a porphyrin based triad TMDAB–ZnP–NQ (b), and a ruthenium based triad PZT–Ru(dmb)$_3$–AQ (c).

opposite direction to the tetramethyl-p-diaminobenzene (TMDAB moiety) to yield an overall charge separated state on the right side of Eq. 1.17. These consecutive ET events are complete in under 500 picoseconds. The resulting charge separated species decays with a time constant of 4 milliseconds, long enough to record its EPR signal, which is remarkably similar to that measured in protein systems. It is an impressive result that adding one more ET event into the scheme extends the overall lifetime of the charge separated species by greater than a factor of a million.

$$\text{TMDAB–ZnP*–NQ} \longrightarrow \text{TMDAB}^{\bullet+1}\text{–ZnP–NQ}^{\bullet-1} \qquad (1.17)$$

Meyer and coworkers have also prepared D-chromophore-A complexes of the type shown in Figure 9 (c) as photophysical models or mimics of the light harvesting and charge separation events in photosynthesis.[18] The model incorporates $[Ru(dmb)_3]^{2+}$ (dmb is 4,4'-dimethyl-2,2'-bipyridine) as a synthetic support from which two distinct types of redox active organic moieties are attached. Each dmb ligand is functionalized, one with PZT, and two with anthraquinone. Absorption of visible light by $[Ru(dmb)_3]^{2+}$ yields an excited state, $[Ru(dmb)_3{}^*]^{2+}$, which simultaneously reduces one of the anthraquinones to its radical anion (λ_{max} = 580 nm, ε = 4000 M^{-1} cm^{-1}), and oxidizes the PZT to its radical cation (λ_{max}= 510 nm), as monitored by time resolved transient absorption spectroscopy, Eq. 1.18. The lifetime of the charge separated species is 150 nanoseconds, where systems functionalized with only a PZT or only an anthraquinone live for a few nanoseconds. This remarkable system demonstrates how light can be efficiently converted into stored energy through carefully tuning intramolecular oxidation and reduction reactions with the excited state of a molecule.

$$\text{PZT–Ru(dmb)}_3\text{*–AQ} \longrightarrow \text{PZT}^{\bullet+1}\text{–Ru(dmb)}_3\text{–AQ}^{\bullet-1} \qquad (1.18)$$

C. Proton-Coupled Electron Transfer

1. Introduction

Protons can significantly affect the rates of biological electron transfer. Many proteins and enzymes derive their function by mediating the rates of electron transfer by a proton. Nowhere is this better demonstrated than in the active site of cytochrome *c* oxidase. Although the distances separating the two heme centers from the binuclear Cu_A centers are similar, electron transfer to heme *a* is 10^2 - 10^4 faster than that to heme a_3.[19] Proton transfer accompanying heme reduction is believed to be the origin of the slow electron transfer to heme a_3 and accordingly the controlling factor for directional electron transport via heme *a*.[20] Such proton-coupled electron transfer (PCET) events continue to emerge in the structure/function relations of a variety of other proteins and enzymes including Photosystem II,[21-23] nitrogenase,[24,25] non-heme iron containing proteins,[26,27] multicopper oxidases,[28] and reductases[29-31] to name a few. Nevertheless, despite the importance of PCET in bioenergetic conversion processes of this diverse biological machinery, the mechanistic details of how the electron couples to the proton remain largely undefined.

2. Photoinitiated ET in Semi-Synthetic Protein Mediated D/A Dyads

a. Histidine-33 Modified Cytochrome c

It was recognized long ago that ET reactions in semi-synthetic proteins could be applied to study the effect of the coupling pathway within the protein. From these studies Gray began to define the role of the protein structure in ET events in natural systems. Their results stem from synthetically tailoring a class of cytrochrome *c* proteins with the redox active pendent groups.[32] The overall electron transfer reactions studied was an ET reaction form a surface modified histidine group to the iron(III) heme imbedded within the protein interior. The net ET reaction is given below, Eq. 1.22. The reaction is initiated by the reductive quenching of the surface $A_5Ru(III)$His-33 by a $[Ru(bpy)_3{}^*]^{2+}$ present in solution. Alternatively the reaction can be initiated using the pulse radiolysis technique, yielding

essentially the same unimolecular rate constant. The reaction rate for the ET reaction listed in Eq. 1.22 is 50 milliseconds, as measured by laser flash photolysis, or by the pulse radiolysis technique. The results of their experiments show that electrons can efficiently tunnel through covalent bonding and hydrogen bonding present within the folded protein structure, Figure 10 (a).

$$A_5Ru(II)\text{-(His-33)–Cyt C–Fe(III)P} \longrightarrow A_5Ru(III)\text{-(His-33)–Cyt C–Fe(II)P} \quad (1.22)$$

b. Dipolar Effects in D/A modified α-Helical Polypeptides

Model helical peptide systems have been developed by Fox and coworkers to examine the effects of helical dipole moments (μ_{helix}) on the rate of ET, Figure 10 (b).[33] ET rates where measured to the excited state electron acceptor (A*) of pyrene (Pyr*), which is reduced by a pendent electron donor (D), N,N-dimethylaminobenzene (DMA), by the mechanism outlined in Eq. 1.23. Owing to the design of the system, the ET could be initiated along a pathway coincident and aginst the permenant dipole of the helix. Measured rates in a variety of solvents reveal k_{ET+}/k_{ET-} to be 27 in THF, showing that an intervening dipole moment can significantly affect ET rates.

$$DMA\text{–}\alpha\text{-helix–}Pyr^* \longrightarrow DMA^{\bullet+1}\text{–}\alpha\text{-helix–}Pyr^{\bullet-1} \quad (1.23)$$

3. Biological Salt Bridge Proton-Coupled Electron Transfer in Sirohemereductase

An important example of PCET in nature is the action of a certain iron-sulfur protein sirohemereductase. Iron-sulfur proteins are well known for their ability to act as electron carriers to supply the electrons required in biological transformations. However, they also catalyze small molecule activation. Sirohemereductases, which encompass sulfite reductase (SiRs) and nitrite reductase (NiRs), catalyze the conversion of sulfite to sulfide (Eq. 1.24). The overall transformation requires the delivery of 6 protons and 6 electrons to the substrate bound protein active site. In the duration of the overall reaction, no intermediate oxidation products can detected free in solution. This is an indication that all

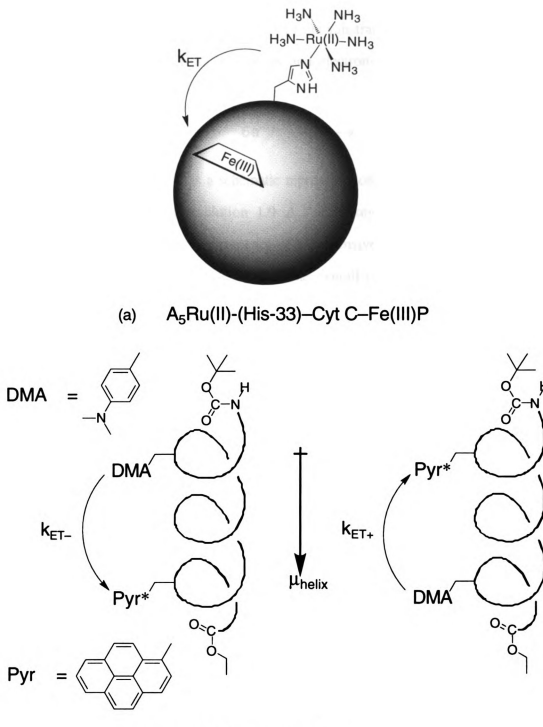

Figure 10. Hydrogen bonded protein mediated ET reactions in (a) a modified cytochrome *c* with a surface $A_5Ru(II)$-His-33 group and (b) a functionalized α-helix in the peptide sequence Boc-NH-Ala-Aib-Ala-(**DMA** or **Pyr-Ala**)-Ala-Aib-Ala-Ala-Aib-Ala-(**Pyr** or **DMA-Ala**)-Aib-Ala-CO_2Et which sets up a helix dipole moment (μ_{helix}).

intermediate reduction and protonation states of the substrate remain bound to the protein active site, implying that the flow of protons and electrons into the protein active site is somehow coupled.

$$SO_3^{2-} + 6H^+ + 6e^- \longrightarrow S^{2-} + 3H_2O \quad (1.24)$$

Displayed in Figure 11 is a schematic representation of SiRs, taken from a protein crystal structure solved at a resolution 1.9 Å.[34] The key features of the structure are highlighted and clearly display the presence of an extensive array of salt bridge hydrogen bonds which act to perform multiple tasks in the overall transformation, including anion recognition, siroheme cofactor stabilization, and to create an access channel to shuttle protons into the active site, while allowing water molecules to exit the active site.

4. Photoinitiated ET in Hydrogen Bonded D/A Dyads

Recent examples of synthetic dyad molecules to study ET reactions have been extended to include naturally relevant hydrogen bonds. The basis for such systems is that hydrogen bonds can be employed to mediate charge separation reactions as the spacer group or linkage in fixed distance D/A ET. These systems emphasize that the spacer group separating D and A need not be a covalent group but can be some non-covalent hydrogen bond. Presented in Figure 10 are systems which fall into this category. In these D/A model systems, the spacer group is some type of hydrogen bond. These studies are peaking interests in a new wave of the ever changing field of ET research. The role of the proton within the hydrogen bond is being defined in the context of bioenergetics and its role in proton-coupled electron transfer (PCET) is being revealed.

a. Carboxylic Acid Dimer D/A Dyads

Nocera and coworkers have led the way in investigating electron transfer through hydrogen bonds and have developed a research program that delves into establishing the

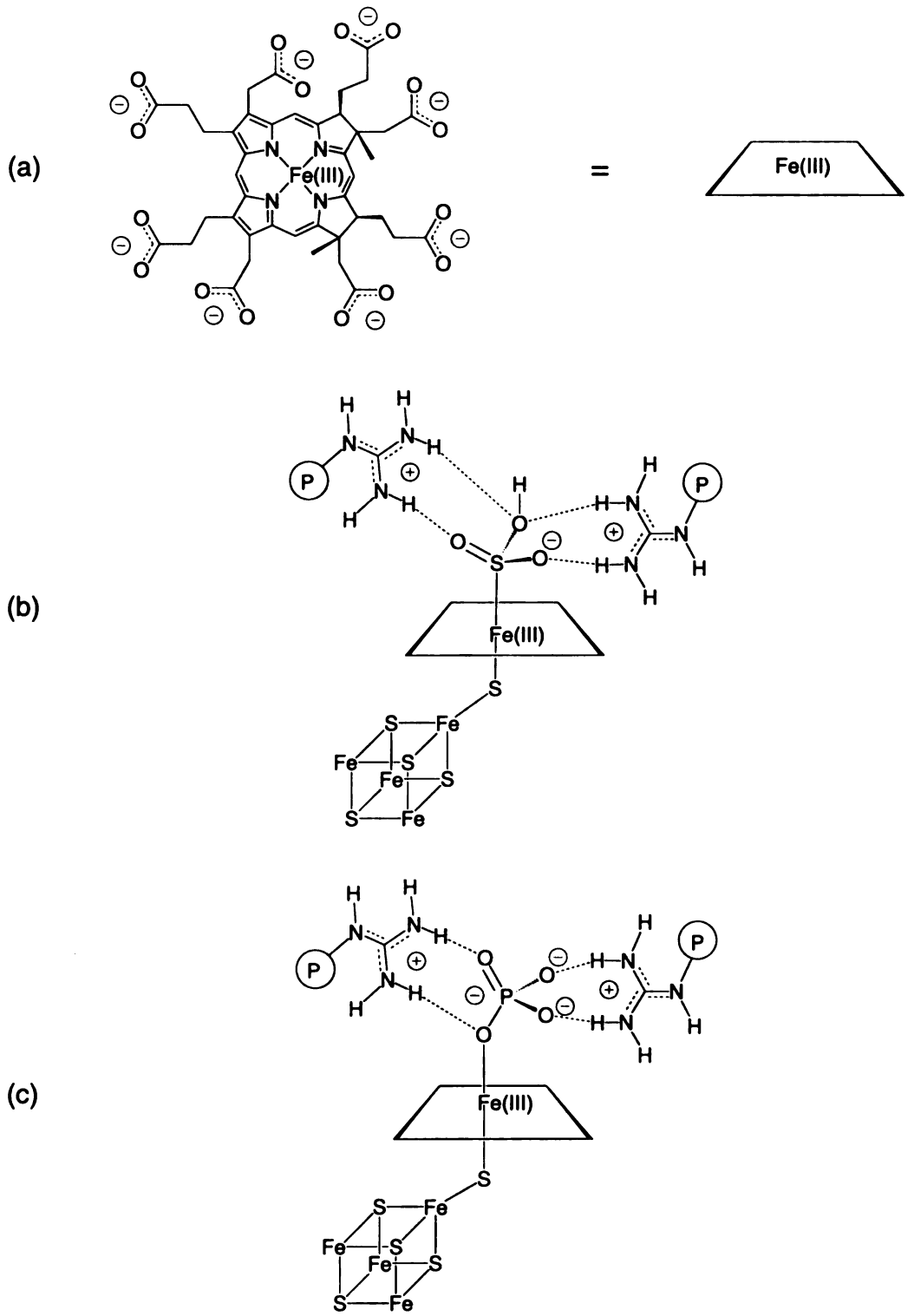

Figure 11. A schematic representation of the active site of SiRs and NiRs proteins. (a) siro heme where a rectangle is used to represent the heme atomic framework; (b), substrate (protonated sulfite) bound enzyme; (c) inhibitor (phosphate ion) bound enzyme.

underpinnings of PCET.[35] The initial studies focused on ET reactions in the midst of a carboxylic acid dimer. One such system is displayed in Figure 12 (a). In their system a zinc porphyrin (ZnP) is funtionalized with an acetic acid group which forms a heteromeric dimer with 3,4-dinitrobenzoic acid. In solvents of low dielectric constant, the carboxylic acid dimer forms spontaneously. In dichloromethane, the association constant for the dimerization is on the order of 500 M^{-1}. Also formed in solution are nearly a statistical distribution of homomeric dimers, which are ET inactive by design, and are not considered in this discussion. Pulsed laser initiated kinetics measurements where performed to assess the dynamics for ET in this system. The lifetimes for the charge separation and charge recombination were assessed by time resolve transient absorption techniques. Fixed distance ET reactions occur form the excited state of the zinc porphyrin to yield charge separated state. For the ^1H isomer charge separation occurs in 20 picoseconds, while charge recombination (not shown) occurs in 100 picoseconds. Similar kinetics studies have been performed where deuterium (^2H) is exchanged into the carboxylic acid dimer. An interesting kinetic isotope effect was observed (k_H/k_D = 1.6) for the forward charge separation step (Eq. 1.19) and similarly a kinetic isotope effect was observed for the charge recombination step (k_H/k_D = 1.7).

$$ZnP^*\text{–}(CO_2{}^{1,2}H)_2\text{–}DNB \longrightarrow ZnP^{+1}\text{–}(CO_2{}^{1,2}H)_2\text{–}DNB^{-1} \quad (1.19)$$

Therien and coworkers have assessed photoinitiated ET reaction in other carboxylic acid dimers.[36] In Figure 12 (b) is displayed a diporphyrin molecule where a benzoic acid dimer substituted in the para position separates a zinc porphyrin by iron porphyrin. The photoinitiated charge separation reaction, Eq. 1.20, is slower than the previous reaction with a time constant of 114 picoseconds. This is in part due to the larger distance separating D and A. Yet again this system demonstrates that coupling through hydrogen bonds is feasible to enable efficient electron transfer.

$$ZnP^*\text{–}(CO_2H)_2\text{–}Fe(III)P \longrightarrow ZnP^{+1}\text{–}(CO_2H)_2\text{–}Fe(II)P \quad (1.20)$$

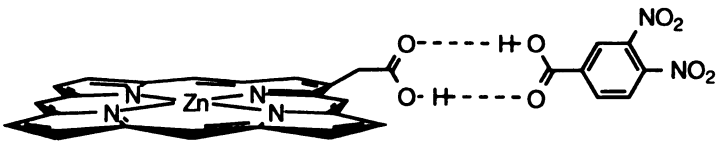

(a) ZnP–$(CO_2H)_2$–DNB

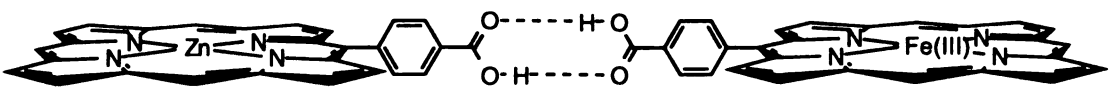

(b) ZnP–(p-$PhCO_2H)_2$–Fe(III)P

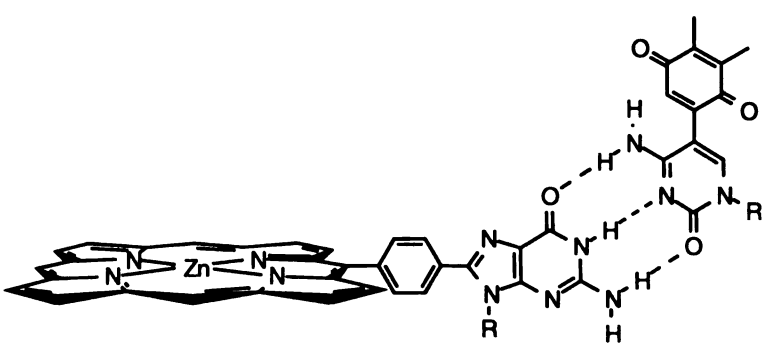

(c) ZnP–GC–BQ

Figure 12. Photoinitiated electron transfer in zinc porphyrin (ZnP) hydrogen bonded complexes where the electron acceptor is a dinitro aromatic, ZnP–$(CO_2H)_2$–DNB (a), an iron(III) porphyrin, ZnP–$(CO_2H)_2$–Fe(III)P (b) and benzoquinone, ZnP–GC–BQ (c).

b. ET in a Guanine-Cytosine Base Paired D/A Dyad

Sessler and coworkers have created an interesting ET assembly based on the hydrogen bonding interactions taken from the natural guanine and cytosine base pairs.[37] Their system is an example of specific hydrogen bonding and molecular recognition. Imparted into their system is the specificity of the guanine-cytosine (GC) base pairing interactions, Figure 12 (c), where the carboxylic acid dimers interactions are nonspecific and in solution there exists competing equilibria yielding dimers of D and dimers of A. The ET reaction takes place between the excited state of the porphyrin and the benzoquinone moiety , Eq. 1.21, with a time constant of 740 picoseconds. The longer time scale for the reaction is in part due to the longer distance created by the GC spacer group. ET is again efficient, and the presence of hydrogen bonds does not greatly purturb ET reaction rates.

$$ZnP^*\text{–}GC\text{–}BQ \longrightarrow ZnP^{+\cdot}\text{–}GC\text{–}BQ^{-\cdot} \quad (1.21)$$

D. Thesis Objectives

1. Association of Amidinium with Carboxylate in Solution and in the Solid State

The salt bridge is presented here as a versatile building block in natural and non-natural molecular architectures. In particular, as depicted in Figure 1, the amidinium-carboxylate salt bridge stands out for its specificity in that it possess only one specific two point hydrogen bonding mode relative to salt bridges based on guanidine and arginine. Chapter 2 presents a study on the factors controlling the amidinium-carboxylate salt bridge formation. Shown in Figure 13 (a) is the equilibrium expression for the formation of an amidinium-carboxylate salt bridge in solution. In the solid state there are other points of contact for maximizing all possible hydrogen bonding by forming additional one point secondary hydrogen bonds, Figure 13 (b), not to be confused with secondary electrostatic interactions. The factors governing hydrogen bond formation in the amidinium-carboxylate

salt bridge will be described. These include electronic, concentration, ionic strength, counter ion, secondary hydrogen bonding and finally pH effects on the observed equilibrium constant, K. In doing so, experimental challenges include the preparation and isolation of the individual components of the salt bridge, namely the challenge of synthesizing the individual molecules with either the amidinium or carboxylate functional groups.

2. The Amidinium-Carboxylate Salt Bridge and Proton-Coupled Electron Transfer

With the amidinium-carboxylate salt bridge moiety understood, we will study PCET by tethering a D/A system via the salt bridge, Figure 13 (c). A series of studies aimed at exploring the coupling of the motion of an electron to the motion of the proton through the synthesis of a series of novel compounds where electron donors and acceptors are tethered together through the dynamic interactions of the amidinium functional group to the carboxylate functional group. These compounds are presented as one possible way in which the proton motion couples to electron motion through a highly polar salt bridge created by the intrinsic electrical fields germane to groups mentioned above. In these systems the positive charge of an amidinium group is the result of protonation. Likewise the charge of the carboxylate group is the result of deprotonation. How an electron transfer reaction proceeds in the presence of such a salt bridge is revealed by electron transfer measurements. PCET reactions are initiated by either photoexcitation or pulse radiolysis.

Chapters 3, 4 and 5 present measurements of ET rates in D/A systems modified with the amidinium-carboxylate salt bridge, Figure 13 (c). Orientation of the salt bridge is an important issue with regard to PCET as the proton is postulated to set up a potential energy gradient that the electron must interact with on its journey from D to A, and also will exhibit Franck-Condon barriers and electronic coupling barriers that are dependent on the

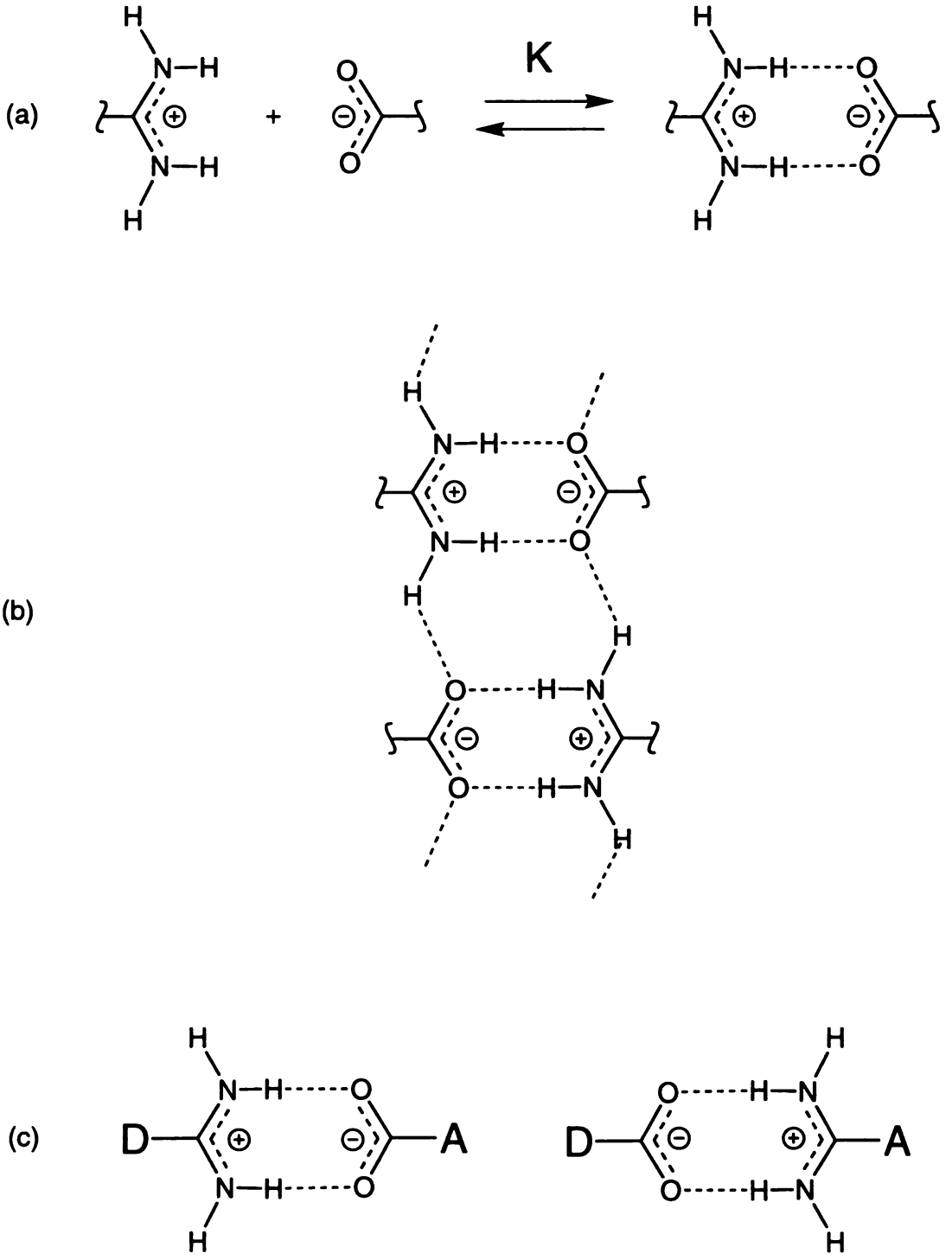

Figure 13. The amidinium-carboxylate salt bridge formed by the equilibrium between an amidinium and a carboxylate group to yield a primary two-point hydrogen bond (a); stacking of amidinium-carboxylate salt bridges through secondary one-point hydrogen bonding (b); D/A amidinium-carboxylate salt bridge complexes with two distinct orientations of the salt bridge for the study of fixed distance ET (c).

position of the proton within the salt bridge interface. Represented in Figure 13 (c) are the two distinct orientations of the amidinium-carboxylate salt bridge with respect to D and A.

Chapter 3 presents the results of photoinduced electron transfer measurements on donor–(salt bridge)–acceptor complexes based on $[Ru(bpy)_3{}^*]^{2+}$. Laser flash excitation prompts an electron to transfer from the reducing excited state of a derivatized Ru(II) bipyridine donor complex to a dinitrobenzene acceptor juxtaposed by the salt bridge interface in an oxidative electron transfer reaction, Eq. 1.25. The rate of electron transfer through the D–(amidinium-carboxylate)–A salt bridge is compared to electron transfer in the switched salt bidge complex, D–(carboxylate-amidinium)–A.

$$D^*\text{–salt bridge–}A \longrightarrow D^{\bullet+1}\text{–salt bridge–}A^{\bullet-1} \qquad (1.25)$$

Laser flash excitation also prompts an electron to transfer to the excited state of other derivatized Ru(II) bipyridine complexes. In this system the excited state of a derivatized Ru(II) bipyridine complex acts as an electron acceptor to a dialkyaminoaromatic donor compounds juxtaposed by the salt bridge interface in an reductive electron transfer reaction, Eq. 1.26.

$$A^*\text{–salt bridge–}D \longrightarrow A^{\bullet-1}\text{–salt bridge–}D^{\bullet+1} \qquad (1.26)$$

Chapter 4 describes the preparation of porphyrins modified the amidine functional group which undergo a reaction with carboxylic acids to form an amidinium–carboxylate salt bridge. The synthesis of porphyrin amidines permits donor-acceptor complexes to be juxtaposed by a zwitterionic hydrogen-bonded interface, formed upon the molecular recognition of a carboxylic acid by the porphyrin amidine. It is demonstrated that the salt bridge not only pre-organizes the donor-acceptor pair, but it also mediates electron transfer from the photoexcitable Zn(II) porphyrin to a nitroaromatic acceptor, Eq. 1.25.

Chapter 5 presents a PCET system as an extension of the Closs and Miller systems, and utilizes the pulse radiolysis technique to study ET reactions in radical anions of aromatic groups linked by the amidinium-carboxylate salt bridge, Eq. 1.27.

$$D^{\bullet -1}\text{–salt bridge–A} \longrightarrow \text{D–salt bridge–}A^{\bullet -1} \qquad (1.27)$$

Chapter 2

SOLUTION AND SOLID STATE AMIDINIUM-CARBOXYLATES

A. Introduction

Innumerable types of hydrogen bonding motifs are continually being revealed in nature where three dimensional structures are constructed from an assembly of hydrogen bonds and covalent bonds. One particular type of hydrogen bond is the salt bridge. In nature salt bridges act both as active catalysts and as passive structural motifs. More than 100 years ago Pinner isolated benzamidinium-benzoate salts in his pursuit of a synthetic methodology toward the amidinium functional group.[38]

Since Pinner's pioneering work, a series of benzamidinium-benzoates have been prepared by Krechl and coworkers, Eq 2.1, where the para substituent, X, is H, NH_2, t-butyl, C_6H_5, Br, and NO_2.[39] They found that the NMR chemical shifts in solution could be correlated to electronic contributions from either the benzamidinium or the benzoate

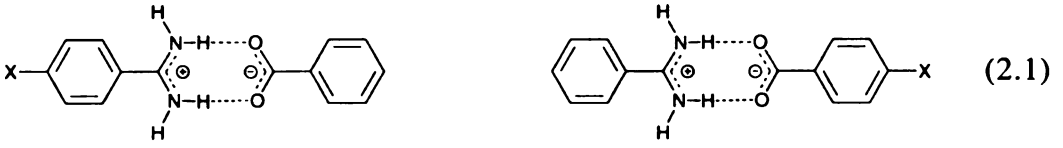

(2.1)

groups across the salt bridge in DMSO-d_6 solution. Yet in D_2O there is no influence on the NMR chemical shifts. From their results it was concluded that the salt bridge fromed by the 1:1 interaction of benzamidinium with the benzoate group is formed readily in DMSO-d_6 solution but not in D_2O. The factors that govern the equilibrium to form a salt bridge

between the benzamidinium group and benzoate group in either solution or in the solid state have only begun to be uncovered.

Before initiating a study of the factors involved in the formation of the benzamidinium-benzoate salt bridge, it is necessary to isolate pure salts of both the benzamidinium group and the benzoate groups. General methodologies are described here that allow for the convenient isolation and purification of large quantities of benzamidinium chloride salts and tetrabutylammonium benzoate salts. With these compounds in hand, it is possible to assess the equilbria in solution through the formation of a strong two point hydrogen bonding interaction.

In solution, the amidinium group of a para substituted benzamidinium (Am) spontaneously interacts with the carboxylate group of benzoate (Ca) to form the benzamidinium-benzoate salt bridge (AmCa) as described by the equilibrium depicted in Eq. 2.2. By carefully changing the relative concentration of amidinium and carboxylate, the equilibrium constant, K, describing the equilibrium between Am and Ca forming the AmCa

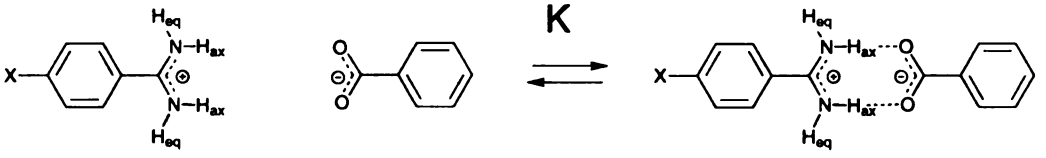

(2.2)

Am Ca AmCa

salt bridge may be assessed. Factors that influence the equilibrium to form the AmCa salt bridge include the electronic structure of the benzamidinium portion of the salt bridge system, the solution pH, and the ionic strength. At high ratios of Ca to Am, secondary hydrogen bonding interactions are observed. For the equilibrium displayed in Eq. 2.2, where X is hydrogen, methyl, phenyl or trifluoromethyl group an interesting substituent effect on the observed K is observed and may be rationalized in terms of a standard

Hammett equation relating changes in K to the electronic structure of the para benzamidinium substituent.

Solution studies of the salt bridge may be extended to the solid state. The molecule 3-amdininium-benzoate, shown in Eq. 2.3, combines both the carboxylate and amidinium groups into one molecule and is synthesised and structurally characterized by

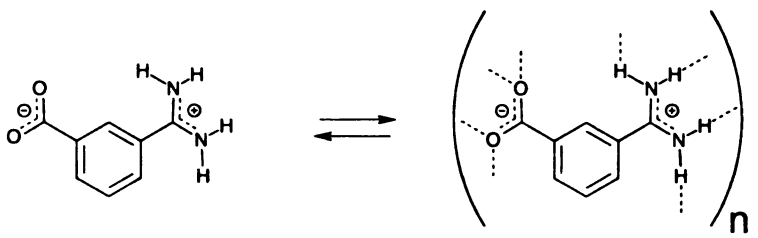

(2.3)

solution solid state

crystallographic techniques for the first time. Its solid state structure provides a link to the observed solution primary two point and secondary one point hydrogen bonding modes in the benzamidinium-benzoate system. The data presented here, from solution to the solid state, shows conclusively both the weaker secondary hydrogen bonding interactions and the strong primary two point hydrogen bonding interactions in both solution and the solid state. These results advance our understanding of the solution behavior of the amidinium-carboxylate salt-bridge as well as the factors that contribute to stabilizing this interesting structural motif in solution. The link between the solution and solid state salt bridge structures are clear in terms of a propensity of the system to achieve a closed set of hydrogen bonding interactions. In this closed set, the carboxylate group yearns to donate 4 lone pairs of electrons to 4 hydrogen bonding protons donated from the nitrogens of the amidinium group. Similarly, the amidinium group yearns to donate all 4 of its protons to 4 lone pairs of electrons. The formation of this closed set of hydrogen bonds in 3-amidinium-benzoate is represented in Eq. 2.3. In the solid state, there appears to exist a propensity to achieve closure inasmuch as one lone pair of electrons is donated to each proton.

B. Synthesis

1. Tetrabutylammonium Benzoate

The carboxylate form of acids are conventionally obtained by neutralization of the acid proton with strong base. Often sodium carboxylate salts of common carboxylic acids are commercially available. The drawback of sodium carboxylate salts is their poor solubility in organic solvents, thus they do not pose as viable compounds for solutions studies of salt bridges involving the introduction of carboxylates into aprotic organic solvents. However the tetrabutylammonium ion is exceedingly soluble in organic solvents, as it is commonly employed in phase transfer catalysts. For our studies we wish to examine salt bridge formation in non-aqueous aprotic solvents; therefore, we require the carboxylate form of carboxylic acid as its tetrabutylammonium salt.

Treatment of benzoic acid with an equivalent of tetrabutylammonium hydroxide in methanol yields an equivalent each of water and the tetrabutylammonium benzoate, as summarized by the reaction shown in Figure 14 (a). Removal of the methanol under reduced pressure yields a tarry residue, which is dissolved in freshly distilled benzene and treated with basic alumina, as described by Kemp.[40] Filtration to remove the basic alumina followed by freeze drying the solution, yields tetrabutylammonium benzoate in its anhydrous cyrstalline form.

2. Benzamidinium Chloride

Classically, rather harsh and cumbersome conditions are required for the preparation of amidinium chloride salts from nitriles. Dry hydrochloric acid consumes a nitrile in dry alcohol to yield the corresponding imidate ester as a hydrochloride salt. Addition of dry ammonia to the imidate ester hydrochloride salt affords the amidinium chloride salt as developed by Pinner at the end of last century. Conversely, as shown in Figure 14 (b), base catalyzed addition of alcohol to para-substituted benzonitriles generates

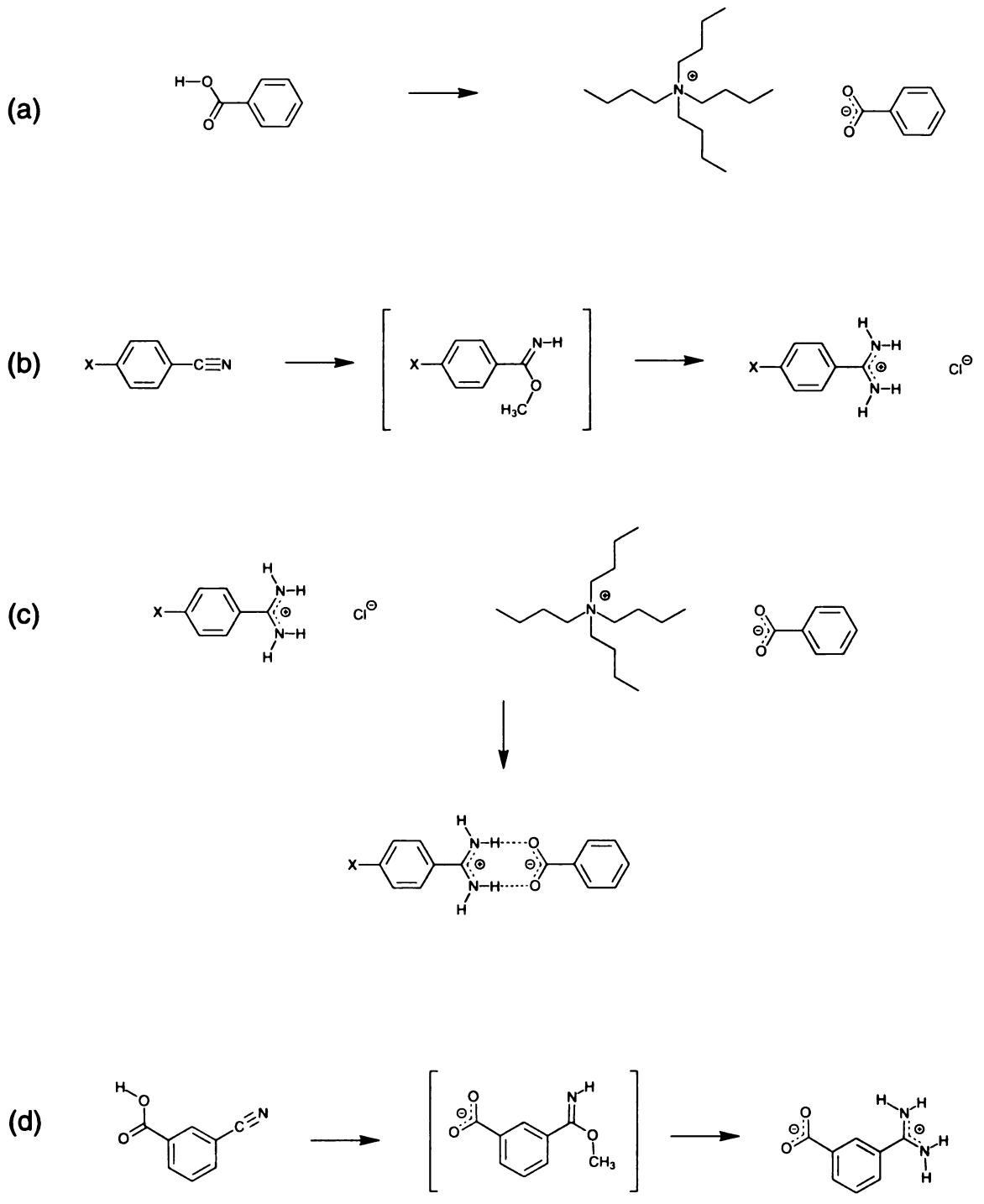

Figure 14. Synthetic reaction sequence employed for the preparation of (a) tetrabutylammonium benzoate by treatment of benzoic acid with tetrabutylammonium hydroxide; (b) para-substituted benzamidinium chloride salts by reaction of para substituted benzonitriles with sodium methoxide followed by ammonium chloride; (c) benzamidinium-benzoate salt bridges by precipitation from water; and (d) the preparation of 3-amidinium-benzoate by reaction of 3-cyanobenzoic acid with sodium methoxide, tetrabutylammonium hydroxide and crystallization from water (d).

free base imidate esters (bracketed in Figure 14 (a)). Addition of ammonium chloride to the free base imidate ester yields para-substituted benzamidinium chloride salts.

3. Benzamidinium-Benzoate

With both tetrabutylammonium benzoate and para-substituted benzamidinium chloride salts in hand it is possible to obtain benzamidinium-benzoate salt bridges free of extraneous counter ions by spontaneous assembly in aqueous solution, Figure 14 (c). When an aqueous solution of an amidinium chloride salt is combined with an equivalent of a tetrabutylammonium carboxylate salt, a precipitate forms. The ^{1}H and ^{13}C NMR as well as mass spectroscopy confirm the presence of both the amidinium and carboxylate portions of the salt bridge. Integration of the peaks in the ^{1}H NMR spectrum reveal the stoichiometry of the amidinium to carboxylate is 1:1. This reaction sequence is similar to a procedure developed where sodium benzoate salts are used instead of tetrabutylammonium benzoate salts.

4. 3-Amidinium-benzoate

An interesting molecule can be prepared that contains both the amidinium and carboxylate functional groups in one molecule. This molecule 3-amidinium-benzoate is prepared from the corresponding 3-cyanobenzoic acid as described in Figure 14 (d). This synthesis essentially combines both steps shown in Figure 14 (a), (b) and (c) into one. An excess of sodium methoxide performs dual duty, first to deprotonate the benzoic acid to yield the 3-cyanobenzoate and then to catalyze the transformation of the nitrile group to the free base imidate ester intermediate, shown as a bracketed intermediate in Figure 14 (d). Addition of an excess of ammonium chloride yields an intractable white solid, which crystallizes from hot water to yield large prismatic crystals suitable for x-ray crystallography.

C. Equilibrium Measurement via the NMR Technique

Displayed in Eq. 2.2 is the equilibrium for a para substituted benzamidiniun, Am with benzoate, Ca to form the benzamidinium-benzoate salt bridge, AmCa, in solution. The equilibrium constant, K, for the equilibrium depicted in Eq. 2.2 is defined in Eq. 2.4 as a function of the equilibrium concentrations of Am, Ca, and AmCa, denoted as [Am], [Ca], and [AmCa] respectively. Simple equilibria of this type have an exact mathematical solution derived from solving a quadratic formula relating the change in initial non-equilibrium

$$K = \frac{[AmCa]}{[Am][Ca]} \tag{2.4}$$

concentrations for Am and Ca, designated by $[Am]_0$ and $[Ca]_0$ respectively, upon achieving some equilibrium concentration of the AmCa salt bridge complex, [AmCa], as governed by K. The solution to this quadratic formula can be derived to define [AmCa] as expressed in Eq. 2.5 in terms of the initial non-equilibrium concentration values of $[Am]_0$ and $[Ca]_0$, as determined by preparing standard stock solutions of either benzamidinium chloride or tetrabutylammonium benzoate employing the usual analytical volumetric techniques and K.

$$[AmCa] = \frac{1}{2}\left[\frac{1}{K} + [Am]_0 + [Ca]_0 - \sqrt{\left(\frac{1}{K} + [Am]_0 + [Ca]_0\right)^2 - 4[Am]_0[Ca]_0}\right] \tag{2.5}$$

The ^{1}H NMR spectrum provides chemical shift information for freely solvated Am and the salt bridge complex AmCa. The chemical shifts for the N-H_{ax}, the protons involved in the primary two point salt bridge hydrogen bonding motif are designated δ_{Am} and δ_{AmCa}, respectively, and are separated in the ^{1}H NMR spectrum by some difference in chemical shift, $\Delta\delta_{max}$, as defined by the expression shown in Eq. 2.6. Next the observed carboxylate-concentration-dependent chemical shift, δ_{obs}, for N-H_{ax}, is defined as the weighted average of δ_{AmCa} for the AmCa salt bridge form of N-H_{ax}, and δ_{Am} for Am, the non-salt bridge forms of N-H_{ax}. This is due to the exchange rate of the salt bridge being

faster then the time scale for the ^{1}H NMR experiment. Finally, upon substitution of Eq 2.5 into Eq 2.7, Eq. 2.8 is obtained, where δ_{obs} is defined in terms of one dependent variable, K. The chemical shift dependence of N-H_{ax} is evident experimentally as shown in Figure 15 where displayed are ^{1}H NMR spectra for benzamidinium chloride and benzaminium chloride with benzoic acid and varying amounts of tetrabutylammonium benzoate.

$$\Delta\delta_{max} = \delta_{AmCa} - \delta_{Am} \tag{2.6}$$

$$\delta_{obs} = \delta_{Am} + \frac{[AmCa]}{[Am]_0} \bullet \Delta\delta_{max} \tag{2.7}$$

$$\delta_{obs} = \delta_{Am} + \frac{\Delta\delta_{max}}{2[Am]_0}\left[\frac{1}{K} + [Am]_0 + [Ca]_0 - \sqrt{\left(\frac{1}{K} + [Am]_0 + [Ca]_0\right)^2 - 4[Am]_0[Ca]_0}\right] \tag{2.8}$$

In the ^{1}H NMR spectrum of benzamidinium chloride both N-H_{ax} and N-H_{eq} appear as a single broad peak centered at 9.3 ppm, the bottom spectrum in Figure 15. Integration of the area of this peak corresponds to the expected 4 protons. Addition of benzoic acid to a solution of benzaminidinium chloride transforms the broad peak into two resolvable peaks corresponding to N-H_{ax} and N-H_{eq}, second spectrum from the bottom of Figure 15, where the integral region of each peak is equivalent to two protons each. A small effect is observed on the δ_{obs} for N-H_{ax} and N-H_{eq}, but they essentially remain centered at 9.3 ppm. The change in the appearence of the line shapes for these two peaks in the presence of benzoic acid reflects the change in the relaxation dynamics of the nuclear spin of the protons corresponding to N-H_{ax} and N-H_{eq}. Effects such as this are well known for altering the media surronding a spin system such as by changing the acidity of the solution. The chemcial exchange of the N-H protons with the acidic proton of the carboxylic acid group may also contribute to the appearence of the peaks corresponding to N-H_{ax} and N-H_{eq} in the ^{1}H NMR spectrum.

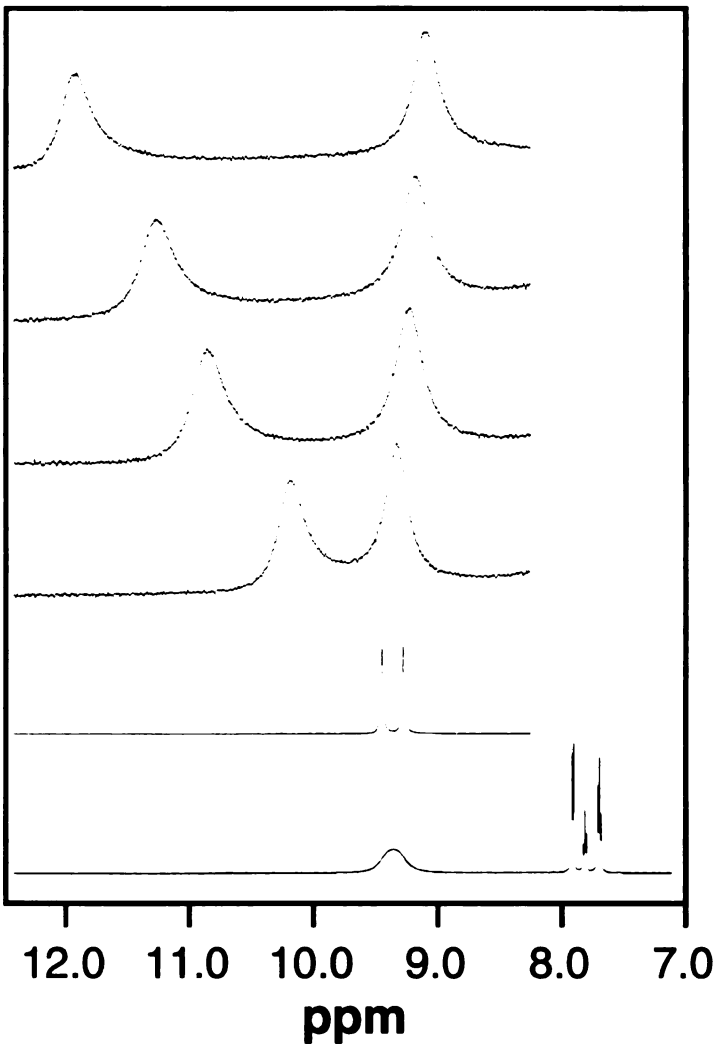

Figure 15. ^{1}H NMR spectrum of benzamidinium chloride at a concentrtion 5.2 mM in DMSO-d_6 (bottom). The ^{1}H resonances of the aromatic ring appear between 7.5 and 8.0 ppm. The amidinium protons appear as a broad singlet at 9.3 ppm, but separate and sharpen to two singlets in the presence of 16.6 mM benzoic acid (second from the bottom). Selected spectra are shown upon addition of the tetrabutylamonium benzoate at concentrations 0.0, 0.0, 1.5, 2.3, 3.0, and 5.0 mM (bottom to top).

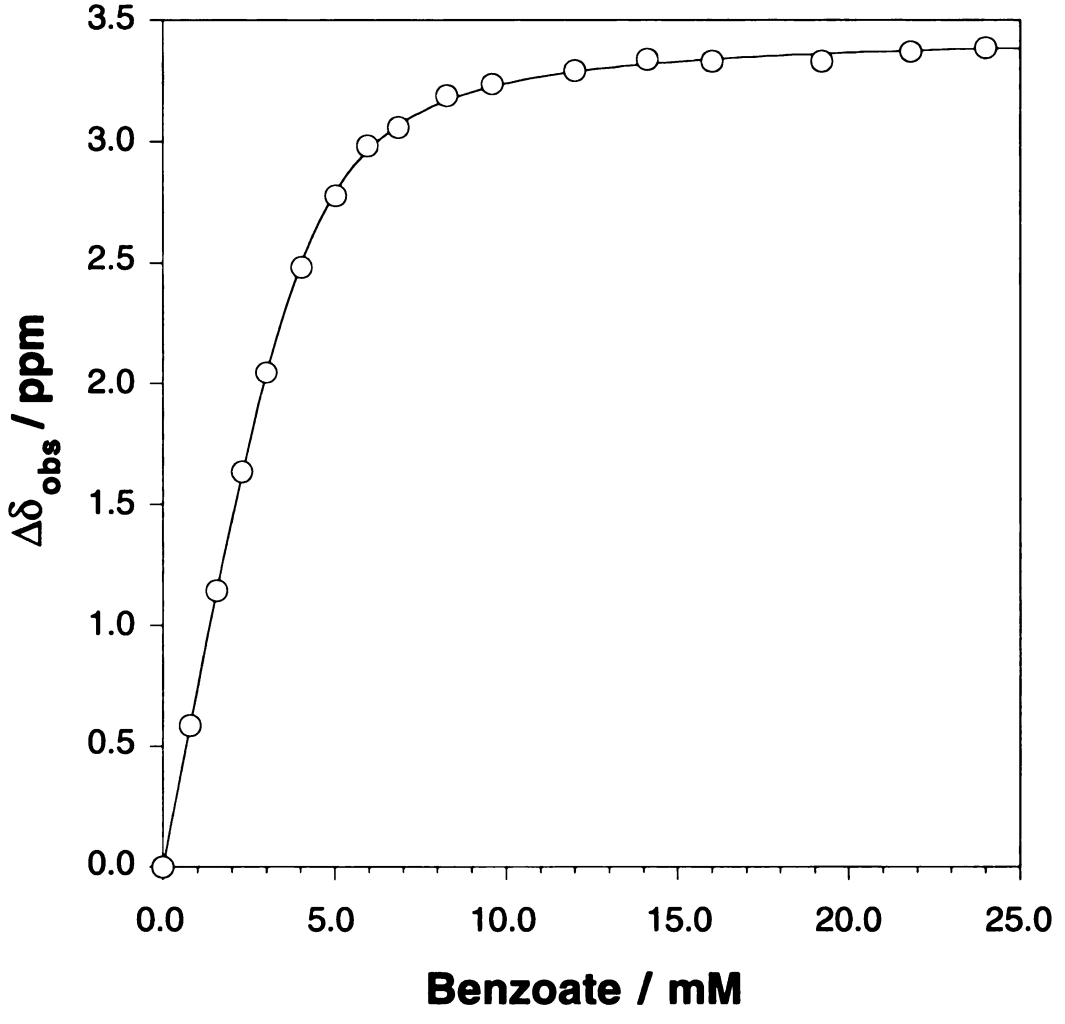

Figure 16. Plot of the change in chemical shift of the benzamidinium N-H_{ax} proton versus the concentration of benzoate from 0.0 to 25 mM. The concentration of benzamidinium chloride is 5.5 mM, and the concentration of benzoic acid is 16.6 mM throughout all concentrations of benzoate (as the tetrabutylamonium salt).

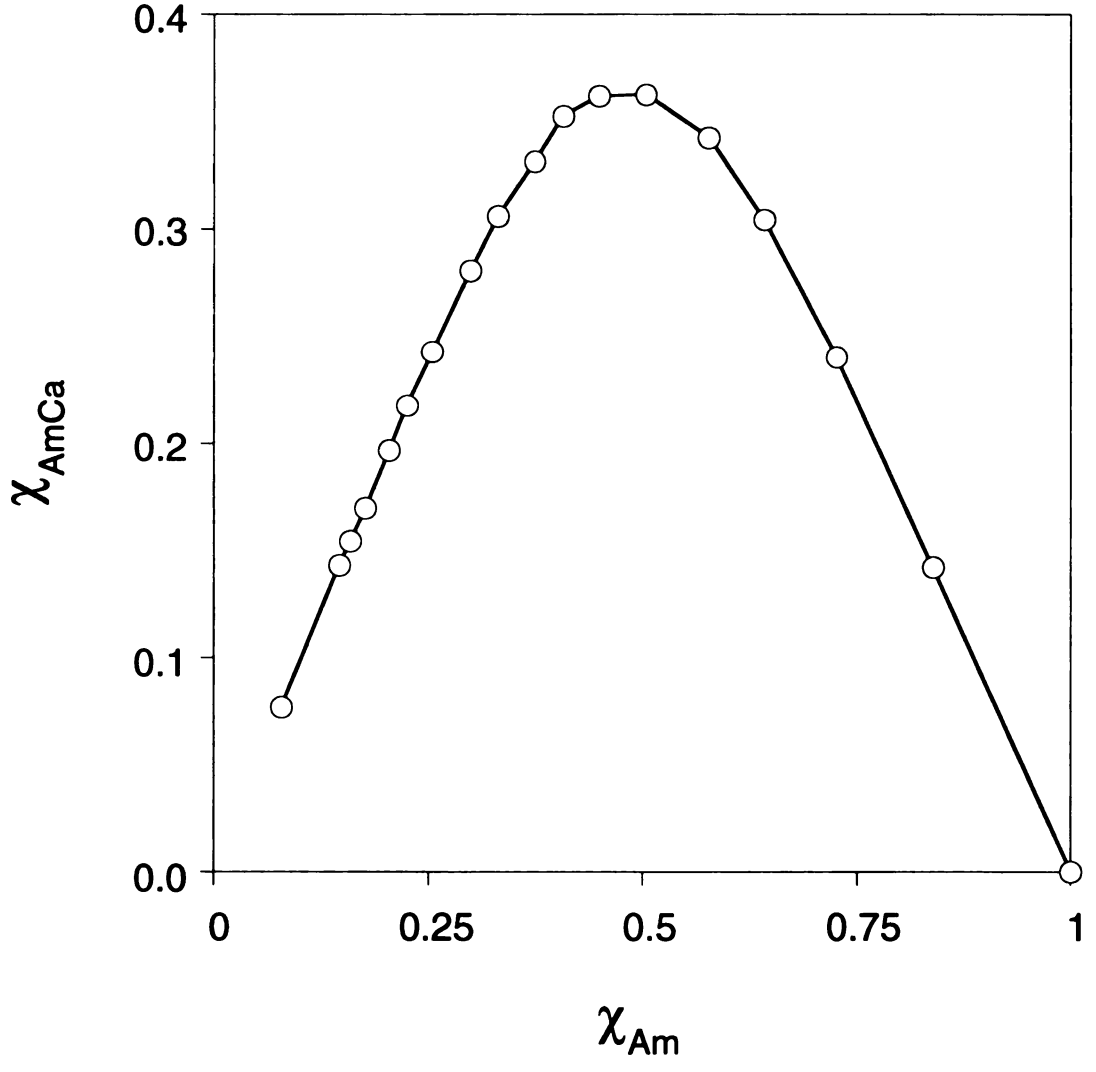

Figure 17. Job's plot of the mole fraction of the benzamidinium-benzoate salt bridge complex vs. the mole fraction of benzamidinium (6.3 mM) as the concentration of benzoate is varied from 0.0 to 25 mM

Addition of tetrabutylammonium benzoate to the solution containing benzamindium chloride and benzoic acid has large effects on δ_{obs} for both N-H_{ax} and N-H_{eq} of the amidinium group of benazminidium chloride. The large downfield changes in δ_{obs} for N-H_{ax}, over 3.0 ppm is a direct indication of AmCa salt bridge formation as shown in Eq. 2.2. Likewise the N-H_{eq} experiences a slight upfield shift of around 0.5 ppm. The chemical shift information, in conjuction with the concentration information, is used in Eq. 2.8 to fit the data to K using a non-linear least squares method. Plotted in Figure 16 is δ_{obs} as a fucntion of the benzoate concentration. A fit to Eq. 2.8 is shown in Figure 16 for which a K of 2500 M^{-1} is obtained. The fit gives a good K for the entire concentration range studied for this systems. The stoichiometry of the AmCa salt bridge is confirmed by a Job plot Figure 17. In the Job plot the method of continuos variation is employed to reveal that the mole fraction of the AmCa has is optimum when the mole fraction of Am is 0.5. That is the concentration ratio of Am and Ca that yields the optimum mole fraction AmCa in solution.

There are limitations to this technique, primarily concentration at which one works. Also for the titration procedure a great limitation is the presence of spectator ions. For each amidinium group there will be a chloride ion in solution. Likewise for each carboxylate group there will be a tetrabutylammonium ion present in solution. The affects of these groups is accounted for by a separate ion dependence on the association constant study. The observed binding constant is also dependent on the concentration of acid present in solution. This can be accounted for by measuring K at different concentrations of benzoic acid while at a constant concentration of benazamidinium chloride. Conversely the affects of chloride ion on K can be assessed by measuring K at different concentrations of benzamidinim chloride while maintaining constant concentration of benzoic acid. The results of these experiments are presented in the proceeding sections of this chapter.

D. Effects on Salt Bridge Equilibrium Constant

1. Salt Bridge Hammett Effects from para Substituted Bemzamidiniums

Recently it was shown by Wilcox that solution hydrogen bonding interactions between N-arylureas, with substituted in the para-position, and sulphonates display a strong correlation between the observed association and the σ^- Hammett parameter. Furthermore, calculated surface electric potentials are shown to effectively predict the observed association energy within the same series of compounds. Thus the correlation between the electrostatic nature of hydrogen bonding and observed association energies is established. These results reinforce the power of the Hammett parameter in predicting electronic effects on chemical equilibria. We thought that the electrostatic nature of the amdinium-carboxylate salt bridge was a logical next step to pursue the electrostatic effects on solution hydrogen bond formation.

Presented here is a similar Hammett study on K, Eq. 2.02, as a function of the electron donating and electron withdrawing groups of para substituted benzamidinium group. Listed in Table 1 are the substituents used in this study along with the corresponding Hammett σ_{para} parameters and the observed K for each substituent. The results of this study reveal that the electronic structure of the molecule is important in controlling the primary two point hydrogen bond formed in the amidinium-carboxylate salt bridge. These effects are due to polarization of the para substituted benzamidinium group due to the electrostatic nature of the salt bridge hydrogen bond. Changes in the electronic structure are manifested in changes in polarity of the hydrogen bonding group, in this case the Hammett parameters are adjusted for modifying the electronic structure about the amidinium group. However the a benzoate group can be nearly equally perturbed as shown by results aimed at exploring the simple chemical shift data.

Table 1. Hammett effects on the association constants of para-substituted benzamidiniums (X) with benzoate.

X	σ_{para} [a]	K [b]
CH_3	-0.14	1490
H	0.00	2504
C_6H_5	0.05	2846
CF_3	0.53	13253

[a]Values for σ_{para} are from March, J. *Advanced Organic Chemistry, 4th Edition* J. Wiley and Sons: New York, 1992, p. 280. [b]In DMSO-d_6 at 25.0 °C, the error in values of K are ± 15%.

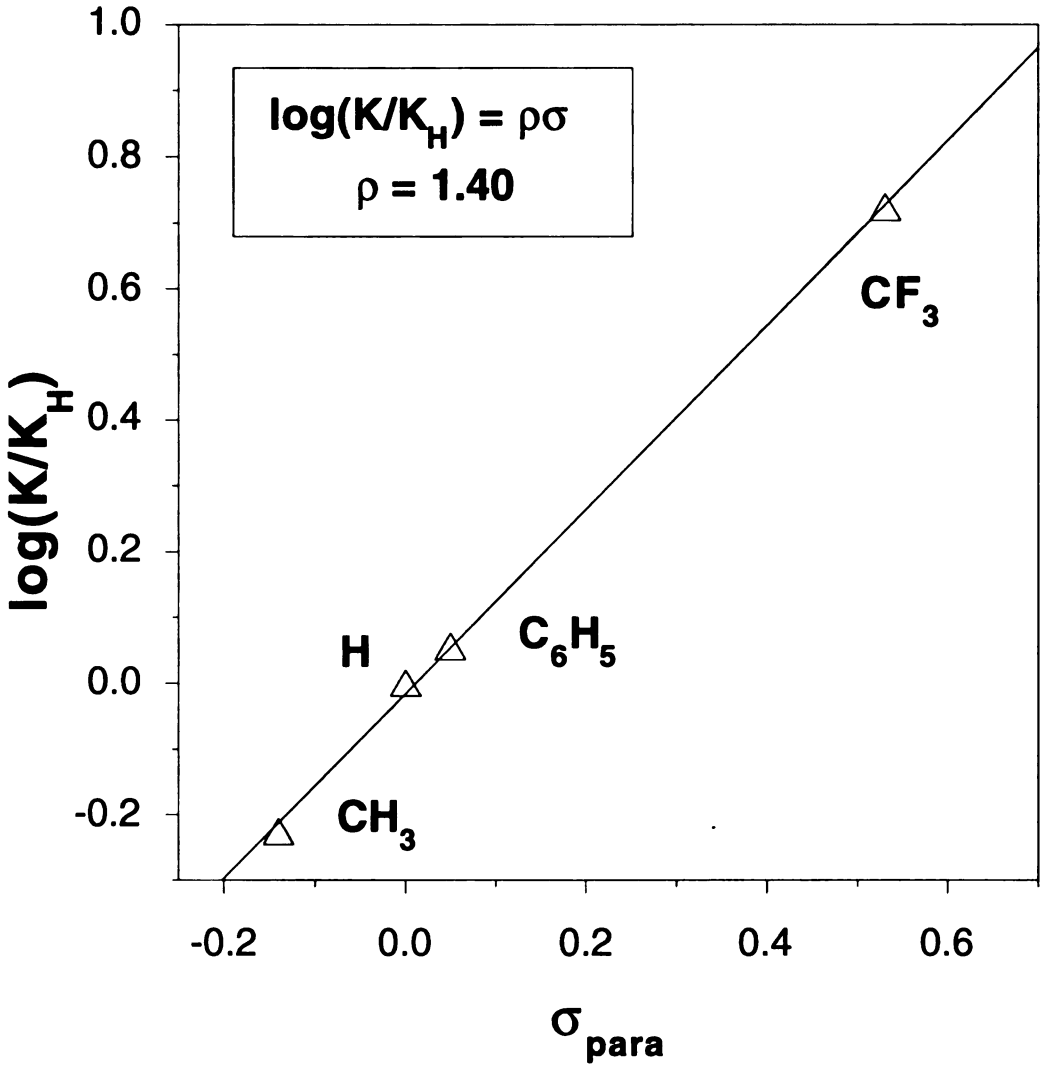

Figure 18. Hammett plot for K and para substituted benzamidiniums.

The effects can be explained in terms of simple electron donor/acceptor interactions. The donation of electron density into the amidinium group results in stronger N-H bonds but decreases the relative charge on the H. This weakening of the charge results in a direct weakening of the electrostatic interaction of the salt bridge. Conversely, removing electron density by the inductive action of the trifluoromethyl groups weakens the N-H bonds, and makes the charge on the H higher thereby directly increasing the electrostatic attraction to the carboxylate moiety, yielding an overall increase in observed K.

These results are summarized in Figure 18 where the slope of the plot of the log of K versus σ_p yields ρ. The value of 1.4 for ρ, obtained in the fit, reflects the strong electrostatic nature of the hydrogen bonding interation within the amidnium-carboxylate salt bridge.

2. Effect of Benzoic Acid Concentration on the Solution Salt Bridge Equilibrium

The effects on the binding constant are not limited to the electronic effects. Due to the polar nature of the salt bridge other factors are involved in controlling the binding such as the addition of other hydrogen bonding groups. Especially important is the effect of adding excess benzoic acid to solutions due to the fact that the protons in the salt bridge are more easily observed when the conjugate acid is present at some concentration.

Figure 19 is the result of three separate titration experiments where the concentration of chloride and amidinium is constant at 5.2 mM and the concentration of benzoic acid is constant at 10, 50 and 100 mM. The fit of the data is arbitrary and is in place only as a visual aid. The results show that there is a sizable decrease in the observed K with increasing benzoic acid concentration. This is due to several factors. First the increase in the polarity of the solution will change the dielectric properties of the solution, directly decreasing the electrostatic interaction. The carboxylic acid is amphoteric in that it can compete for hydrogen bonding to the amidinium group through one and two point

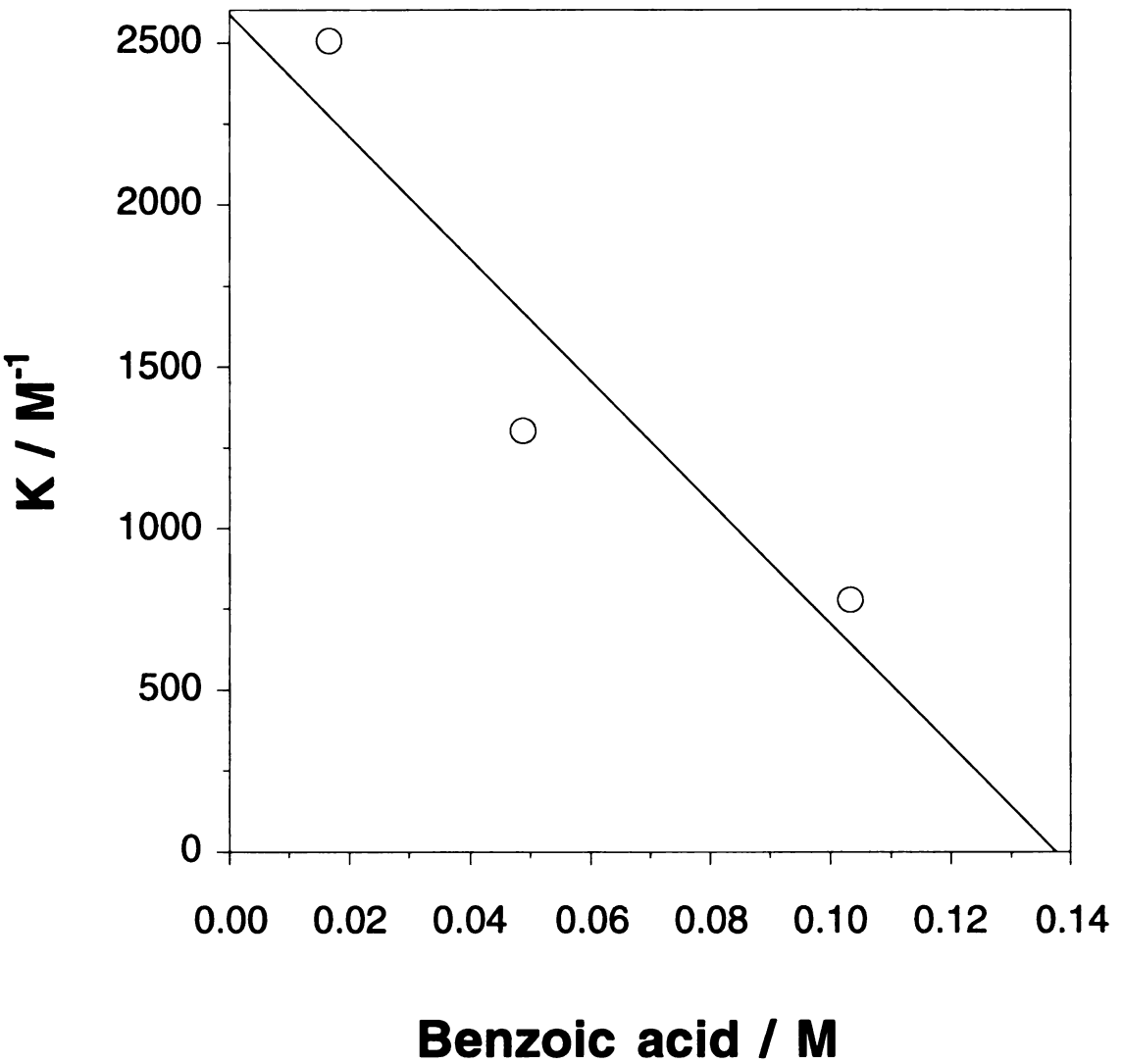

Figure 19. The effect of benzoic acid concentration on K. The chloride concentration is held constant at 0.005 M.

hydrogen bonds. Finally by increasing the pH of the solution will also affect the hydrogen bonding interactions.

3. Effect of Chloride Ion Concentration on the Salt Bridge Equilibrium

The ionic strength of a solution affects equilibria present in that solution. The interaction energy of the amidinium-carboxylate salt bridge, determined by Coulombs's law, is directly effected by the ionic strength of the solution as described by the Debye-Huckle equation. Therefore, the association constant for the formation of salt bridges should also depend on the ionic strength of the solution. This quantitiy can be systematically varied with the addition of extraneous counter ions by changing the initial concentration of the amidinium chloride in a particaular titration experiment, or by the addition of extraneous ions in the form of tetrabutylammonium chloride.

As shown in Figure 20, there are large effects on the observed binding constant with ions present. These effects suggest that the lone pair electrons and protons that interact with the solvent give a direct pathway to tuning the electronic interactions in the salt bridge by the solvent. Added chloride ions, which can weakly donate 4 lone pair electrons and has a net negative charge, compete with carboxylate to interact with the positively charged amidinium group. This interaction need not be bonding. Furthermore the chloride can perturb the system by simple non-specific ion-ion interactions, thereby scrambling the electrostatic interactions between net ion partners. These non-specific ionic interactions effectively lower the observed binding constant for the observed salt bridge interaction.

4. Carboxylate Concentration Effects

The preceding discussion has focused upon the interesting concentration dependent chemical shifts at low concentrations, and the effects on the equilibrium constant for the formation of the amidinium-carboxylate salt bridge. However, when the concentrations of benzoate is raised far above and beyond the concentrations used in assessing K in the primary hydrogen bonding mode expressed by Eq. 2.2, it is evident that secondary

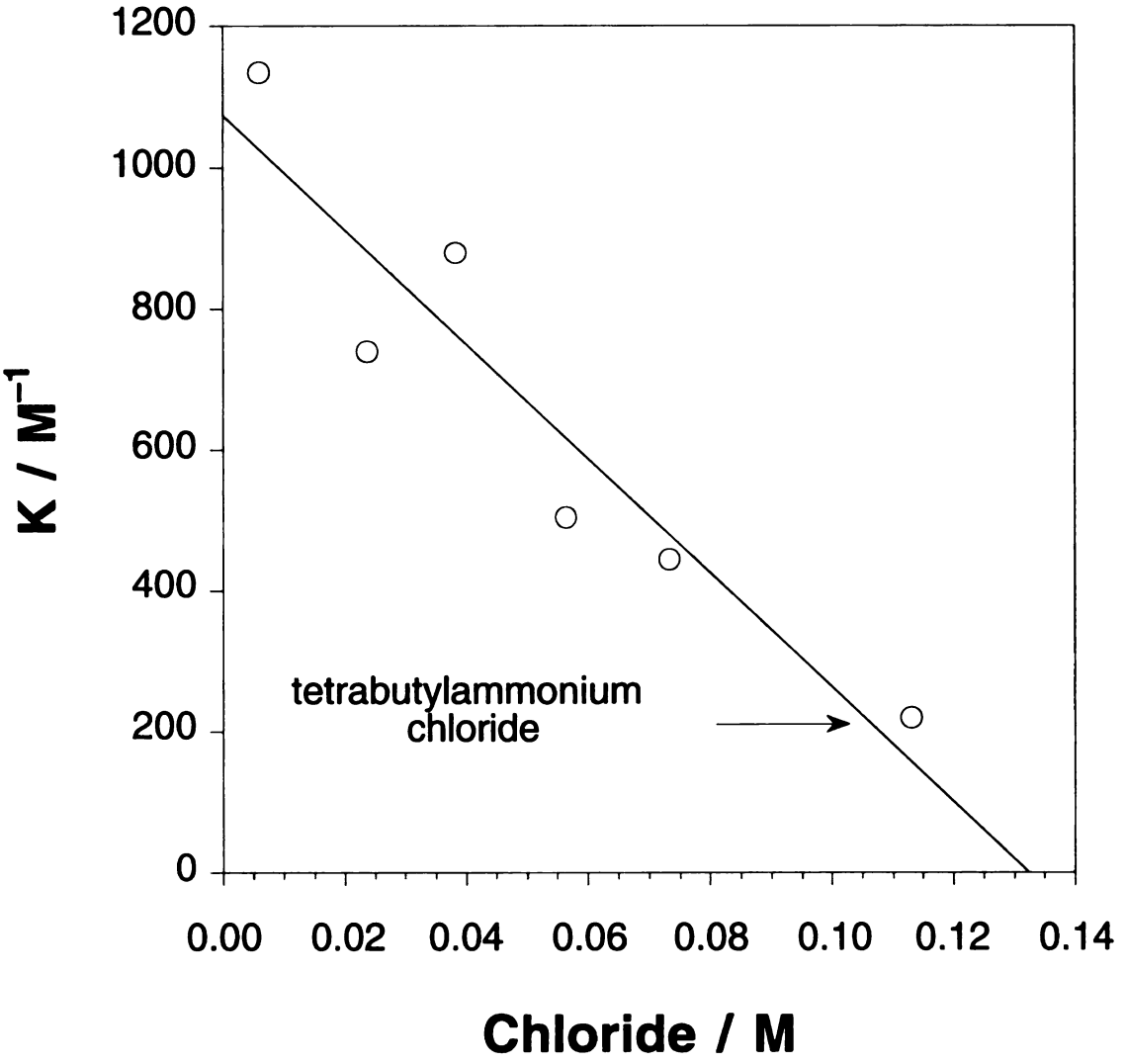

Figure 20. Affect of chloride ion concentration on the observed binding constant (K). The concentration of benzoic acid is constant 0.050 M for each measurement of K.

hydrogen bonding equilibria are present, though with much lower relative equilibrium constants relative to the primary two point hydrogen bonding salt bridge interaction.

Figure 21 displays the concentration dependence of the amidinium protons at 63.0 mM over a concentration range of carboxylate from 0.0 to 864.0 mM with the carboxylic acid concentration constant at 226.0 mM. The early concentration dependence fits to the equilibrium expression shown in Eq. 2.2, where a K of 125 M^{-1} is obtained. This primary hydrogen bonding mode fits well to the equation below 5 equivalents, but not at higher concentrations. This suggests that secondary equilibria are also present. In particular, the concentration dependence of the NH_{eq} becomes obvious when the concentration of carboxylate approaches 10 equivalents or more. This suggest an association constant weaker then the primary mode yet observable nonetheless.

A model to explain the behavior of NH_{eq} at concentrations of benzoate near saturation is outlined in Figure 22. First, the primary two point hydrogen bonds form, then in a stepwise manner, a second and a third benzoate associate with the two NH_{eq}'s to form a total of four hydrogen bonds to the benzamidinium group through the two additional weaker one point hydrogen bonds. This creates a net closed set of hydrogen bonds to the amidinium group as put forth by Etter and Ward.

E. Solid State Structure of 3-Amidinium-benzoate

Evidence for the weaker secondary hydrogen bonds in the amidinium-carboxylate salt bridge observed in the benazamindinium-benzoate salt bridge in the presence of exceedingly high concentrations of benzoate is revealed in the examination of the solid state structure of 3-amidinium-benzoate. The construction of solids by self-assembly requires that the noncovalent interactions of structural subunits, referred to as supramolecular synthons,[41] be controlled in an exact and predictable manner. Hydrogen-bonding, dipole, hydrophobic, aromatic -stacking and van der Waals forces are some of

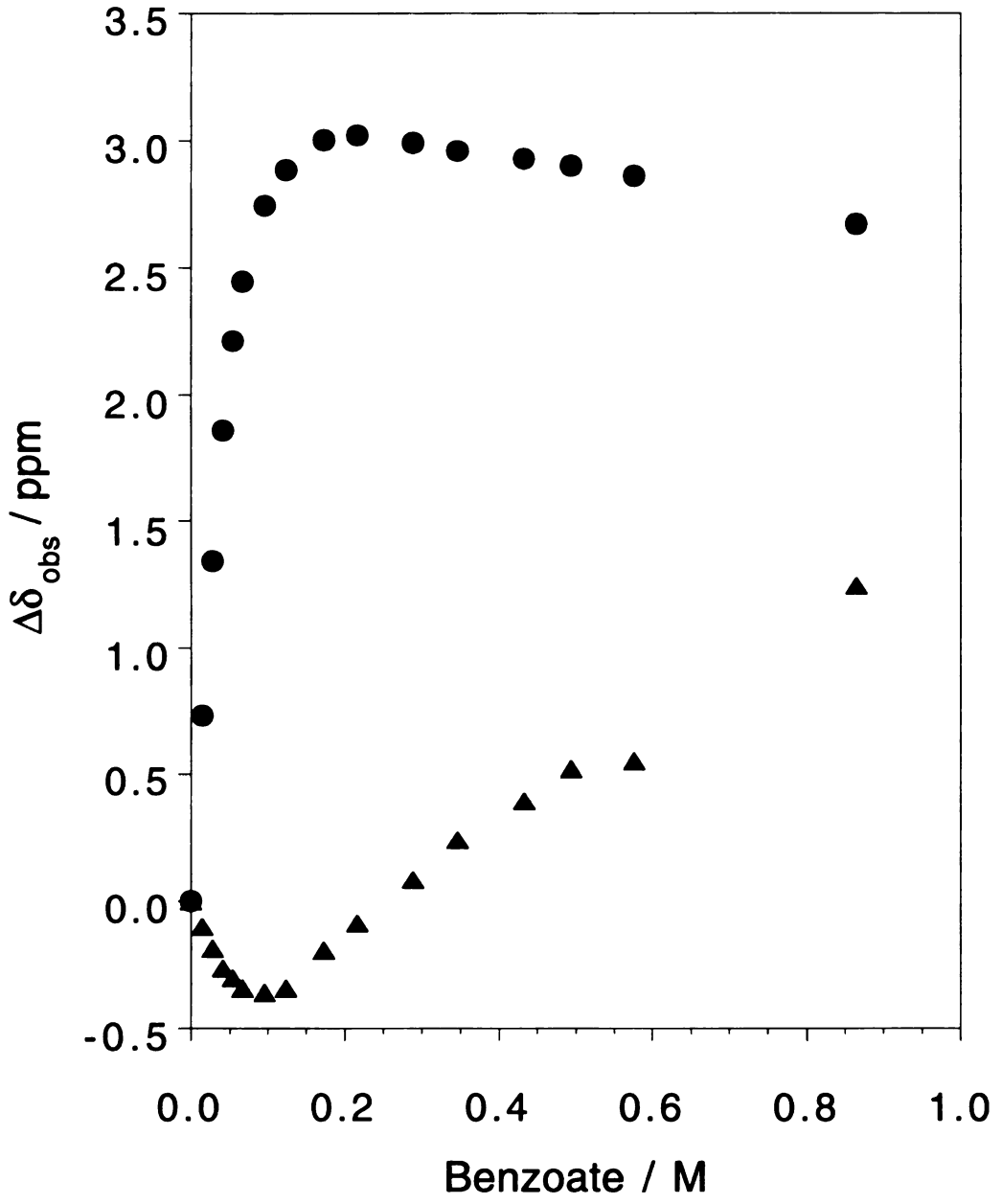

Figure 21. Change in chemical shift of benzamidinium NH_{ax} (●) and NH_{eq} (▲) with the addition of benzoate 0 to 886 mM.

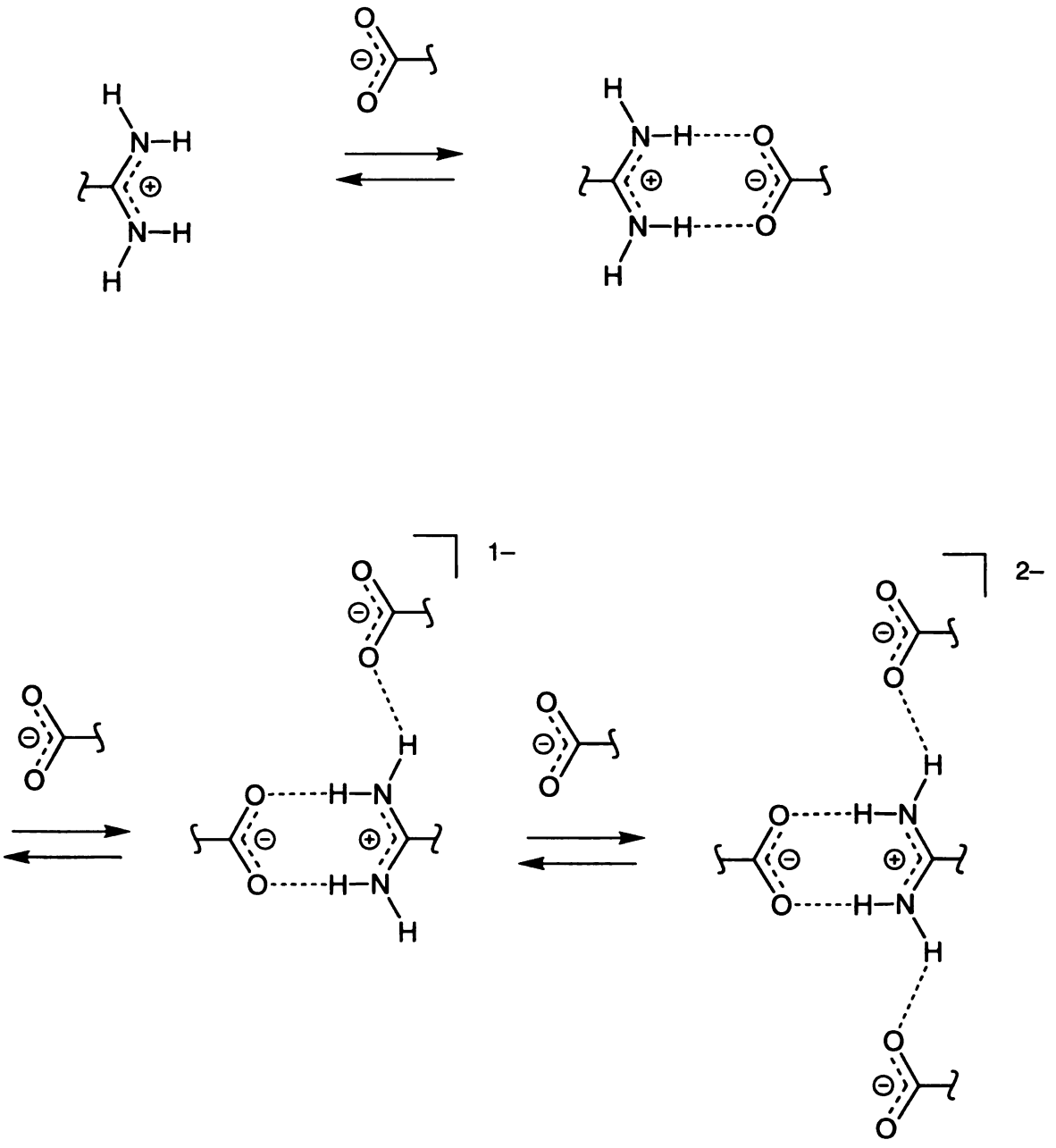

Figure 22. Proposed mechanism for stepwise association of three carboxylates to one amidinium, yielding a net four hydrogen bonds to the amidinium in solution.

the noncovalent intermolecular interactions that have been exploited to self-assemble organic molecules into solids.[42] Though less common, electrostatic forces are emerging as a particularly important noncovalent interaction in assembling subunits in extended arrays.[43] The nondirectionality of the electrostatic interaction, the inability to de-solvate charged species from polar environments, and the need for counterions to maintain charge neutralization in the crystalline environment is overcome when the synthon is a salt bridge. The pioneering work of Etter and Ward[44] and others[45,46] has shown that salt bridges can be used to assemble tapes and layers. Yet the ability to set the dimensionality between tapes or layers can be difficult. We wondered whether the control offered by a salt bridge in establishing the three-dimensional structure of these biological systems would be useful for the design of the extended crystalline arrays. Our approach centered on the amidinium-carboxylate salt bridge as a synthon for self–assembly. We now report the three dimensional structure of 3–amidinium benzoate (**1**), Figure 23, and show that Whiteside's recent prediction[47] is correct; namely, favorable secondary electrostatic interactions of synthons with small substituents are important in establishing the three-dimensional motif of crystalline solids.

Figure 24 shows the bc plane of the crystal structure of **1**.[48,49] This view highlights the primary interaction of the two-point hydrogen bond of the amidinium-carboxylate salt bridge. Two favorable secondary electrostatic interactions[50] confer significant stability on the interface[51] as indicated by the relatively short N to O distances of 2.766(1) and 2.790(2) Å and by the ability to self assemble the interface from water. A zig–zag tape pattern results from the catenation of the salt bridges along chains. The tapes align in a head-to-head arrangement along the c-axis of the unit cell and pack together at a van der Waals contact distance to create the sheets of the bc plane. The repeat distance between positional atoms of neighboring tapes is 6.93 Å thereby establishing the b-dimension of the unit cell. Whereas the phenyl rings lie in the bc plane, a rotation of the amidinium group by

30.0(1)° from the plane of the aromatic ring is complemented by a 23.3(1)° counter-rotation of the carboxylate group. This 7° difference in rotation of the two groups results in a slight twist of the amidinium-carboxylate interface (dihedral angle of 8.41° for the planes defined by the CN_2 and CO_2 atoms of the salt bridge) with respect to the bc plane.

The canting of the salt bridges permits the formation of secondary hydrogen bonding interaction, which extends the dimensionality of the structure beyond the sheets of zig-zag tapes, shown in Figure 24. The amidinium protons outside the salt bridge form hydrogen bonds to carboxylate oxygens of tapes from adjacent sheets above and below the bc plane. This secondary interaction generates ladders as shown in Figure 25, where the crystal structure has been rotated such that one of the ladders is projected in the plane of the paper. The hydrogen-bonding arrangement of the ladder necessarily enforces the amidinium–carboxylate salt bridges in neighboring sheets to arrange such that their dipoles are opposed, thereby setting the head-to-tail orientation of tapes along the ladder. This orientation has the added benefit of satisfying the dominant dipole interaction within the 3-D structure. The dipoles of salt bridges above and below a plane in the ladder structure are at a distance of 3 Å whereas the dipoles within the bc plane are at a distance of 7 Å. Consequently, the maximum stabilization of the dipoles arising from the Coulombic potential is derived from interlayer salt bridges in the head-to-tail arrangement.

The crystal structure of **1** in the ac plane (Figure 24) shows that ladders intersect the bc plane at an oblique angle to interconnect the intralayer planes of zig-zag tapes within sheets to form a layered structure with a d-spacing of 3.16 Å. The ladders are parallel to each other but alternately tilt in and out of the ac plane owing to the rotation of the amidinium and carboxylate groups with respect to the aromatic rings (*vide supra*). Though the one-point hydrogen bond is slightly weaker than the two point interaction, as evidenced by the longer N to O distances of 2.878(5) Å and 2.904(6) Å, it composes the ladders that radiate from the aromatic subunits to provide the scaffolding to support the layer structure,

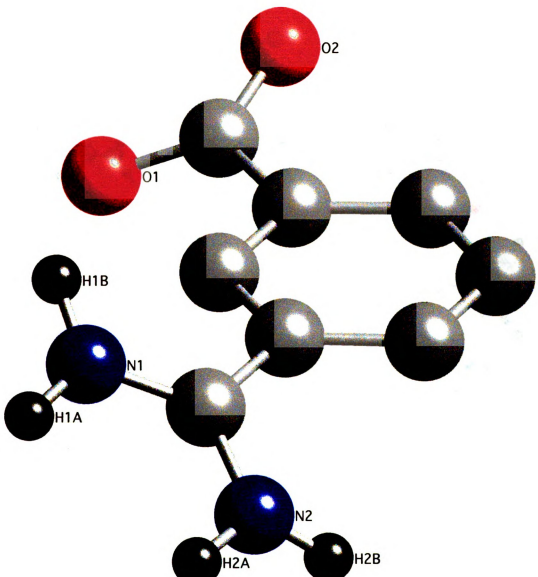

Figure 23. Structure of 3-aminidinium-benzoate; oxygen (red), nitrogen (blue), carbon (light gray) and hydgrogen (dark gray). The aromtic hydrogens are omitted for clarity.

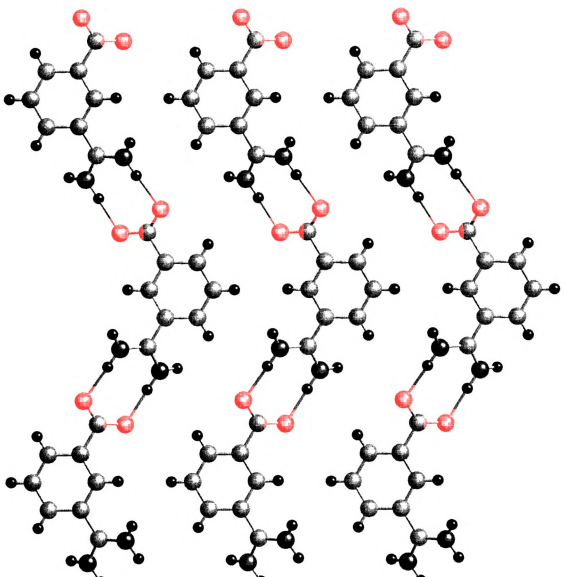

Figure 24. The packing of the zig-zag tapes in the bc plane of the crystal strucutre of **1**. The amidinium-carboxylate salt brdgie is roatated 26.1° (plane defined by the oxygen and nitrogen atoms of the salt bridge) out of the plane of the aromatic ring.

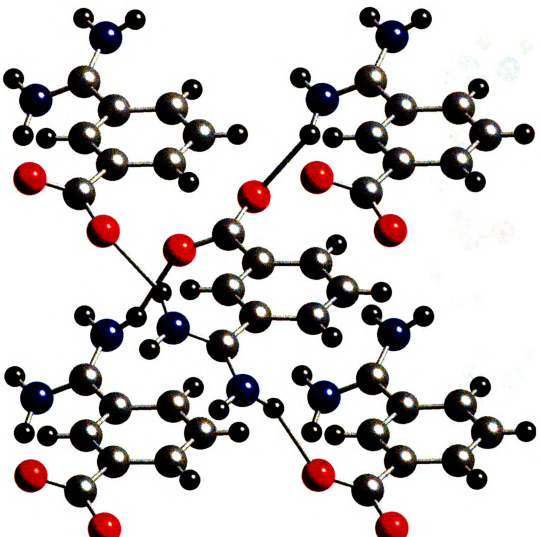

Figure 25. View of the interlayer one-point secondary hydrogen bonding network. Each subunit of **1** is connected to four other distinct subunits of **1** via the secondary one-point hydrogen bonding interaction (two above and two below with respect to the the layers of two-point primary interactions displayed in Figure 24).

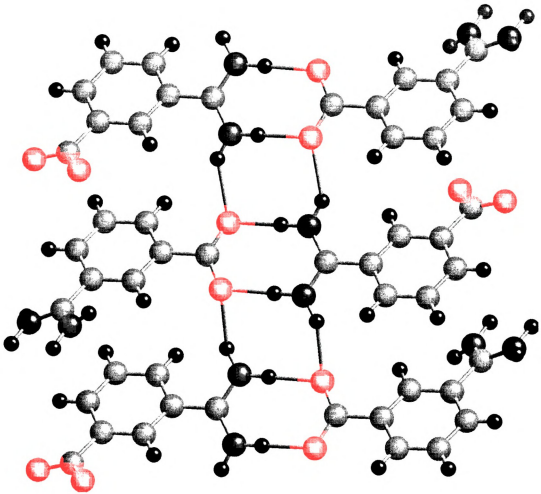

Figure 26. Rotation of the crystal structure of **1** such that the ladder is viewed in the plane of the paper. The ladder structure is formed from the hydrogen bonding between protons external to the salt bridge of a given tape and the carboxylate oxygens of salt bridges in neighboring interlayers.

Table 2. Primary hydrogen bond distances for **1**.

Atom1	Atom2	Distance
O(1)	N(2)	2.766(1)[a]
O(1)	H(2A)	1.779[b]
O(2)	N(1)	2.790(2)[a]
O(2)	H(1A)	1.825[b]

[a]Numbers in parentheses are estimated standard deviations in the least significant digits.
[a]Determined from difference maps used to calculate the position of the hydrogen.

Table 3. Secondary one-point hydrogen bond distances for **1**.

Atom1	Atom2	Distance[a]
O(1)	N(2)	2.878(5)[a]
O(1)	H(2B)	2.011[b]
O(2)	N(1)	2.904(6)[a]
O(2)	H(1B)	2.104[b]

[a]Numbers in parentheses are estimated standard deviations in the least significant digits.
[a]Determined from difference maps used to calculate the position of the hydrogen.

which is further stabilized by the van der Waals interactions of the aromatic rings from neighboring sheets.

The most successful approaches to crystal engineering take advantage of the highly directional and relatively strong nature of the hydrogen bond. In the crystal structure of **1**, the full complement of four protons and four lone pairs of the amidinium-carboxylate salt bridge creates closure of the hydrogen bonding network. Two protons internal to the salt bridge establish a primary interaction with two lone pairs of an individual carboxylate to comprise zig-zag tapes that are analogous to that of isophthalic acid.[52] Here the two point intermolecular hydrogen bond is established with a carboxylic acid dimer. However, in this structure, there is no secondary interaction to connect the layers owing to the absence of protons external to the hydrogen bonding interface. For the amidinium-carboxylate salt bridge of **1**, the two external protons of the salt bridge are complemented by two lone pairs of oxygens from adjacent interlayer carboxylates to form the common ladder structure characteristic of benzamidinium-carboxylate bridges.[53] The one-point hydrogen bond of the salt bridge is strong with respect to other non-covalent secondary interactions used for traditional crystal engineering and it is the important interaction that establishes the three-dimensional motif of the crystal. The results reported here thus further establish the importance of salt bridges as useful synthons in crystal engineering.

F. Experimental

Synthesis of 3-amidinium-benzoate The intermediate imidate ester carboxylate is prepared in situ by adding an excess of freshly generated sodium methoxide to a methanol solution of 3-cyanobenzoic acid, under an argon atmosphere. An excess of ammonium chloride is added after 24 h of stirring, at ambient temperature. The product was filtered and washed several times with water, methanol and ether. The proton NMR spectrum (D_2O, 300 MHz) shows the appropriate peaks for the unsymetrically substituted meta aromatic ring: δ 7.67 (1H, t), 7.89 (1H, d), 8.18 (doublet, 1H) and 8.20 ppm (1H,

s). Calcd. for: $C_8H_8N_2O_2$: C, 58.48%; H, 4.87%; N, 17.05%. Found: C, 57.55%; H, 4.88%; N, 16.18%.

Chapter 3

Ruthenium(II)tris(2,2'-bipyridine) Complexes to Probe PCET

A. Introduction

Pioneering work of Meyer and coworkers showed that photoexcited ruthenium(II)tris-2,2'-bipyridine ($[Ru(bpy)_3*]^{+2}$) effeciently undergoes ET reactions in solution via oxidative or reductive quenching. $[Ru(bpy)_3*]^{+2}$ in the presence of nitroaromoatic groups ($ArNO_2$) undergoes an oxidative ET reaction as shown in Eq. 3.1. In the presence of dialkylaminoaromatics ($ArNR_2$), $[Ru(bpy)_3*]^{+2}$ undregoes a reductive ET reaction as described by Eq. 3.2. Based on these systems, salt bridge complexes for the study of proton–coupled electron transfer (PCET) have been developed.

$$[Ru(bpy)_3*]^{+2} + ArNO_2 \longrightarrow [Ru(bpy)_3]^{+3} + ArNO_2^{\bullet -1} \quad (3.1)$$

$$[Ru(bpy)_3*]^{+2} + ArNR_2 \longrightarrow [Ru(bpy)_3]^{\bullet +1} + ArNR_2^{\bullet +1} \quad (3.2)$$

Three bipyridine ligands for this study are displayed in 3.3. These bidentate ligands are distinguished for their electron donating and withdrawing capabilities. The bpy ligand acts a benchmark with no electron donating or withdrawing functional groups attached to it, while the tmbpy ligand, a bipyridine appended with four methy groups, is relatively electron rich. The decb ligand has two ester functional groups which act to withdraw electron density from its π system rendering it relatively electron deficient. These ligands are ancillary to the salt bridge and can be used ot establish the proper electronics for PCET studies.

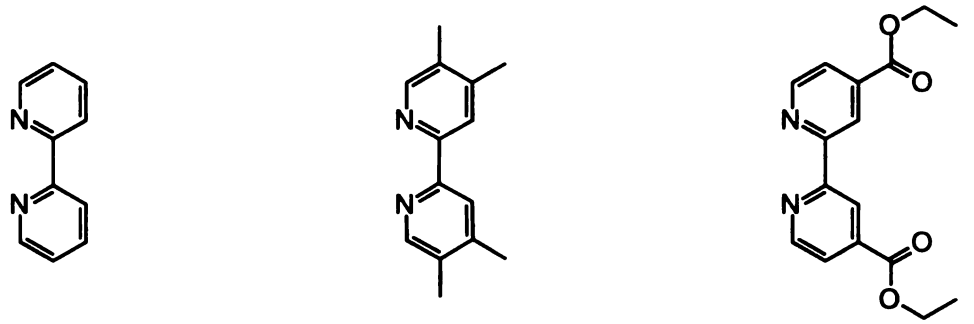

(3.3)

bpy tmbpy decb

The salt bridge is established with the ligands displayed in 3.4. The Mebpy-amH$^+$ and Mebpy-COO$^-$ ligands can establish the formation of the amidinium-carboxylate salt bridge moiety; the known Mebpy-COOH bipyridine ligand funcitonalized with the carboxylic acid group is capable of forming symmetrical carboxylic acid dimers and also is the synthetic precursor to Mebpy-COO$^-$.

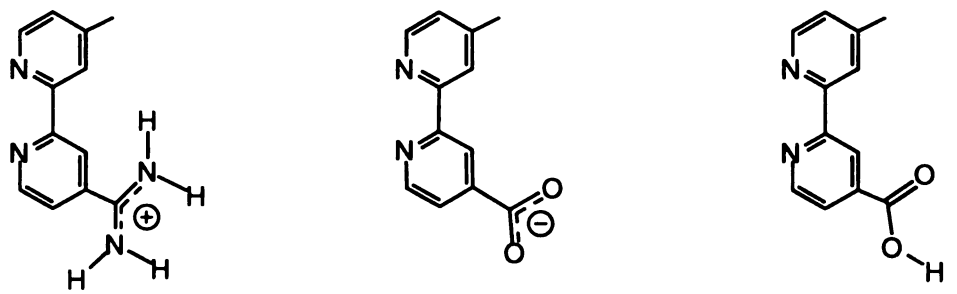

(3.4)

Mebpy-amH$^+$ Mebpy-COO$^-$ Mebpy-COOH

The 4′-methyl-2,2′-bipyridine (Mebpy) ligand with amidine or carboxylate functionalities is derived from the aldehyde, which may be converted to the nitrile following Olah's procedure[54] in good yields. Conversion of the aldehyde to the carboxylic acid is accomplished under standard oxidation conditions.[73] The amidine group is afforded by adapting Garigipati's method[55] of reacting nitrile with Weinreb's amide transfer reagent, methyl aluminum(III) chloroamide, In our hands, the amidinium chloride is directly obtained from this conversion, Eq. 3.5.

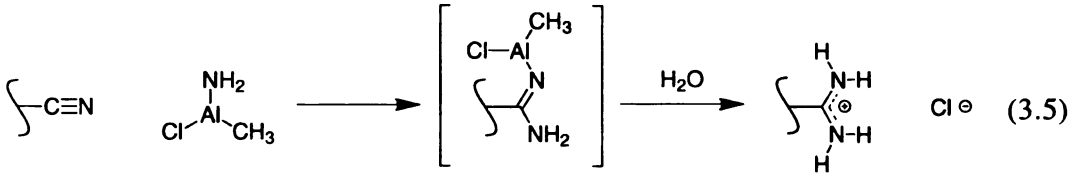

(3.5)

Alternatively, for the polypyridine modification, we have obtained 4-methyl-4′-amidinium-2,2′-bipyridine (Mebpy-amH$^+$) chloride in higher yields by the base-catalyzed reaction of the nitrile with methoxide to afford the imidate ester, which smoothly reacts with ammonium chloride[56] as shown in Eq. 3.6.

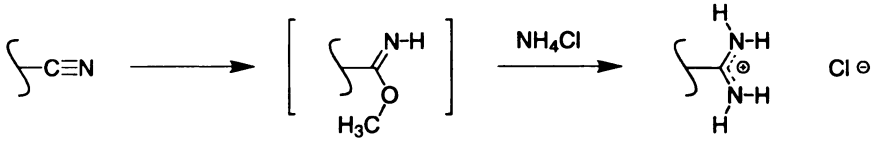

(3.6)

The oxidative quenchers for this study are based on the electron acceptror 1,3-dinitrobenzene and are listed in Eq. 3.7.

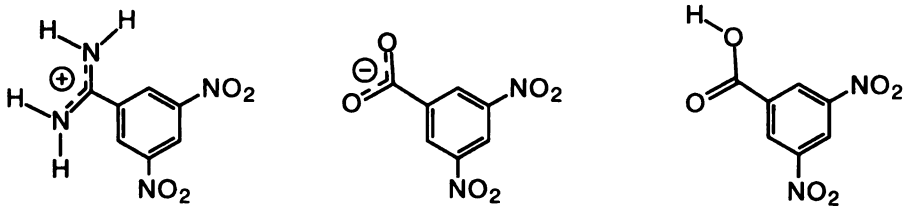

(3.7)

3,5-DNB-amH$^+$ 3,5-DNBCOO$^-$ 3,5-DNBCOOH

The reductive quenchers for this study are based on the electron donor on N,N-dimethylbenzene, and are listed in Eq. 3.8.

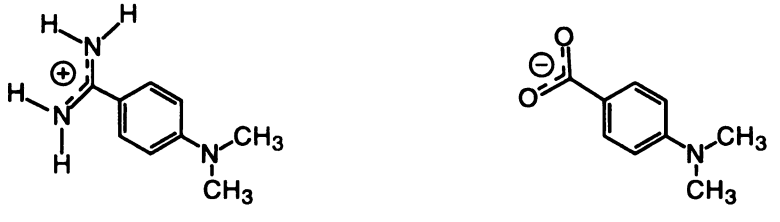

(3.8)

4-DMAB-amH$^+$ 4-DMAB-COO$^-$

B. BPY Complexes of Ru(II) to Mediate Oxidative PCET

Reported here is the rate of proton-coupled electron transfer (PCET) through the amidinium-carboxylate salt bridge. The donor is electronically excited $Ru(bpy)_3^{2+}$ (bpy = bipyridine), the acceptor is 3,5-dinitrobenzene (3,5-DNB), and a salt bridge is formed from the association of an amidine to a carboxylic acid. The influence of proton motion on the rate of electron transfer through the salt bridge is revealed by a deuterium isotope effect. PCET in **2** is compared to **3** where a symmetric $-(COOH)_2-$ interface has been introduced between the donor/acceptor pair, Figure 27.

1. Results and Discussion

a. Solution Association of D/A PCET Complexes

The amidinium-carboxylate salt bridge is formed directly upon mixing the appropriate carboxylic acid with free base amidine. Two favorable secondary electrostatic interaction[18] within the amidinium-carboxylate interface are manifested in high association constants even when the solvent is polar. Figure 28 shows the ^1H NMR spectrum of $(bpy)_2Ru^{II}(Mebpy\text{-}amH)^{3+}$ in DMSO-d_6 at 19.5 °C. The ascending traces highlight the changes in the chemical shifts of the amidinium protons, which appear as broad singlets at ~9.5 ppm, upon titration with the tetramethylammonium salt of the carboxylate. A concentration-dependent downfield shift of >2.0 ppm is observed for the protons involved in hydrogen bonding to the carboxylate whereas the chemical shift of the adjacent protons, which are not bound to the carboxylate, varies marginally from 9.55 to 9.65 ppm over all concentrations.

A least squares fit of a plot of the chemical shift of the hydrogen-bonded amidinium protons vs the carboxylate concentration at 19.5 °C yields $K_{assoc} = 1136 \pm 93\ M^{-1}$, Figure 29.[19] Unfortunately, the solubility of **2** in CH_2Cl_2, the solvent in which electron transfer kinetics were determined, is too low to permit K_{assoc} to be reliably ascertained by NMR titration experiments. Nonetheless we observe the association constant for **2** to increase

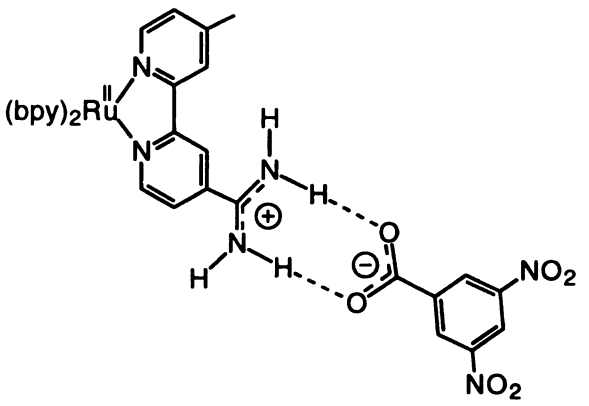

2

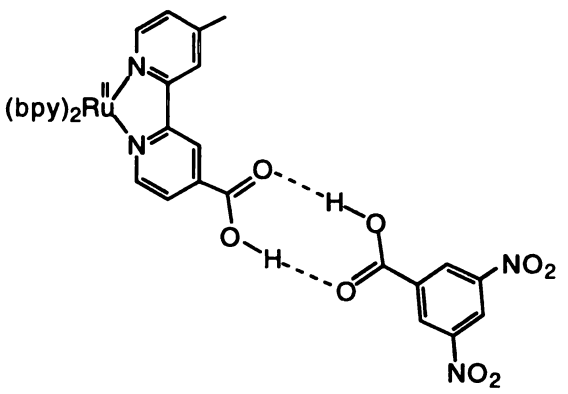

3

Figure 27. Complexes to study PCET; **2** is based on $[(bpy)_2Ru^{II}(Mebpy\text{-}amH^+)]^{3+}$ and is based on $[(bpy)_2Ru^{II}(Mebpy\text{-}COOH)]^{2+}$.

with decreasing solvent polarity (K_{assoc} = 2432 M^{-1} in CH_3CN at 19.5 °C). On this basis, the DMSO and CH_3CN association constants represent a lower limit for the formation of **2** in our electron transfer experiments. A Job's plot, Figure 30, confirms the 1:1 stoichiometry of the amidinium-carboxylate salt bridge complex. For the case of **3**, K_{assoc}, measured by techniques previously described by us for the symmetric $-(COOH)_2-$ interface,[8] is 702 M^{-1} in CH_2Cl_2, which is comparable to our previous measurements of a dicarboxylic interface bridging a dinitrobenzoic acid acceptor to a porphyrin donor (K_{assoc} = 552 M^{-1}).

b. Photophysical Behavior

The luminescence of $[(bpy)_2Ru^{II}(bpy\text{-}am)]^{2+}$ in CH_2Cl_2 is quenched upon the addition of 3,5-dinitrobenzoic acid (3,5-DNBCOOH). This result is consistent with an electron transfer quenching mechanism, which is well-established for the reaction between electronically excited Ru^{II}*tris*(polypyridyl) complexes and nitroaromatic acceptors.[15] In the absence of 3,5-DNBCOOH, the decay of the $(bpy)_2Ru^{II}(bpy\text{-}amH)^{3+}$ excited state is monoexponential with a lifetime of 1300 ns, which decreases upon complexation to aliphatic carboxylates or benzoate (τ_o = 850 ns). However, when 3,5-DNBCOOH is present, a biexponential decay of the luminescence is observed whereupon one lifetime component is dependent on the concentration of acceptor and the other is not over a 3,5-DNBCOOH concentration range of 0.1 to 5 mM ($[(bpy)_2Ru^{II}(Mebpy\text{-}am)^{2+}]$ = 0.1 mM).

The origin of the concentration-dependent decay is easily understood. The Stern-Volmer plot of the concentration-dependent lifetime is linear over the entire quencher concentration range and the intercept is unity. The bimolecular rate constant of 2.4×10^9 $M^{-1}s^{-1}$ is in accordance with that measured by Meyer et al. for $Ru(bpy)_3^{2+}$ and 3,5-dinitrobenzoic acid ($k_{ET} = 1.6 \times 10^9$ $M^{-1}s^{-1}$).[15] More significantly, the bimolecular kinetics of **2** is similar to that for the reaction of the $(bpy)_2Ru^{II}(Mebpy\text{-}amH)^{3+}$ with the ester, 3,5-DNBCOOEt ($k_{ET} = 1.9 \times 10^9$ $M^{-1}s^{-1}$), which is unable to associate with the amidine

(association of the amidinium with the nitro functionality is not likely,[20] which we also confirmed by NMR). The concentration independent lifetime decay component is attributable to electron transfer for the associated pair shown **2**. An intramolecular rate constant of $4.3(9)\times 10^6$ s^{-1} is determined from the concentration-independent lifetime decay component.

The reaction of $(bpy)_2Ru^{II}(Mebpy\text{-}COOH)^{2+}$ with 3,5-DNBCOOH in CH_2Cl_2 exhibits similar characteristics to the reaction of the quencher with $(bpy)_2Ru^{II}(Mebpy\text{-}am)^{2+}$. Lifetime decays are biexponential, also exhibiting concentration-independent and dependent components. The bimolecular rate constant derived for the latter is 1.4×10^9 $M^{-1}s^{-1}$, which is comparable to the reaction rate constant of $(bpy)_2Ru^{II}(Mebpy\text{-}COOH)^{2+}$ with the ester 3,5-DNBCOOEt ($k_{ET} = 1.1\times 10^9$ $M^{-1}s^{-1}$). Despite a 0.07 V smaller driving force ($\Delta G(\mathbf{2})$ = –0.21 V, $\Delta G(\mathbf{3})$ = –0.14 V),[21] the intramolecular rate constant of $8.0(4)\times 10^6$ s^{-1} for **3** is nearly a factor of two greater than that observed for **2**.

c. Kinetic Isotope Effects on PCET

Does the attenuated PCET process in **2** suggest that the salt bridge is affecting the rate of the ET? To more directly address this issue, we exchanged the ^{1}Hs of the amidine and carboxylic acid by ^{2}H and measured the electron transfer kinetics of the associated pair. The intramolecular rate constant for deuterated **2** was 3.2×10^6 s^{-1}, yielding k_H/k_D = 1.34(3). This isotope effect is in line with that measured for **3** (k_H/k_D = 1.5) and it is consistent with our previous measurement of electron transfer for a porphyrin donor–$(COOH)_2$–acceptor complex (k_H/k_D = 1.6 and 1.7). As recently discussed, a deuterium isotope effect in these hydrogen bonded systems arises from the modulation of the electronic coupling matrix element by proton motion within the interface,[10,22] thereby providing a mechanism for the asymmetric salt bridge to engender a PCET reaction.

The effect of proton motion on the electron transfer rate may be manifested in ways other than the electronic coupling. Unlike the –$(COOH)_2$– interface, significant charge

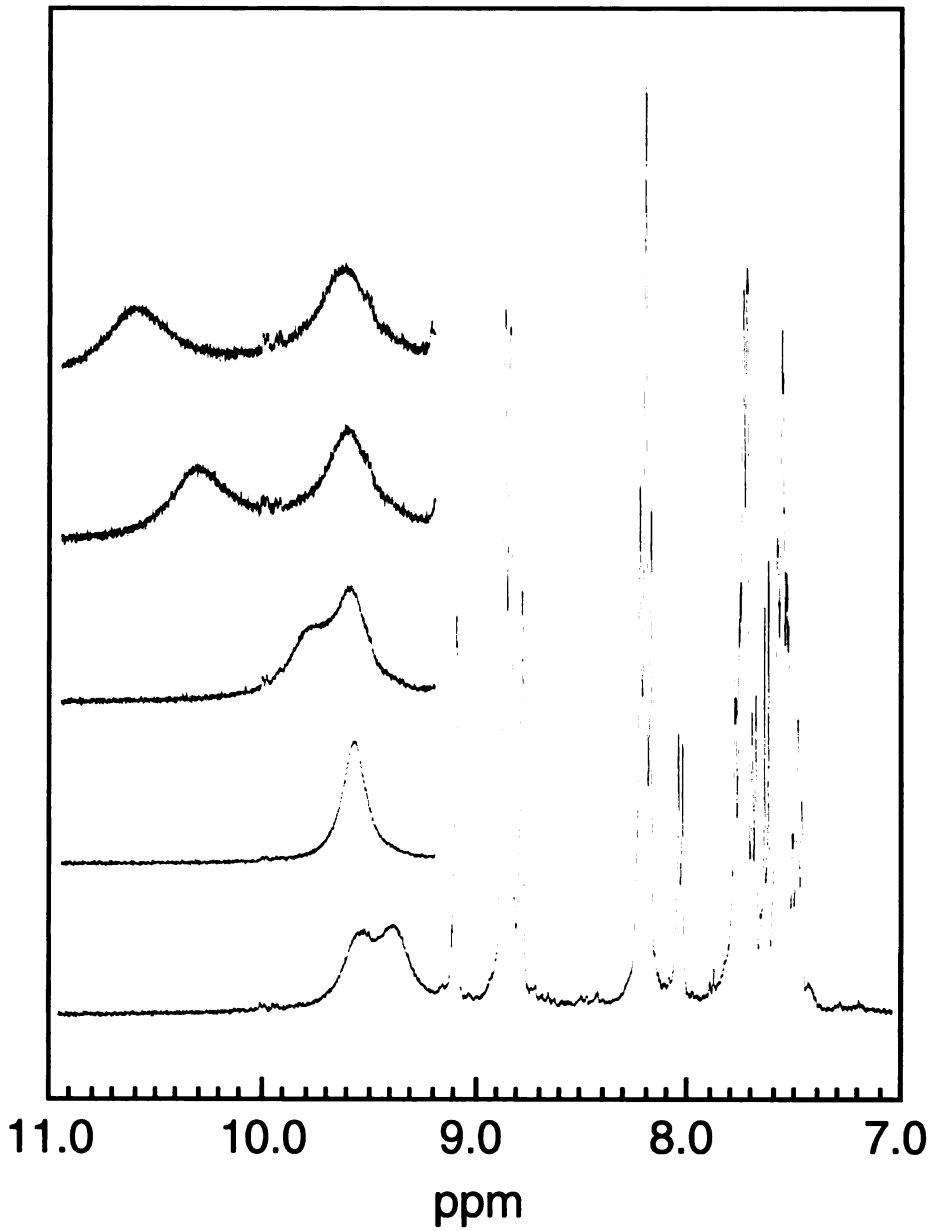

Figure 28. ^{1}H NMR spectrum of $[(bpy)_2Ru^{II}(Mebpy\text{-}amH^+)]^{3+}$. Selected spectra are shown upon addition of the tetramethylammonium salt of 3,5-dinitrobenzoate at concentrations 0, 0.44, 0.89, 2.2, and 3.1 mM in DMSO-d_6 (bottom to top). The ^{1}H resonances of the bipyridines appear between 7.3 and 9.2 ppm, two broad singlets flanking 9.5 ppm signify the ^{1}H resonances of the amidinium protons. For the spectrum at 0.44 M carboxylate added, the two resonances are coincident.

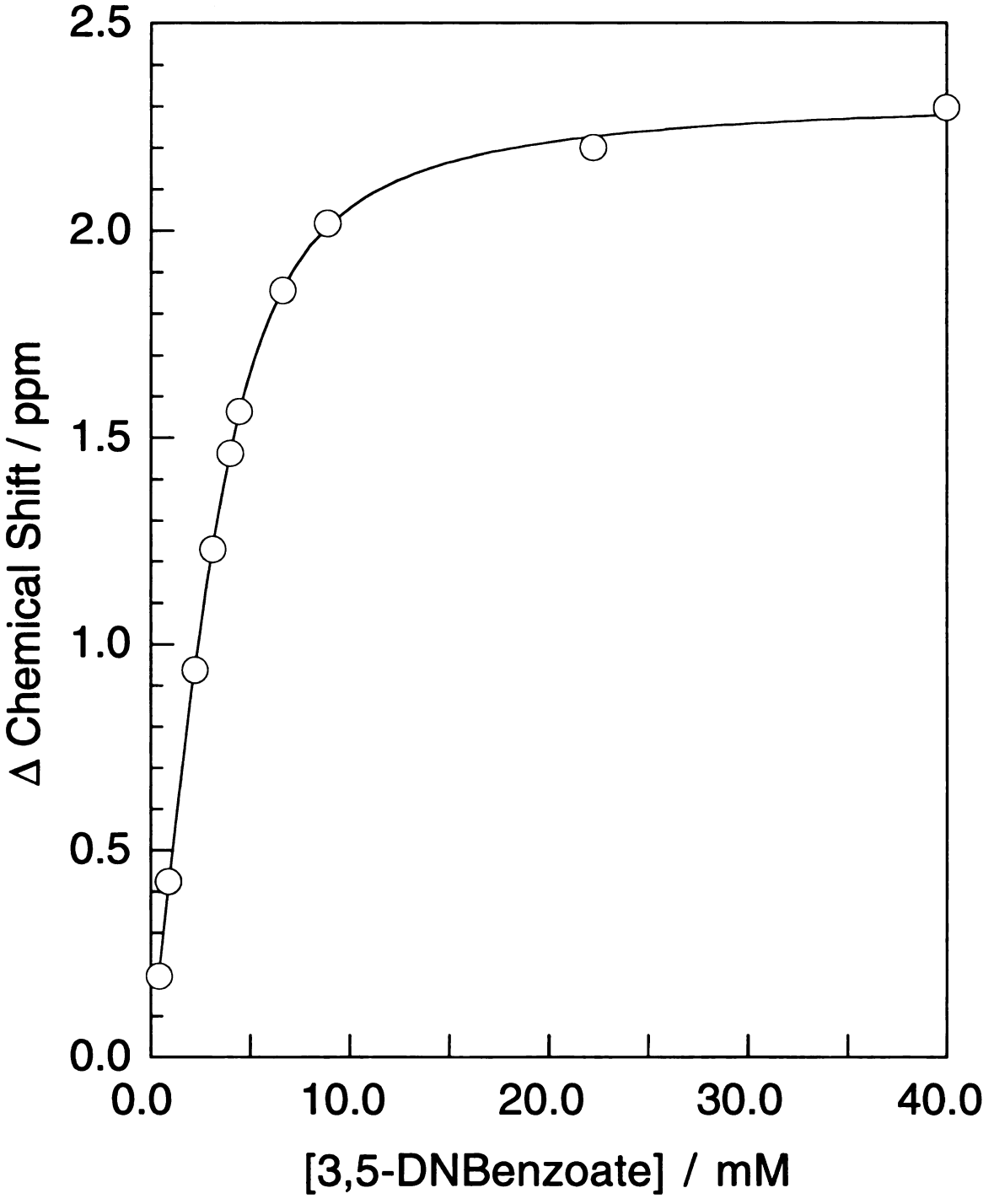

Figure 29. Plot of the chemical shift of the amidinium protons hydrogen-bonded to carboxylate versus concentration of carboxylate from 0.44 to 40 mM.

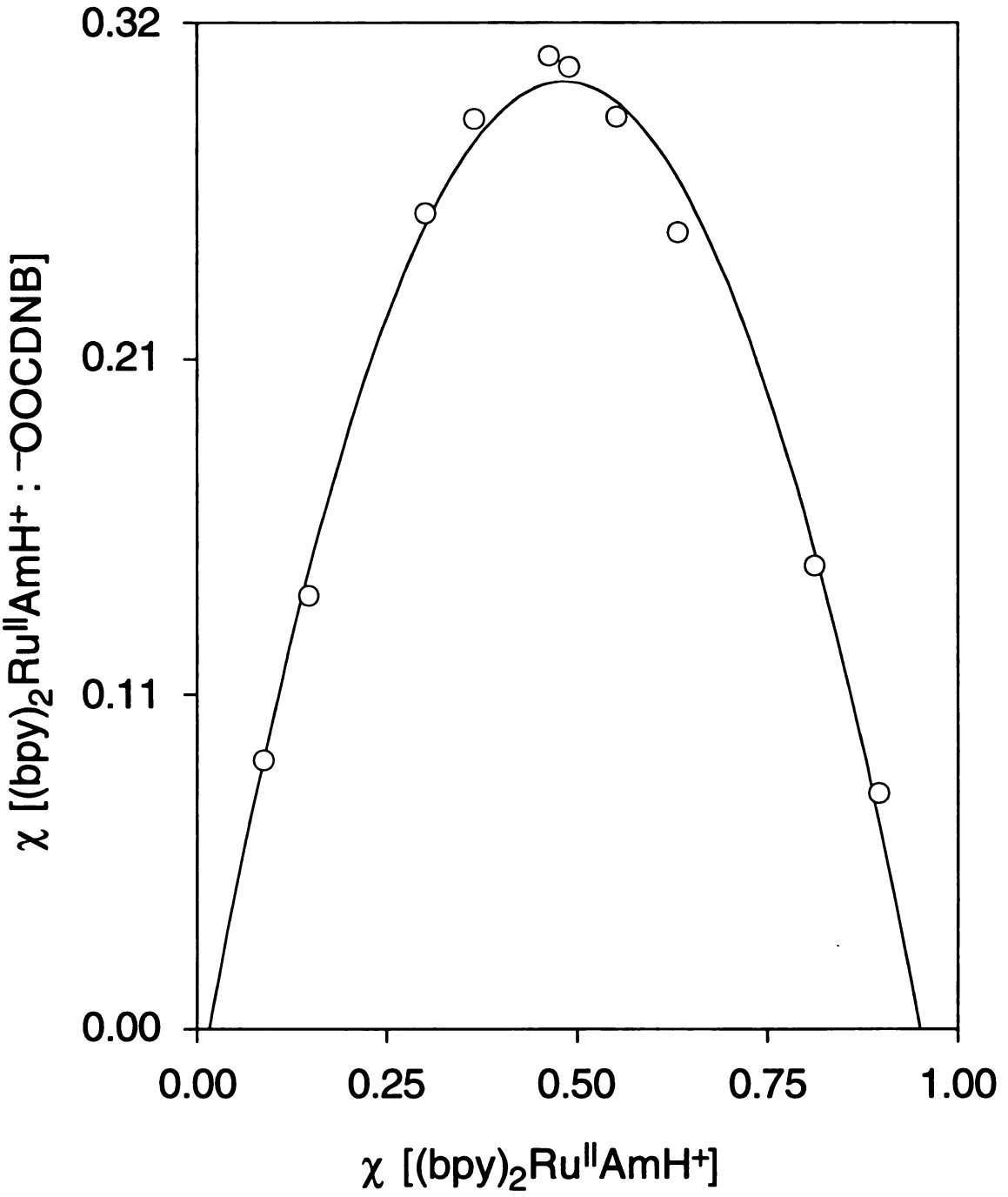

Figure 30. Job's plot of the relative salt-bridge complex concentration vs. the mole fraction of $[(bpy)_2Ru^{II}(Mebpy\text{-}amH^+)]^{3+}$ (3.8 mM) as the concentration of $DNBCOO^-$ is varied from 0.0 to 40.0 mM.

rearrangement occurs upon proton motion in the salt bridge, and this charge redistribution will couple to solvent (i.e. to give rise to additional Franck-Condon factors arising from proton motion).[10b] Moreover, the electron is transferred through the permanent electrostatic field of the salt bridge in **2** thereby modifying the energetics of the overall reaction. These issues may be addressed by comparing the rates of electron transfer for a donor–(amidinium-carboxylate)–acceptor complex to its congener where the interface is switched (i.e. donor–(carboxylate-amidinium)–acceptor). For the systems here, such a comparative study is obscured by the possibility of transferring an electron from the ancillary bipyridine ligand in addition to the transfer of an electron from the derivatized bipyridine ligand because the two metal-to-ligand charge transfer states are close in energy.[23,24] We therefore have gone on to assess the issue of PCET rates for switched interface systems with complexes featuring a single bipyridine ligand, and with complexes in which the energy of the metal-to-ligand charge transfer state for the ancillary ligands are energetically far removed from the derivatized amidinium or carboxylate bipyridine ligand.

C. TMBPY Complexes of Ru(II) to Mediate Oxidative PCET

A direct experimental measure of the affect of a salt bridge on electron transfer is to undertake a comparative kinetics study of a donor–(amidinium-carboxylate)–acceptor supramolecule and its switched interface donor–(carboxylate-amidinium)–acceptor congener. We now report such a study for the supramolecular series of complexes where the donor is $[(tmbpy)_2Ru^{II}(Mebpy\text{-}amH^+)]^{3+}$ or $[(tmbpy)_2Ru^{II}(Mebpy\text{-}COO^-)]^+$ (tmbpy = 3,3′,4,4′-tetramethyl-2,2′-bipyridine, Mebpy-amH$^+$ = 4-methyl-4′-amidinium-2,2′-bipyridine, Mebpy-COO$^-$ = 4-methyl-4′-carboxylate-2,2′-bipyridine) and the acceptor is the complementary carboxylate- or amidinium-modified 3,5-dinitrobenzene (**4** and **5**, respectively in Figure 31). To further extend the study, we have also prepared the same donor/acceptor pair bridged by the symmetric –$(COOH)_2$– interface (**6**, also shown in Figure 31). The metal complexes are afforded by standard reactions of the modified Mebpy

ligands with the cis-dichloride $[(tmbpy)_2RuCl_2]$.[57] Electron transfer measurements of this series of complexes reveal that the salt bridge can extraordinarily influence the rates of electron transfer thereby allowing us to uncover new contributing effects to the mechanism of biologically relevant PCET.

1. Results and Discussion

a. Solution Salt Bridge Association.

The Ru(II) carboxylate and amidinium complexes readily form the salt bridge with the corresponding acceptor. Complexes **4** and **5** have been thoroughly characterized by NMR. Figure 32 shows the ^1H NMR spectral changes resulting for the association of $[(tmbpy)_2Ru^{II}(Mebpy\text{-}amH^+)]^{3+}$ to 3,5-dinitrobenzoate (3,5-DNBCOO$^-$) in DMSO-d_6. As observed previously for guanidinium-carboxylate salt bridges,[58] a signature of the salt bridge is the concentration-dependent downfield shift of amidinium protons involved in hydrogen bonding (NH_{ax}) and an insensitivity of the chemical shift for the amidinium protons external to the salt bridge (NH_{eq}). The chemical shift of the NH_{ax} protons vary by 2.4 ppm upon their hydrogen bonding association to the carboxylate, whereas the chemical shift of the NH_{eq} protons varies by <0.3 ppm over the same concentration range. A nonlinear least-squares fit of chemical shift of the hydrogen-bonded amidinium protons vs. the carboxylate concentration (Figure 33), as described by Wilcox,[59] yields an association constant (K_{assoc}) of 386 M^{-1}. A 1:1 stoichiometry of the supramolecule complexes is established by the Job's plot[60] of the ^1H NMR titration data reproduced in Figure 34, which shows that the optimal formation of **4** occurs at equimolar concentrations of the amidinium and carboxylate (i.e., a 0.5 mole fraction). This is definitive evidence for the 1:1 stoichiometry of the amidinium-carboxylate salt bridge.

Similar behavior is observed for **5** (Figures 35 - 37) The NH_{eq} resonance (9.53 ppm) of 3,5-dinitrobenzamidinium (3,5-DNBamH$^+$) exhibits an insignificant shift upon the addition of $[(tmbpy)_2Ru^{II}(Mebpy\text{-}COO^-)]^+$ (Δ ppm < 0.2 over 10 mM), while NH_{ax} varies

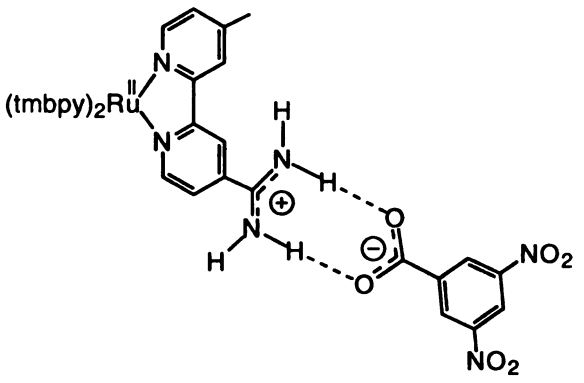

4

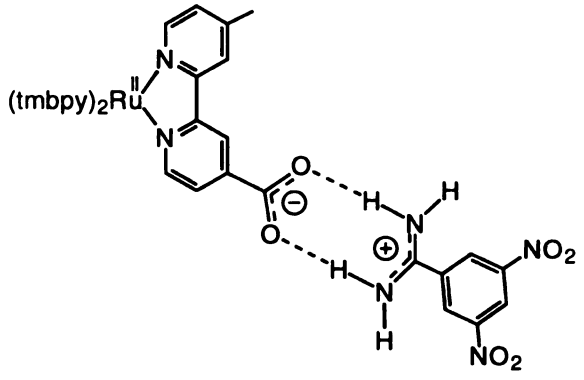

5

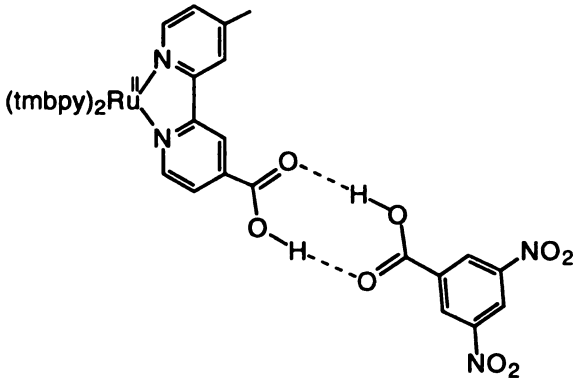

6

Figure 31. Complexes to study PCET; **4** is based on $[(tmbpy)_2Ru^{II}(Mebpy\text{-}amH^+)]^{3+}$, **5** is based on $[(tmbpy)_2Ru^{II}(Mebpy\text{-}COO^-)]^+$ and **6** is based on $[(tmbpy)_2Ru^{II}(Mebpy\text{-}COOH)]^{2+}$.

by 2.5 ppm over the 10 mM concentration range, Figure 35. The larger shift of NH_{eq} resonances over the smaller concentration range as compared to **4** is indicative of the higher association constant of 2297 M^{-1} for **5** in DMSO.

The greater association constant of **5** is consistent with the electron withdrawing nitro groups conferring a decreased basicity of the carboxylate group on 3,5-DNB, resulting in a weaker hydrogen bonding interaction for **4**. In less polar solvents, the association constant greatly increases. The low solubility of **4** and **5** in CH_2Cl_2 (the solvent in which electron transfer kinetics were determined, *vide infra*) precludes reliable determination of K_{assoc} by NMR titration experiments.

b. Photophysics

The design of the excited state structure of the Ru(II) polypyridyl complex is crucial to a proper kinetics study of the electron transfer reactions of **4-6**. The electron transfer reaction to the 3,5-dinitrobenzene acceptor of **4-6** is initiated by laser excitation of the metal-to-ligand charge transfer (MLCT) transition of the Ru(II) polypyridyl complex. Two potential reaction pathways arise for the oxidative quenching reaction, depending on the energetics of the MLCT excited state. For the case where the lowest energy MLCT excited state is localized on the salt bridge modified Mebpy ligand, photoexcitation will place the transferring electron directly into the PCET pathway. Alternatively, a lowest energy MLCT excited state involving the ancillary polypyridine ligand will remove the excited electron from the PCET reaction pathway. Indeed, we have confronted this issue in our earlier studies of the oxidative quenching of $[(bpy)_2Ru^{II}(Mebpy\text{-}X)]^{n+}$ (X = COO^-, n = 1, X = amH^+, n = 3). In the absence of tetramethyl substitution of the bipyridine rings, the MLCT excited states involving the ancillary bpy and the Mebpy-amH^+ and Mebpy-COO^- ligands are close in energy thereby obscuring a comparative PCET study owing to the presence of the two competing reaction pathways.

The electronic spectra of $[(tmbpy)_2Ru^{II}(Mebpy\text{-}amH^+)]^{3+}$, $[(tmbpy)_2Ru^{II}$(Mebpy-

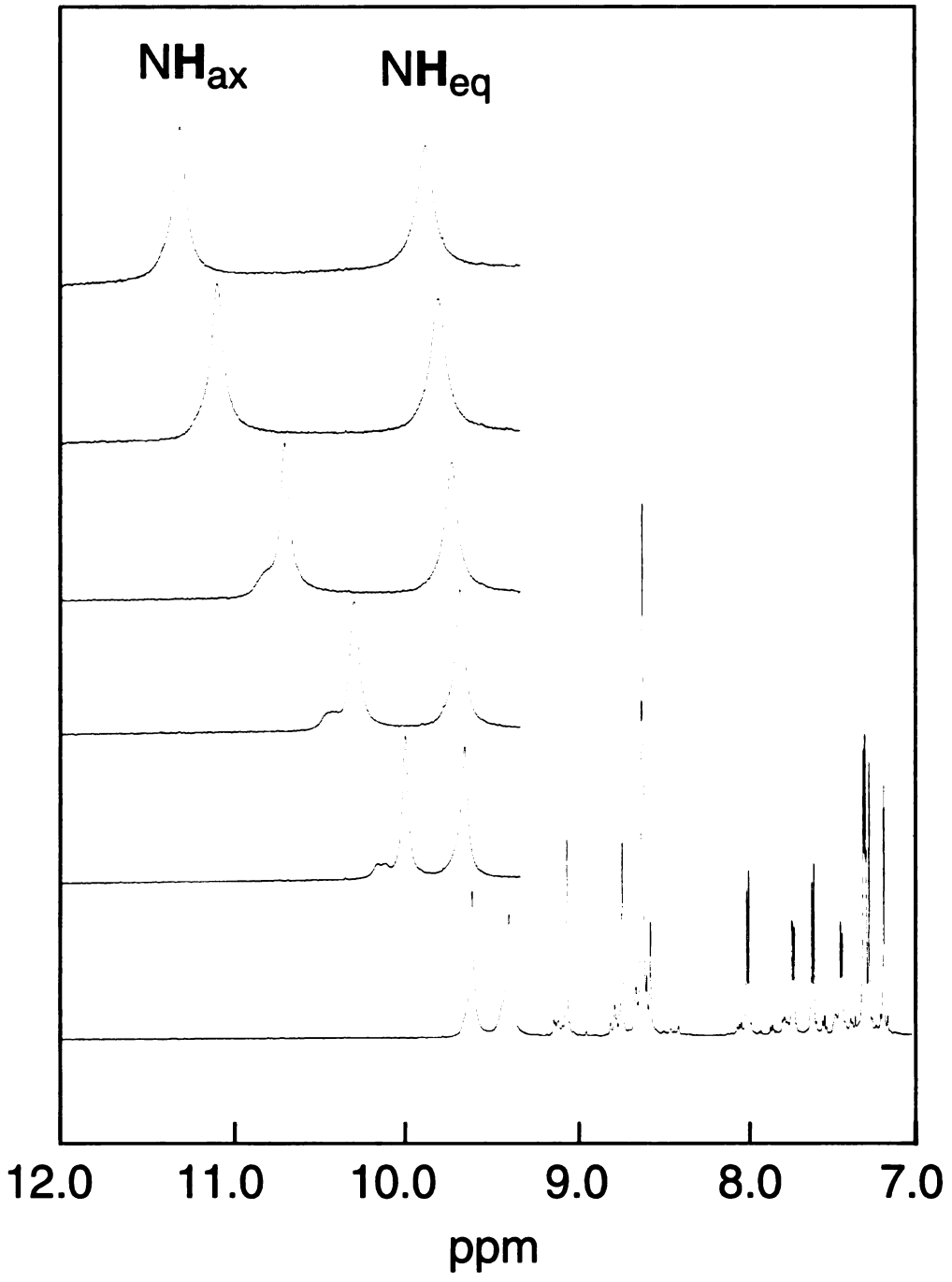

Figure 32. Spectral changes of ^{1}H NMR spectrum of $[(tmbpy)_2Ru^{II}(bpy\text{-}amH^+)]^{3+}$ with added tetrabutylammonium 3,5-dinitrobenzoate. Selected spectra are shown upon addition of 3,5-dinitrobenzoate at concentrations 0.0, 2.3, 3.7, 6.6, 10.3 and 13.9, mM in DMSO-d_6 (bottom to top). The ^{1}H resonances of the bipyridines appear between 7.0 and 9.2 ppm, two broad singlets flanking 9.5 ppm signify the ^{1}H resonances of the axial (internal) and equatorial (external) amidinium protons.

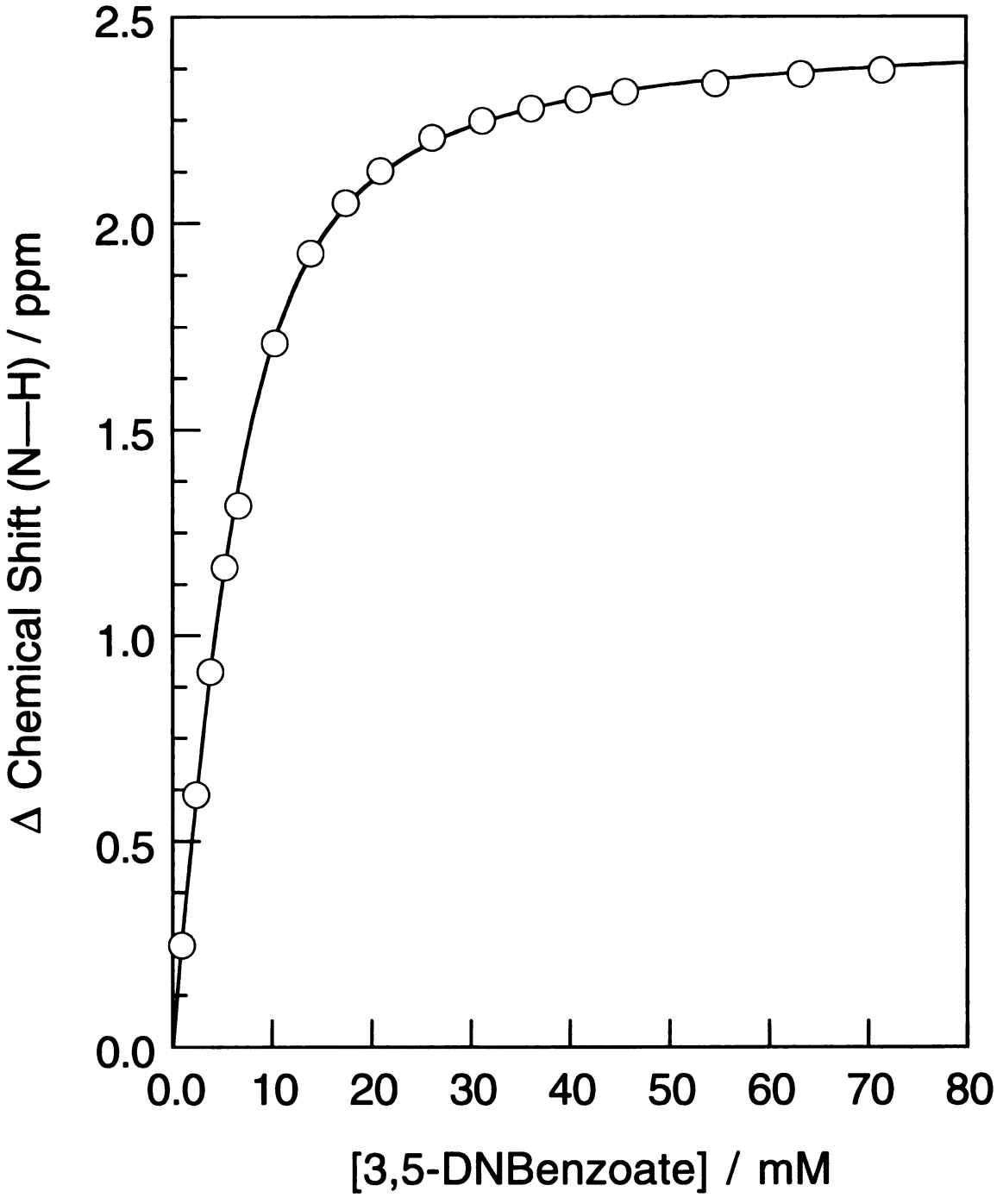

Figure 33. Plot of the chemical shift of the resonances shown in Figure 32 for $[(tmbpy)_2Ru^{II}(Mebpy\text{-}amH^+)]^{3+}$ and additional resonances of the amidinium protons hydrogen-bonded to carboxylate versus concentration of carboxylate from 0.0 to 80 mM.

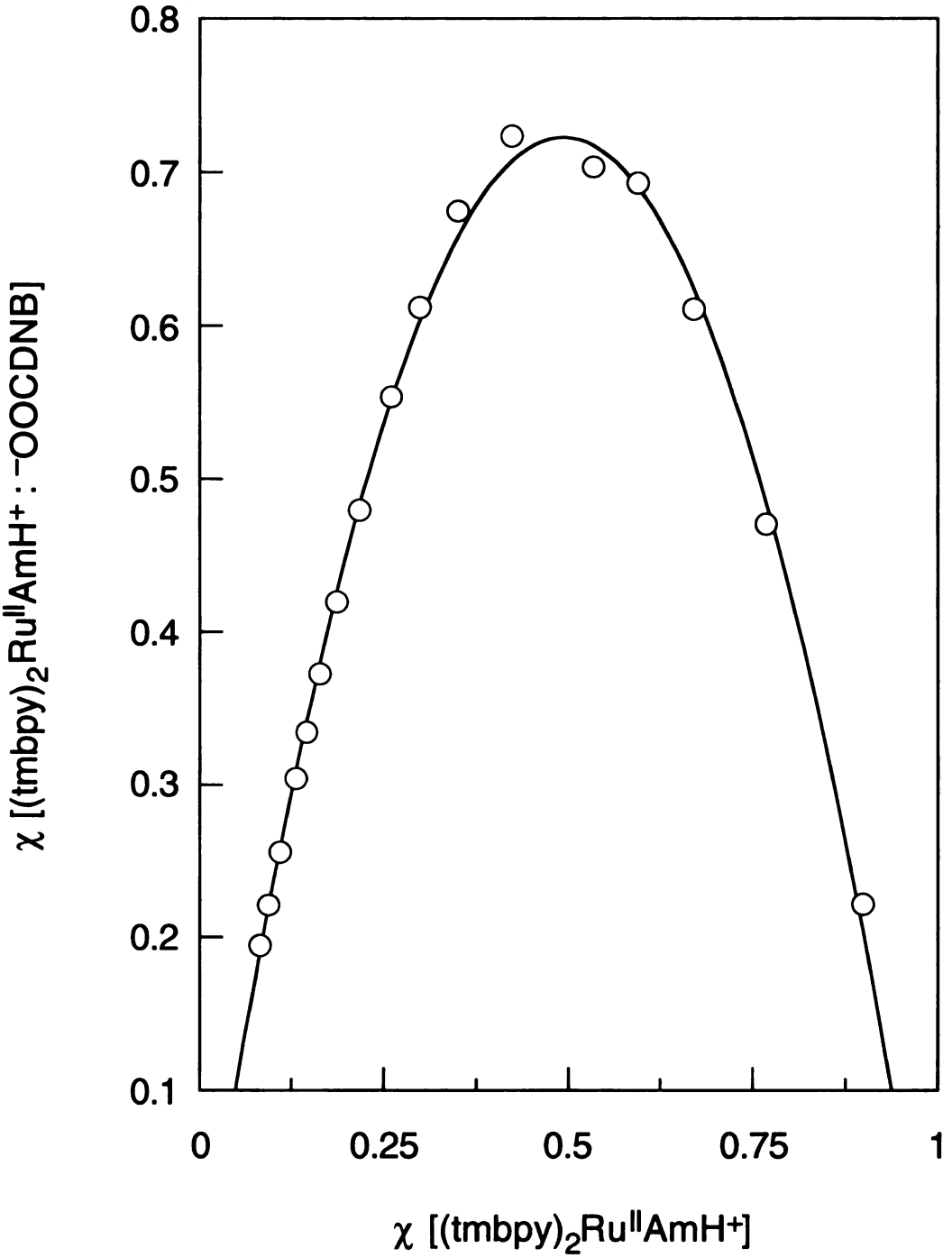

Figure 34. Job's plot of the relative salt-bridge complex concentration vs. the mole fraction of $[(tmbpy)_2Ru^{II}(Mebpy\text{-}amH^+)]^{3+}$ (6.3 mM) as the concentration of 3,5-$DNBCOO^-$ is varied from 0.0 to 80 mM

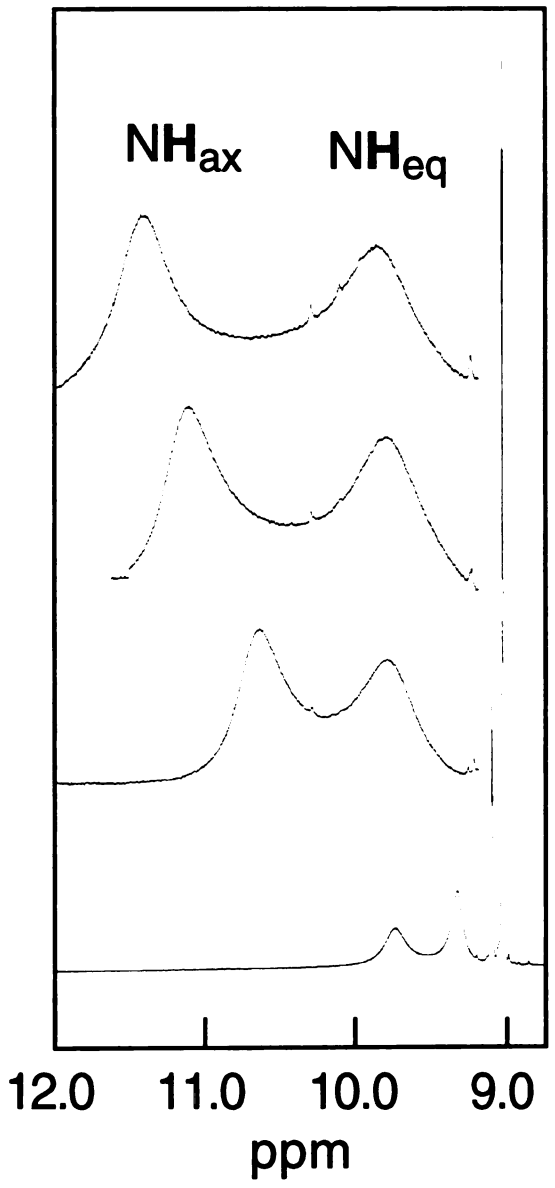

Figure 35. ^{1}H NMR spectrum of the tetraphenylborate salt of 3,5-DNBamH$^+$ with addition of the PF_6^- salt of [(tmbpy)$_2$Ru^{II}(Mebpy-COO$^-$)]$^+$ at concentrations 0.0, 1.8, 2.9 and 3.9 mM in DMSO-d_6 (bottom to top). The ^{1}H resonances of the axial (internal) and equatorial (external) amidinium protons appear between 9.3 and 12.0 ppm.

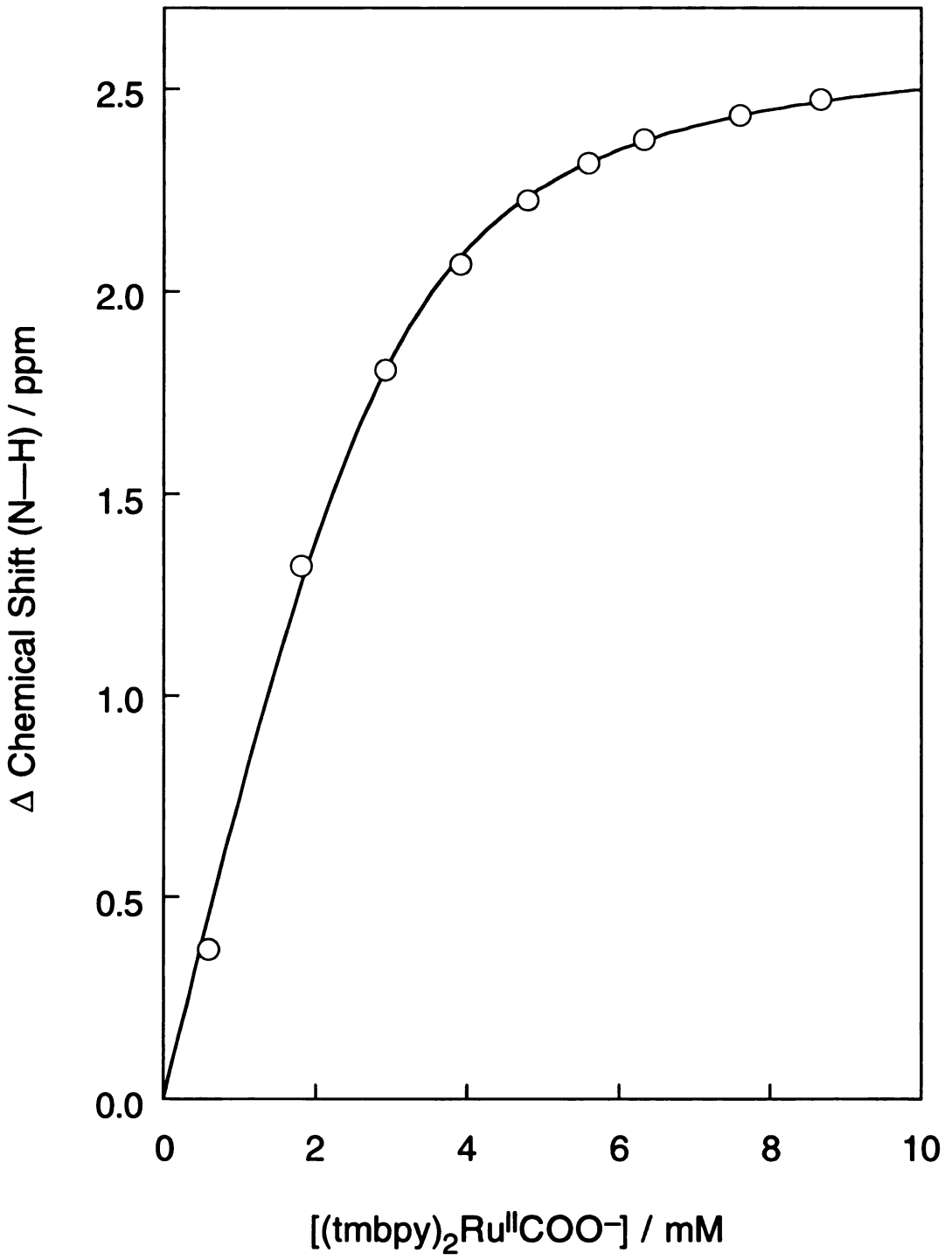

Figure 36. Plot of the chemical shift of the resonances shown in Figure 35 and additional resonances of the amidinium protons hydrogen-bonded to Ru^{II} carboxylate complex from 0.0 to 10 mM.

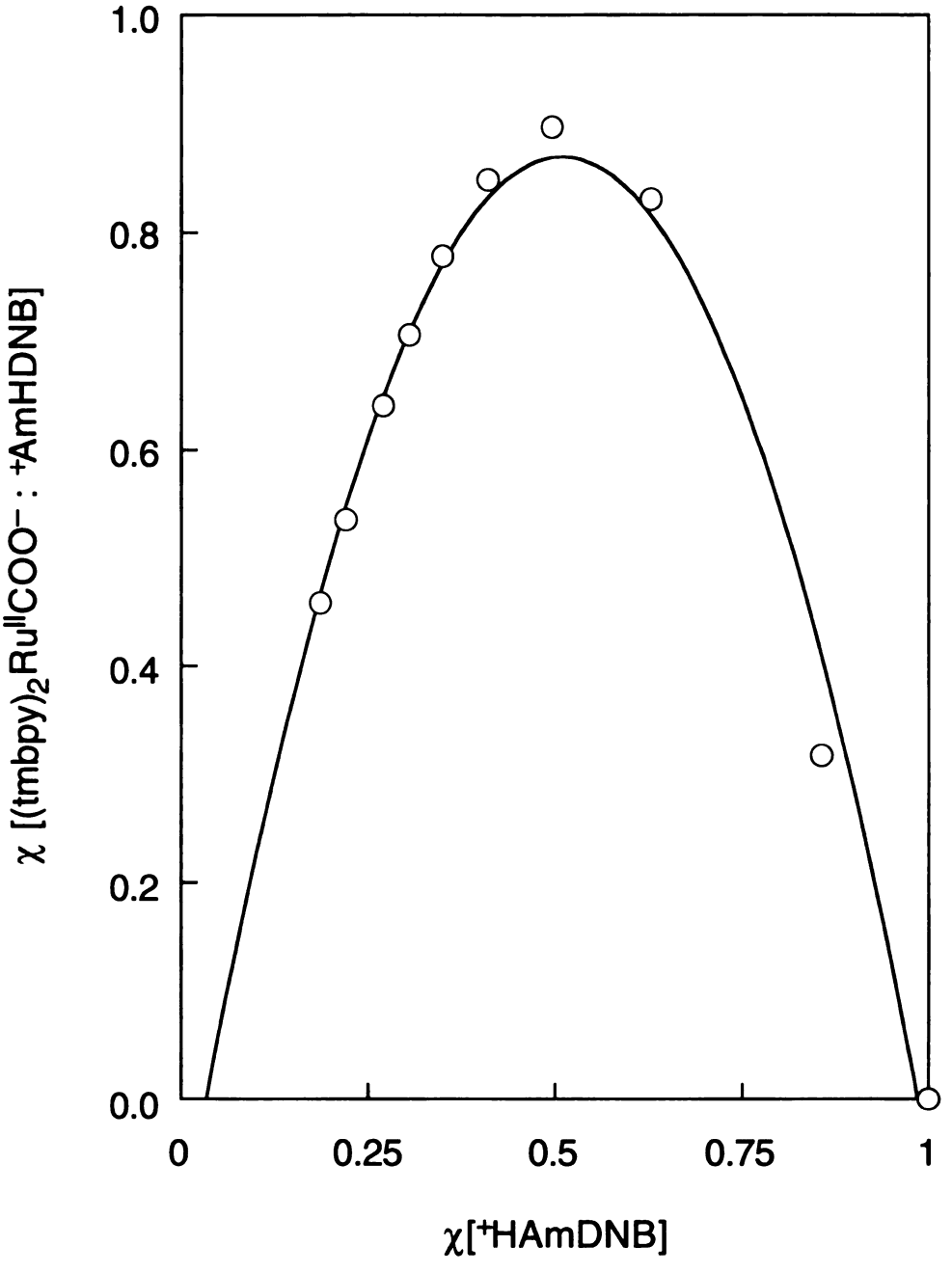

Figure 37. Job's plot of the relative salt-bridge complex concentration vs. the mole fraction of 3,5-DNBamH$^+$ (2.9 mM) as the concentration of the [(tmbpy)$_2$Ru^{II}(Mebpy-COO$^-$)]$^+$ is varied from 0.0 to 10 mM.

$COO^-)]^+$ and $[(tmbpy)_2Ru^{II}(Mebpy\text{-}COOH)]^{2+}$, are typical of Ru(II) polypyridyl complexes. Absorption profiles are dominated by a high energy $\pi\pi^*$ intraligand absorption band and a split lower energy $d\pi$-π^* MLCT absorption band. Nonaqueous solutions of the complexes exhibit a strong red. Luminescence decay exhibits monoexponential behavior and a fit of luminescence data yield lifetimes of 860, 1030 and 770 ns for $[(tmbpy)_2Ru^{II}(Mebpy\text{-}amH^+)]^{3+}$, $[(tmbpy)_2Ru^{II}(Mebpy\text{-}COO^-)]^+$ and $[(tmbpy)_2Ru^{II}(Mebpy\text{-}COOH)]^{2+}$, respectively.

The relative energies of the relevant MLCT excited states for systems **1-3** may be evaluated by analyzing the emission profiles of the various homoleptic complexes as follows,[74]

$$\Delta G_{es}^{\circ} = E_o + \chi \tag{3.9}$$

$$\chi = (\Delta\bar{\nu}_{0,1/2})^2(16k_BT\ln 2)^{-1} \tag{3.10}$$

where the excited state energy (ΔG_{es}°) is related to the energy of the luminescence maximum (E_o) and the reorganization energy (χ) containing solvent and low frequency modes, which are treated classically and related to the full width at half-maximum, $\Delta\bar{\nu}_{0,1/2}$ for a single vibronic component. The relation of the spectroscopic energy to a free energy arises from negligible pressure-volume work (and hence the energy is primary enthalpic)[61] and small electronic entropic contributions accompanying excited state production.[62] Measured values of E_o = 14,843 cm^{-1} and $\Delta\bar{\nu}_{1/2}$ = 2476 cm^{-1} for Ru(II) *tris*-(Mebpy-amH^+) and E_o = 15,359 cm^{-1} and $\Delta\bar{\nu}_{1/2}$ = 1826 cm^{-1} for Ru(II) *tris*-(Mebpy-COO^-) complex yield excited state energies ($E_{o,o}$) of 2.17 and 2.08 eV, respectively, as compared to that reported for $Ru(tmbpy)_3^{2+}$ ($E_{o,o}$ = 2.56 eV[74]). The destabilization of the $d\pi \rightarrow \pi^*$(tmbpy) MLCT by nearly 0.4 eV with regard to the MLCT excited states of Mebpy-amH^+ and Mebpy-COO^- ensures that photoexcitation of **4-6** cleanly promotes the

transferring electron on to the Mebpy ligand, from where it can smoothly advance to the dinitrobenzoic acceptor.

c. PCET

Consistent with these excited state energetics, the Ru(II) excited state undergoes electron transfer reactions with unbound and bound acceptor. The luminescence from the $[(tmbpy)_2Ru^{II}(Mebpy\text{-}COO^-)]^+$ bound to benzamidinium and $[(tmbpy)_2Ru^{II}(Mebpy\text{-}amidinium)]^{3+}$ bound to benzoate is long-lived with observed excited state lifetimes of 1200 and 470 ns, respectively. Owing to the large association constants of **4** and **5** in CH_2Cl_2, these lifetimes are independent of benzamidinium and benzoate at greater concentrations than that of the metal complex. Conversely, the presence of the 3,5-DNB electron accepting group leads to efficient quenching of the Ru(II) excited state luminescence for **4-6**. For each system, biphasic decay kinetics are observed for the quencher concentration range investigated. One component of the emission decay is clearly dependent upon the concentration of quencher whereas the other component remains concentration-independent. The concentration-dependent lifetimes obey typical linear Stern-Volmer quenching kinetics and the rate constants for the bimolecular reactions of the respective constituents of supramolecule assemblies are listed in Table 4. The bimolecular reaction at low concentrations likely involves complexed quencher and free Ru(II) complex as a result of the high association constants of the supramolecule assemblies **4** and **5**. The bimolecular rate constants for **4-6** accord well with the kinetics of equi-exergonic bimolecular reactions between Ru^{II}*tris*(polypyridyl) and nitroaromatic quenchers.[63] Of greater relevance to PCET are the attendant concentration-independent rate constants, which we attribute to the unimolecular electron transfer of the associated complexes.[64] The striking result of these data listed in Table 1 is that the electron transfer rate constant through **4** is considerably slower than for its switched interface congener **5**. The differences in the unimolecular rate

constants for **4** and **5** reveal that the rate of electron transfer depends significantly on the salt bridge and its orientation with respect to the electron transfer pathway.

The slower rate of **4** may have several origins. In **4**, the permanent dipole ($\delta^+\delta^-$) of the salt bridge is in the direction of electron transfer whereas in **5** electron transfer opposes the dipole. Internal electrostatic fields affect the rates of electron transfer by altering the driving force of reaction relative to the isolated constituents.[65-67] By using typical bond distances of $[Ru(bpy)_3]^{2+}$, DNB and the amidinium-carboxylate salt bridge, we calculate that a 0.37 V (less favorable for **4**) field-induced difference between the driving force for intramolecular electron transfer ($\Delta E_C = e^2/\varepsilon r$).[68] This thermodynamic attenuation of the electron transfer rate constant for **4** may be further augmented by a greater reorganization energy associated with the salt bridge. In **4**, accompanying proton transfer (from the Ru^{II} amidinium donor to the carboxylate acceptor) can stabilize the charge of the electron as it develops on the acceptor. In this case, since the proton charge is strongly coupled to the solvent dipoles, as with the electron, charge shift within the salt bridge may be accompanied by significant solvent polarization thereby giving rise to additional Franck-Condon factors. This is not the case for **5**. Here, the proton is already residing on the acceptor, and hence it is likely to remain upon the arrival of the electron. Finally, differences in H-bonding strengths of the asymmetric interfaces may be manifested in differences in electronic coupling efficiencies.[69] The electron withdrawing nitro groups will stabilize the negative charge on the carboxylate, resulting in a weaker hydrogen bond in **6** and hence correspondingly weaker electronic coupling pathway.

2. Conclusions

Our results show that intervening salt bridges can profoundly mediate the rates of intramolecular electron transfer. Unlike a symmetric interface, the salt bridge can significantly affect the rate of electron transfer from contributions of the electrostatic potential, Franck-Condon factors, and electronic coupling arising from the asymmetric

Table 4. Rates for unimolecular and bimolecular electron transfer for donor-acceptor complexes with amidinium-carboxylate and dicarboxylic acid dimer bridges in dichloromethane at 22 °C.

PCET Complex	ΔG° / eV[a]	k_{ET} / 10^9 $M^{-1}s^{-1}$	k_{PCET} / 10^6 s^{-1}
4	–0.14	1.2	8.4
5	–0.34	3.3	310
6	–0.23	3.2	43

[a]Excited state redox potentials of the $[(tmbpy)_2Ru^{II}(Mebpy\text{-}amH^+)]^{3+}$, $[(tmbpy)_2Ru^{II}(Mebpy\text{-}COO^-)]^+$ and $[(tmbpy)_2Ru^{II}(Mebpy\text{-}COOH)]^{2+}$ donors were determined from the simple thermodynamic relation: $E_{1/2}(*Ru^{II/I}) = \Delta G_{es}^\circ - E_{1/2}(Ru^{II/I})$ where $E_{1/2}(Ru^{II/I})$ and $E_{1/2}(*Ru^{II/I})$ are the ground state and excited state $Ru^{II/I}$ reduction potentials, respectively. The excited state free energies (ΔG_{es}°) of 2.23, 2.11 and 2.22 eV were determined from Eqs. (3.9) and (3.10) and the $Ru^{III/II}$ reduction potentials of 1.05, 1.02 and 1.05 eV were measured by cycilc voltammetry (CH_2Cl_2 containing 0.1 M tetrabutylammonium hexafluorophosphate as supporting electrolyte), respectively. Reduction potentials of 3,5-dinitrobenzoate and 3,5-dinitrobenzamidine were measured to be –1.04 and –0.85 V vs SCE, respectively. Protonation of the acceptors was estimated to facilitate reduction by 0.1 V.

charge distribution. Such effects will be present in any biological system where the developing charge resulting from proton motion coupled to the electron transfer pathway is not compensated (e.g. proton pumps, oxygen activation). Current studies are underway to begin disentangling the contributions of the different PCET mechanisms for electron transfer through asymmetric interfaces.

D. DECB and BPY Complexes of Ru(II) to Mediate Reductive PCET

With an electronic framework established for the PCET reactions of Ru(II) polypyridyl complexes established, we wondered whether the influence of the salt bridge on electron transfer rates was specific to an oxidative quenching pathway. To address this issue, we undertook electron transfer reactions of Ru(II) polypyridyls juxtaposed to donors via the amidinium-carboxylate salt bridge. In the case of the reductive quenching pathway, the PCET reaction effectively amounts to hole transfer through the amidinium-carboxylate salt bridge (as opposed to electron transfer for the oxidative pathway). Accordingly, a meaningful PCET study demands that the excited electron be removed from the PCET pathway by MLCT to the ancillary bipyridyl ligand. We now report that modification of the ancillary bpy ligands by diethylcarboxy (decb) permits PCET reactions of Ru(II) polypyridyl excited states to be investigated by reductive quenching, Figure 38. Supramolecule assemblies **7** and **8** have been prepared in which an electron may transfer from N,N´-dimethylaniline to the electronically excited Ru(II) polypyridyl acceptor through the intervening amidinium-carboxylate salt bridge interface. Electron transfer into the Ru(II) metal center is fast when the Ru(II) polypyridyl complex is attached to the amidinium-side of the salt bridge. This behavior is opposite to that previously observed by us for the oxidative quenching pathway where electron transfer is fast when the Ru(II) polypyridyl complex is attached to the carboxylate-side of the salt bridge. These differences in the oxidative and reductive quenching reactions may be understood by considering the orientation of the salt bridge relative to the direction of electron transport. Complex **9** was

also studied however it does not appear to undergo an ET reaction due to thermodynamic constaints.

1. Results and Discussion

a. Solution Association

Amidinium-carboxylate salt bridge complexes **7** and **8** readily form in CH_3CN solutions. The exceptionally high association of the salt bridge agrees well with Jorgensen's classification for two favorable secondary interactions composing the hydrogen bonded interface[70], bolstered by the stabilization imparted by the molecular recognition of the negatively charged carboxylate by the positively charged amidinium. The significantly higher K_{assoc} of **7** is consistent with an increased basicity of the carboxylate group conferred by the electron donating dimethylamino group, resulting in a stronger hydrogen bonding interaction than that observed for switched interface system **9**.

b. Photophysical Behavior

The long-lived luminescence from the Ru(II) polypyridyl complexes is preserved upon formation of the salt bridge in the absence of an electron donating group. Addition of benzoate to acetonitrile solutions of $[(bpy)_2Ru^{II}(Mebpy\text{-}amH^+)]^{3+}$ and $[(decb)_2Ru^{II}(Mebpy\text{-}amH^+)]^{3+}$ lead to a modest attenuation in the observed excited state lifetimes (τ = 975 and 1330 ns, respectively), which remain relatively independent of benzoate concentrations. Similarly, long-lived excited state lifetimes of 900 and 1130 ns are observed for $[(bpy)_2Ru^{II}(Mebpy\text{-}COO^-)]^+$ and $[(decb)_2Ru^{II}(Mebpy\text{-}COO^-)]^+$ associated to benzamidinium. The Ru(II) excited state luminescence of $[(bpy)_2Ru^{II}(Mebpy\text{-}amH^+)]^{3+}$ and $[(decb)_2Ru^{II}(Mebpy\text{-}amH^+)]^{3+}$ is dramatically quenched when phenyl of benzoate is substituted with the dimethylaniline. This result is consistent with an electron transfer quenching mechanism, which is a well-established reaction between electronically excited Ru(II) *tris*(polypyridyl) complexes and dialkylylamine aromatic electron donors.

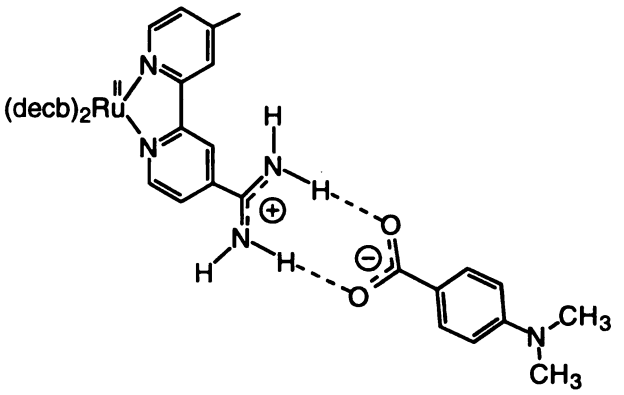

7

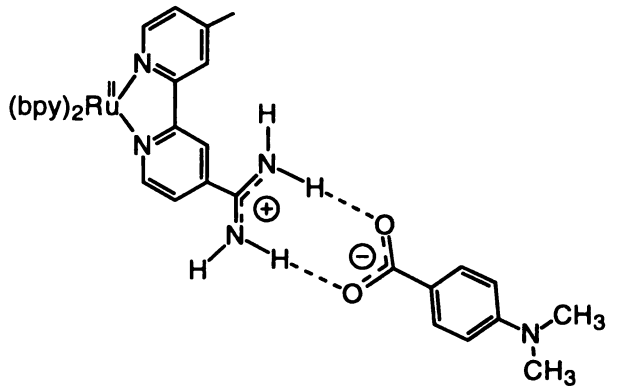

8

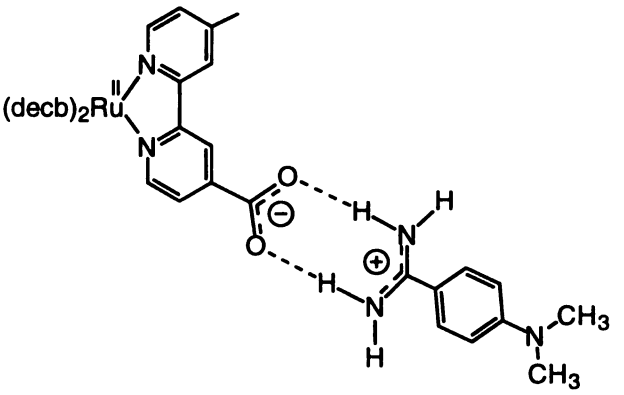

9

Figure 38. Complexes to study PCET; **7** is based on $[(decb)_2Ru^{II}(Mebpy\text{-}amH^+)]^{3+}$, **8** is based on $[(bpy)_2Ru^{II}(Mebpy\text{-}amH^+)]^{3+}$ and **9** is based on $[(decb)_2Ru^{II}(Mebpy\text{-}COO^-)]^+$.

Biexponential decay kinetics are observed where one lifetime component of the emission decay is dependent on the concentration of donor and the other is not over a DMA-COO^- concentration range of 0.062 to 1.24 mM ($[(bpy)_2Ru^{II}(Mebpy\text{-}am)^{2+}]$ = 0.051 mM). The concentration-dependent lifetimes obey typical linear Stern-Volmer quenching kinetics and the bimolecular rate constants of 6.4×10^8 $M^{-1}s^{-1}$ for $[(bpy)_2Ru^{II}(Mebpy\text{-}amH^+)]^{3+}$ and of 3.5×10^8 $M^{-1}s^{-1}$ for $[(decb)_2Ru^{II}(Mebpy\text{-}amH^+)]^{3+}$ accord well with the kinetics of equi-exergonic bimolecular reactions between $Ru(bpy)_3^{2+}$ and dialkylanilines. Analyses of the concentration-independent lifetime decay curves yield intramolecular rate constants of 1.9×10^7 s^{-1} and 1.7×10^9 s^{-1} for **8** and **7**, respectively. The independence of the rate constant on quencher concentration is consistent with an electron transfer quenching reaction occurring within the associated pair.

When the interface is carboxylate and amidinium moieties are interchanged on the Ru(II) acceptor and DMA donor, as in **9**, no electron transfer quenching of the Ru(II) luminescence is observed. The lifetime of $[(bpy)_2Ru^{II}(Mebpy\text{-}COO^-)]^+$ and $[(decb)_2Ru^{II}(Mebpy\text{-}COO^-)]^+$ is invariant with the addition of DMA-amH^+ over a quencher concentration range of $1.0 - 140 \times 10^{-5}$ M.

The significant differences in the electron transfer reactivity between the **7**,**8** and **9** systems are reflected in the electron transfer driving forces. For N,N′-dimethylaminobenzamidinium, a reversible half-wave potential at 1.10 V vs. SCE was observed in the cyclic voltammogram. Conversely, N,N′-dimethylaminobenzoate (TBA^+ salt) was electrochemically irreversible as evidenced by the presence of only an anodic wave in the cyclic voltammetric scan. Accordingly, the potential for this compound was estimated from a Marcus curve by using methods previously described by Schuster and co-workers and gives a redox potential of 0.70 V vs. SCE.

Consistent with the equilibrium measurements, the Ru(II) excited state undergoes electron transfer with unbound and bound donor when the reaction is exergonic. The luminescence from $[(bpy)_2Ru^{II}(Mebpy\text{-}amH^+)]^{3+}$ and $[(decb)_2Ru^{II}(Mebpy\text{-}amH^+)]^{3+}$ is

efficiently quenched by DMA-COO^-. That the bimolecular rate for the reaction of the bpy complex, **8**, is greater than that of the decb complex, **7**, is sensible in light of the greater driving force of the bimolecular electron transfer reaction of the former ($\Delta\Delta G$ = 0.13 V). Along these lines, the inversion of the relative ordering of the rate constants, and their large difference (**8** is ~10^2 less than that of its decb congener **7**), for the salt-bridge assembled acceptor-donor pair appears peculiar. We believe that the origins of this behavior arise from disparate MLCT energetics and consequently electronic structure of the Ru(II) polypyridyl acceptor complex.

The electron transfer reactions of **7** and **8** is established by photogenerating a hole at the Ru(II) center by MLCT excitation. The energy ordering decb ~ Mebpy-amH^+ << bpy follows a simple trend where the energy of the MLCT excited state increases as the electron withdrawing ability of the substituents on the polypyridyl rings decreases. In the case of **8**, simple Boltzmann considerations suggest that MLCT excitation places an electron on the Mebpy-amH^+ and thus the electron transfer pathway contains a photoreduced Mebpy ligand. For **7**, the decb and Mebpy-amH^+ MLCT excited states are nearly equi-energetic and therefore the photoexcited electron is partly removed from the electron transfer pathway. In an electronic sense, the transferring electron traverses a less obstructed pathway from DMA to the photogenerated hole on the metal.

The electronics of **7** and **8** are straightforward with regard to photoinitiating the electron transfer reaction. The energetics for the $d\pi \rightarrow \pi^*$(polypyridine) MLCT excited state are decb < bpy < Mebpy-COO^-. Photoexcitation of **9** cleanly establishes a hole at the metal ion without any contribution of a photoreduced ligand along the electron transfer pathway. Nevertheless, electron transfer is not observed for the salt-bridge complex. Moreover, the corresponding bimolecular electron transfer reaction of **9** is negligible. Inspection of the free energy involved in ET in **9** reveal that the electron transfer reactions for this systems is endergonic.

The reactivity difference between the Ru(II) polypyridyl amidinium systems (**7** and **8**) and carboxylate congener (**9**) is primarily a result in a shift of the DMA donor potential upon the presence of amidinium at the para position of dimethylaniline. DMA-amH$^+$ is 0.40 V more difficult to oxidize than DMA-COO$^-$, which is a slightly better reductant than DMA ($E_{1/2}$ = 0.81 V vs. SCE). The increased difficulty in oxidizing DMA-amH$^+$ is sufficiently destabilizing to drive the electron transfer reaction of **9** energetically uphill.

2. Conclusions

The overall electron transfer kinetics of **7** and **8** follows the emerging trend that electron transport through salt bridges is fast for the D–(carboxylate-amidinium)–A complexes. In this orientation, electron transfer is in the direction of the permanent dipole of the salt bridge and the internal electric field contributes favorably to the driving force of reaction relative to the isolated constituents.[71,72] The thermodynamics may be further augmented by favorable kinetics associated with a D–(carboxylate-amidinium)–A orientation. Charge redistribution within the salt-bridge may be strongly coupled to the solvent dipoles, thereby giving rise to Franck-Condon factors in excess of that expected for simple electron transfer. In the case of the D–(carboxylate-amidinium)–A complex, the proton already resides on the acceptor and hence it is likely to remain upon the arrival of the electron. Franck-Condon factors arising from proton motion within the salt bridge are therefore minimized. On the basis of the thermodynamic and kinetics considerations, we can account for the differences in the oxidative and reductive quenching pathways. For the oxidative quenching reaction, electron transfer should be fast out of the electronically excited Ru(II) complex. Conversely, fast electron transfer into the metal center should be observed for a reductive quenching pathway. In both cases, the orientation of the salt bridge with regard to the direction of electron transfer is the same and favorable with regard to electron transfer. Unfortunately, as was previously provided by a comparative kinetics studies of switched interface systems for the oxidative quenching pathway, a more explicit

analysis of the effect of the salt bridge on electron transfer pathway is obviated by the large difference in the electron transfer driving forces of **7** and **9**.

E. Materials and Methods

Synthesis of 4-methyl-4′-amidinium-2,2′-bipyridine. The ligand synthesis began with the preparation of 4-methyl-4′-carbonitrile-2,2′-bipyridine. Hydroxylamine hydrochloride (1.8 g, 26 mmol) was added to a 40 ml formic acid solution of 4-methyl-4′-carboxaldehyde-2,2′-bipyridine[73] (4.0 g, 20 mmol). The solution was refluxed for 24 h under an argon atmosphere. After cooling to room temperature, the solution was poured into 200 ml of ice. Neutralization with an aqueous sodium carbonate solution produced a white precipitate, which was extracted into dichloromethane (3x50 ml). The organic extracts were combined, dried over magnesium sulfate, and the solvent was removed under reduced pressure to give the product, 4-methyl-4′-carbonitrile-2,2′-bipyridine. Yield: 3.15 g, 80%; MS: 195.1 m/z; m.p. 134-137 °C; ^{1}H NMR (CD_3CN): δ 8.79 (1H, d), 8.60 (1H, s), 8.50 (1H, d), 8.21 (1H, s), 7.62 (1H, d), 7.25 (1H, d), 2.12 ppm (3H, s); ^{13}C NMR (CD_3CN): δ 158.16, 154.76, 151.16, 150.23, 149.82, 126.68, 126.15, 123.54, 122.58, 122.03, 117.76, 21.22 ppm.

Conversion to the amidinium was achieved by charging a solution of freshly prepared sodium methoxide in methanol (20 ml, 0.04 M) with 4-methyl-4′-carbonitrile-2,2′-bipyridine (1.50 g, 7.7 mmol) under argon. The resulting solution was stirred at room temperature for 24 h, ammonium chloride (0.43 g, 8.0 mmol) was added in one portion, and stirring was continued for an additional 24 h under argon. Large colorless crystals of (4-methyl-4′-amidinium-2,2′-bipyridine)Cl (Yield: 0.70 g, 71%) were collected and dissolved in a minimal amount of water. The conversion of the Cl^- salt to the PF_6^- salt was quantitative upon the addition of a saturated aqueous solution of ammonium hexafluorophosphate to an aqueous solution of (4-methyl-4′-amidinium-2,2′-bipyridine)Cl. MS: 212.1 m/z; ^{1}H NMR (CD_3CN): δ 8.87 (1H, d), 8.65 (1H, s), 8.52

(1H, d), 8.27 (1H, s), 8.02 (4H, s), 7.64 (1H, d), 7.39 (1H, d), 2.41 ppm (3H, s); ^{13}C NMR (CD_3CN): δ 166.79, 158.25, 154.82, 151.51, 150.21, 137.12, 126.82, 122.93, 122.44, 119.84, 21.26 ppm.

Synthesis of $[(tmbpy)_2Ru(Mebpy\text{-}amH^+)][(PF_6)_3]$. The ligand 4-methyl-4′-amidinium-2,2′-bipyridine chloride (0.09g, 0.36 mmol) was reacted with $(tmbpy)_2Ru^{II}Cl_2$[74] (0.30 g, 0.50 mmol) in refluxing 95% ethanol (20 ml) for 4 h. After removing the solvent under reduced pressure, the resulting solid was dissolved in a minimal amount of water and filtered. Addition of an aqueous saturated solution of NH_4PF_6 yielded $[(tmbpy)_2Ru^{II}(Mebpy\text{-}amidinium)]^{3+}$ as its PF_6^- salt, which was washed with water (5 x 15 ml), dried in air, and washed with anhydrous ethyl ether (5 x 15 ml). Yield: 0.17g, 40%; ES/MS $[M]^{2+}$: 369.6 m/z; ^1H NMR (DMSO-d_6): δ 9.60 (2H, s), 9.37 (2H, s), 9.03 (1H, s), 8.71 (1H, s), 8.59 (4H, s), 7.97 (1H, d), 7.70 (1H, d), 7.59 (1H, d), 7.42 (1H, d), 7.29 (1H, s), 7.28 (1H, s), 7.26 (1H, s), 7.17 (1H, s), 2.55 (3H, s), 2.41 (12H, s), 2.08 ppm (12H, s).

Synthesis of $[(tmbpy)_2Ru(Mebpy\text{-}COOH)][(PF_6)_2]$ and $[(tmbpy)_2Ru(Mebpy\text{-}COO^-)][(PF_6)]$. A 95% ethanol (20 ml) solution containing 4-methyl-4′-carboxylic acid-2,2′-bipyidine[73] (0.05g, 0.23 mmol) and $(tmbpy)_2Ru^{II}Cl_2$ (0.24 g, 0.39 mmol) was refluxed for 24 h. The solution was cooled and the solvent was removed under reduced pressure. The remaining solid was dissolved in a minimal amount of water and filtered. The orange PF_6^- salt of $[(tmbpy)_2Ru^{II}(Mebpy\text{-}COOH)]^{2+}$ was obtained upon the addition of an aqueous saturated solution of NH_4PF_6. The product was further purified by charging a column of neutral alumina, activity 1, with a solution of the complex salt and eluting with dichloromethane and ethanol 6:1 (v/v). Yield: 0.12g, 52%; ES/MS $[M]^{2+}$: 370.0 m/z; ^1H NMR (CD_3CN): δ 8.89 (1H, s), 8.45, (1H, s), 8.27, (4H, m), 7.72 (1H, d), 7.60 (1H, d) 7.46 (1H, d), 7.36 (1H, s), 7.33 (1H, s), 7.32 (1H, s), 7.27 (1H, s), 7.15 (1H, d), 2.50 (3H, s), 2.42 (6H, s), 2.41 (6H, s), 2.07 (6H, s), 2.06 ppm (6H, s).

The carboxylate form of the complex was obtained by dissolving the chloride salt of $[(tmbpy)_2Ru^{II}(Mebpy\text{-}COOH)]^{2+}$ in a minimal amount of water. The pH was adjusted to ~10 with sodium hydroxide and addition of saturated solution of sodium hexafluorophosphate, added dropwise, yielded an orange precipitate. The precipitate was filtered onto a fine frit and washed with water. Because the complex is slightly soluble in aqueous solution, a minimal amount of water should be used for washing (3 x 5 ml). The gummy, air-dried solid was washed with copious amounts of anhydrous ethyl ether to remove any vestiges of water, thereby yielding a microcrystalline solid. ^{1}H NMR (DMSO-d_6): δ 8.85 (1H, s), 8.73 (1H, s), 8.57 (2H, s), 8.55 (2H, s), 7.66 (1H, d), 7.60 (1H, d), 7.45 (1H, d), 7.29 (5H, m), 2.50 (3H, s), 2.41 (9H, s), 2.39 (3H, s), 2.07 (6H, s), 2.06 ppm (12H, s).

Synthesis of [NBu_4][3,5-dinitrobenzoate]. Twenty three ml of a 1.0 M tetrabutylammonium hydroxide methanol solution was added via burette to a flask containing 3,5-dinitrobenzoic acid (5.0 g, 23 mmol). The mixture was stirred until the acid was completely dissolved. A viscous oil remained upon removal of the methanol under reduced pressure. The oil was dissolved in freshly distilled benzene and 10 g of basic alumina was added to the solution, which was stirred for 10 min and filtered. The filtrate was freeze-dried to yield the product as a fluffy white solid. Yield: 8.5g, 81%; MS: 212.1 m/z; ^{1}H NMR (DMSO-d_6): δ 8.90 (2H, s), 8.75 (1H, s), 3.20, (8H, s), 1.57 (8H, p) 1.28, (8H, s), 0.89 ppm (12H, t); ^{13}C NMR (DMSO-d_6): δ 162.97, 147.46, 146.00, 128.25, 117.91, 57.551, 23.11, 19.22, 13.42 ppm.

Synthesis of [3,5–dinitrobenzamidinium][BPh_4]. The chloride salt of 3,5-dinitrobenzamidinium (0.5 g, 2.03 mmol), which has previously been prepared by Creary,[75] was dissolved in a minimal amount water and residual solid was removed by filtering through a fine frit. An aqueous solution of sodium tetraphenylborate (1.0 g, 2.92 mmol) was added to the filtrate to afford a lemon yellow precipitate. This solid was filtered, washed with water (5 x 15 ml), dried in air, and washed with anhydrous ethyl ether (5 x 15

ml). The metathesis reaction proceeded with nearly quantitative conversion. MS: 210.0 m/z; ^{1}H NMR (DMSO-d_6): δ 9.59 (4H, s), 9.15, (1H, s), 9.10, (2H, s), 7.24 (8H, s), 6.97 (8H, t), 6.83 ppm (4H, t); ^{13}C NMR: δ 164.44, 163.79, 163.13, 162.48, 162.21, 147.87, 135.64, 131.071, 129.31, 125.37, 123.03, 121.60 ppm.

Synthesis of [Ru(decb)$_2$Cl$_2$]. An absolute ethanol (50 ml) solution containing 2,2′-bipyridine-4,4′-dicarboxylic acid (1.0 g, 4.1 mmol), $RuCl_3 \bullet (H_2O)_3$ (0.5 g, 1.9 mmol), LiCl (1.0 g, 23.6 mmol) and concentrated hydrochloric acid (1 ml) was refluxed for 24 h. The reaction mixture was allowed to cool to room temperature and poured into ice water (250 ml). A black microcrystalline precipitate forms immediately. The solid was collected on a fine frit, washed with water, dried in air, and washed with anhydrous ether. The product was obtained by column chromatographic separation on silica gel with CH_2Cl_2 and ethanol 50:1 v/v as the eluant. Yield: 0.70 g, 71%; ES/MS [M]$^+$: 772.4 m/z; ^{1}H NMR (CD_3CN): δ 10.22 (1H, d), 8.95 (1H, s), 8.77 (1H, s), 8.18 (1H, d), 7.77 (1H, d), 7.43 (1H, d), 4.51 (2H, q), 4.35 (2H, q), 1.47 (3H, t), 1.34 ppm (3H, t); ^{13}C NMR ($CDCl_3$): δ 164.00, 163.49, 160.22, 157.89, 154.95, 152.43, 136.24, 134.94, 124.89, 124.40, 121.76, 121.50, 62.51, 62.34, 14.24, 14.11 ppm.

Synthesis of [Ru(decb)$_2$(Mebpy-COOH)][(PF$_6$)$_2$]. The ligand 4-methyl-4′-carboxylic acid-2,2′-bipyidine (0.020 g, 0.093 mmol)[76] was combined with $Ru(decb)_2Cl_2$ (0.060 g, 0.078 mmol) in ethylene glycol (2 ml) and the mixture was heated at 120 ℃ for 20 min. The ethylene glycol was removed by liquid-liquid extraction with ether (2 l) to yield a tar-like orange residue, which was dissolved in a minimal amount of water. Addition of ammonium hexafluorophosphate to the aqueous solution yielded an orange precipitate. The solid was purified by neutral alumina, activity 1, and eluted with dichloromethane and ethanol 6:1 (v/v). Yield: 32 mg, 34%; ES/MS [M]$^{2+}$: 458.0 m/z; ^{1}H NMR (CD_3CN): δ 9.03 (4H, s), 9.01 (1H, s), 8.60 (1H, s), 7.85 (9H, m), 7.73 (1H, d), 7.47 (1H, d), 7.26 (1H, d), 4.44 (8H, q), 1.39 (12H, t).

Synthesis of $[Ru(decb)_2(Mebpy\text{-}amH^+)][(PF_6)_3]$. The metal complex was prepared by a chloride substitution reaction with [4-methyl-4′-amidinium-2,2′-bipyridine][Cl]. A freshly distilled ethanol solution containing $Ru(decb)_2Cl_2$ (0.084 g, 0.11 mmol) and [4-methyl-4′-amidinium-2,2′-bipyridine][Cl] (0.048 g, 0.19 mmol) was refluxed under argon for 18 days. A solution color change from deep purple to dark orange was observed over the course of the reaction. The reacted solution was added to a short silica gel column, and eluted with dichloromethane and ethanol 10:1 (v/v). Several bands separated from the product, which remained immobilized on the silica gel. After all mobile impurities were eluted from the column, the silica gel containing the product was collected from the top of the column. A solution of ammonium hexafluorophosphate (0.5 g) in dichloromethane and ethanol 10:1 (v/v) released the product from the silica gel. The silica gel was removed by filtration. The mother liquor was taken to dryness, and water was added to remove the excess ammonium hexafluorophosphate. The resulting solid was collected on a fine frit, dried in air, and washed with dry ether to afford $[Ru(decb)_2(Mebpy\text{-}amH^+)][(PF_6)_3]$. Yield: 0.056 g, 38%; ES-MS $[M]^{2+}$: 456.9; ^1H NMR (CD_3CN): δ 9.08 (4H, s), 8.67 (1H, s), 8.46 (1H, s), 8.06 (4H, s), 7.90 (9H, m), 7.58 (1H, d), 7.50 (1H, d), 7.33 (1H, d), 4.44 (8H, q), 2.62 (3H, s), 1.42 ppm (12H, t).

Synthesis of $[NBu_4]$[4-(N,N′-Dimethylamino)benzoate] . An equivalent of a 1.0 M tetrabutylammonium hydroxide (31.5 ml) in methanol was added to N,N′-dimethylaminobenzoic acid (5.20 g, 31.5 mmol). The mixture was stirred until the acid was completely dissolved. A viscous oil remained upon removal of the methanol under reduced pressure. The oil was dissolved in freshly distilled benzene and 10 g of basic alumina was added to the solution, which was stirred for 10 min and filtered. The filtrate was freeze-dried to yield the product as a fluffy white solid. Yield: 11.95 g, 93%; ES/MS $[M+2H]^+$: 166.2 m/z; ^1H NMR (CD_3CN): δ 7.76 (2H, d), 7.60 (2H, d), 3.09 (8H, m), 2.88 (6H, s), 1.56 (8H, m), 1.31 (8H, m), 0.91 ppm (12H, t); ^{13}C NMR (CD_3CN): δ 170.69, 151.88, 131.46, 131.25, 111.70, 59.12, 40.83, 24.32, 20.28, 13.84 ppm.

Synthesis of [4-(N,N-Dimethylamino)benzamidinium][PF_6]. In a dry Schlenk tube, 4-(N,N′-dimethylamino)benzonitrile (1.68 g, 11.5 mmol) was added via cannula to a 1.0 M solution of methylchloroaluminumamide (35 ml). The mixture was heated to 80 °C for 3 days. The reaction mixture was quenched with a chloroform slurry of silica and the resulting mixture was stirred until gas evolution ceased. This suspension was poured into a fine frit, and thoroughly washed with a chloroform/methanol solution. Removal of solvent yielded the chloride salt of the product (1.48 g, 64%). The hexafluorophosphate salt was obtained by dissolving this chloride salt in a minimal amount of water, followed by the addition of a saturated solution of ammonium hexafluorophosphate. The metathesis reaction proceeded with nearly quantitative conversion. ES/MS $[M]^+$: 164.4 m/z; ^{1}H NMR (CD_3CN): δ 7.59 (2H, d), 7.30 (2H, s), 7.06 (2H, s), 6.78 (2H, d), 3.05 (6H, s); ^{13}C NMR (CD_3CN): δ 166.167, 155.70, 130.58, 112.16, 111.78, 40.22 ppm.

Electrospray mass spectrometric (ES/MS) analyses were obtained with a Finnegan mat (San Jose, CA) quadrupole mass spectrometer using a CH_3CN mobile phase. A CH_3CN solution of the sample was infused directly into the vaporization nozzle of the electrospray ion source at a flow rate of 3 ml min^{-1}. Nitrogen was used as the nebulizing gas at a pressure of 35 PSI. NMR spectra were recorded on a Varian VXR 300 and samples were thermostatted at 298 (0.2) K.

Association constants for **4** and **5** were determined by measuring the ^{1}H NMR chemical shift of amidinium protons by titrating DMSO-d_6 solutions of the appropriate amidinium compound with varying amounts of the complementary carboxylate compound. Thus for **4**, the hexafluorophosphate salt of $[(tmbpy)_2Ru^{II}(Mebpy\text{-}amH^+)]^{3+}$ (6. 3 mM) was titrated with tetrabutylammonium 3,5-dinitrobenzoate whereas 3,5-dinitrobenzamidinium tetraphenylborate (2.9 mM) was titrated with $[(tmbpy)_2Ru^{II}(Mebpy\text{-}COO^-)]^+$ (PF_6^- salt).

Chapter 4

FUNCTIONALIZATION OF PORPHYRIN WITH THE AMIDINE GROUP

A. Introduction

Due to the relavence of porphyrins in biological ET we became interested in developing a facile route to amidine-modified porphyrins. Although a common synthetic approach to amidines is the conversion of a nitrile to its imidate ester followed by aminolysis, this method can be limited by the insolubility of porphyrin nitriles in methanol. Therefore we have adapted Garigipati's strategy[77] to prepare porphyrin amidines for the first time by using a metal-mediated amide transfer to a nitrile. We also show that an amidinium-carboxylate salt bridge is readily formed from the porphyrin amidine donor and carboxylic acid acceptor, thereby permitting us to measure the rate of a PCET reaction through the salt-bridge. Zinc porphyrins have been popular donors in photoinitiated electron transfer schemes because they can readily donate an electron from their singlet excited state to a variety of acceptors.[78]

B. Results and Discussion

1. Synthesis

The synthesis of the Zn(II) porphyrin vinyl amidine employed for PCET measurements is displayed in Figure 39. The amidine group is afforded by reaction of Weinreb's amide transfer reagent,[79] methyl aluminum(III) chloroamide, with the acrylonitrile, which in turn was obtained from the corresponding aldehyde. We have found

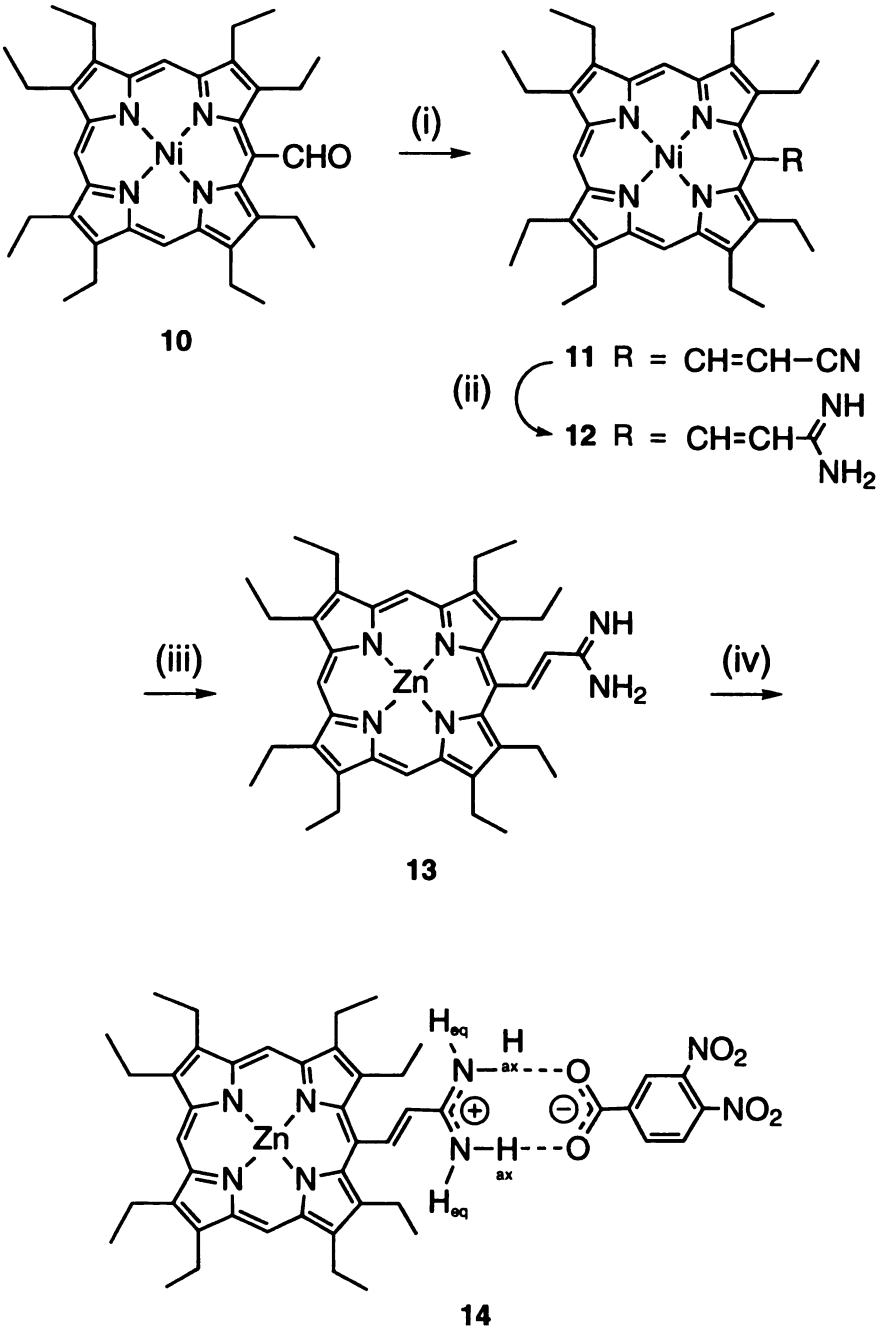

Figure 39. Preparation of ocatethyl porphyrin with the amidine functional group: (i) $(EtO)_2PCH_2CN$, $NaNH_2$; (ii) $MeAl(Cl)NH_2$, NaOH; (iii) 6M H_2SO_4, NaOH, $Zn(OAc)_2$, NaOH; (iv) 3,4–dinitrobenzoic acid.

that amide transfer to the nitrile proceeds efficiently only with Ni(II) in the porphyrin ring; no appreciable reaction is observed for free base or zinc porphyrins. The starting material Ni^{II}OEP aldehyde, **10**,[80,81] was converted to the corresponding acrylonitrile by using a modified Wittig reaction employing diethyl cyanomethylphosphonate. Amidine **3** was obtained by reaction of the nitrile **11** with Wienrebs reagent, methyl aluminum(III) chloroamide, in toluene. This reaction mixture is stirred at 80 °C for 2 days under an argon atmosphere and then quenched upon addition to a chloroform/silica gel slurry. The hydrochloride salt of **12** is released by thoroughly chloroform/methanol (20:1 v/v), and it was isolated as a crystalline solid by removing the solvent mixture under reduced pressure. Addition of 5 equivalents of NaOH to a methanol solution of the hydrochloride salt of **12**, and trituration with water, yielded **12** as a pink solid. This product was washed with water, and dried by rinsing with copious amounts of anhydrous ethyl ether. Removal of Ni(II) and insertion of Zn(II) was accomplished with standard procedures to yield **13** quantitatively.[82]

2. Solution Salt Bridge Association

The binding constants of **12** and **13** to carboxylates were nearly identical. Figure 40 shows the major ^{1}H NMR spectral changes resulting for the association of **12** to the electron acceptor, 3,4–dinitrobenzoic acid (3,4–DNBCOOH) in DMSO–d_6. The positions of the nearly coincident singlets for the porphyrin meso protons at 9.6 ppm and the doublet of the vinylic proton at 10.3 ppm are concentration invariant. Most striking is the behavior of the amidinium protons, which appear as broad singlets. A concentration-dependent downfield shift of >1.0 ppm is observed for the protons involved in hydrogen bonding to the rinsing the carboxylate (sometimes called NH_{ax}[83]) whereas the chemical shift of the adjacent protons (NH_{eq}), which are not bound to the carboxylate, remains virtually unchanged at 9.25 ppm over all concentrations.

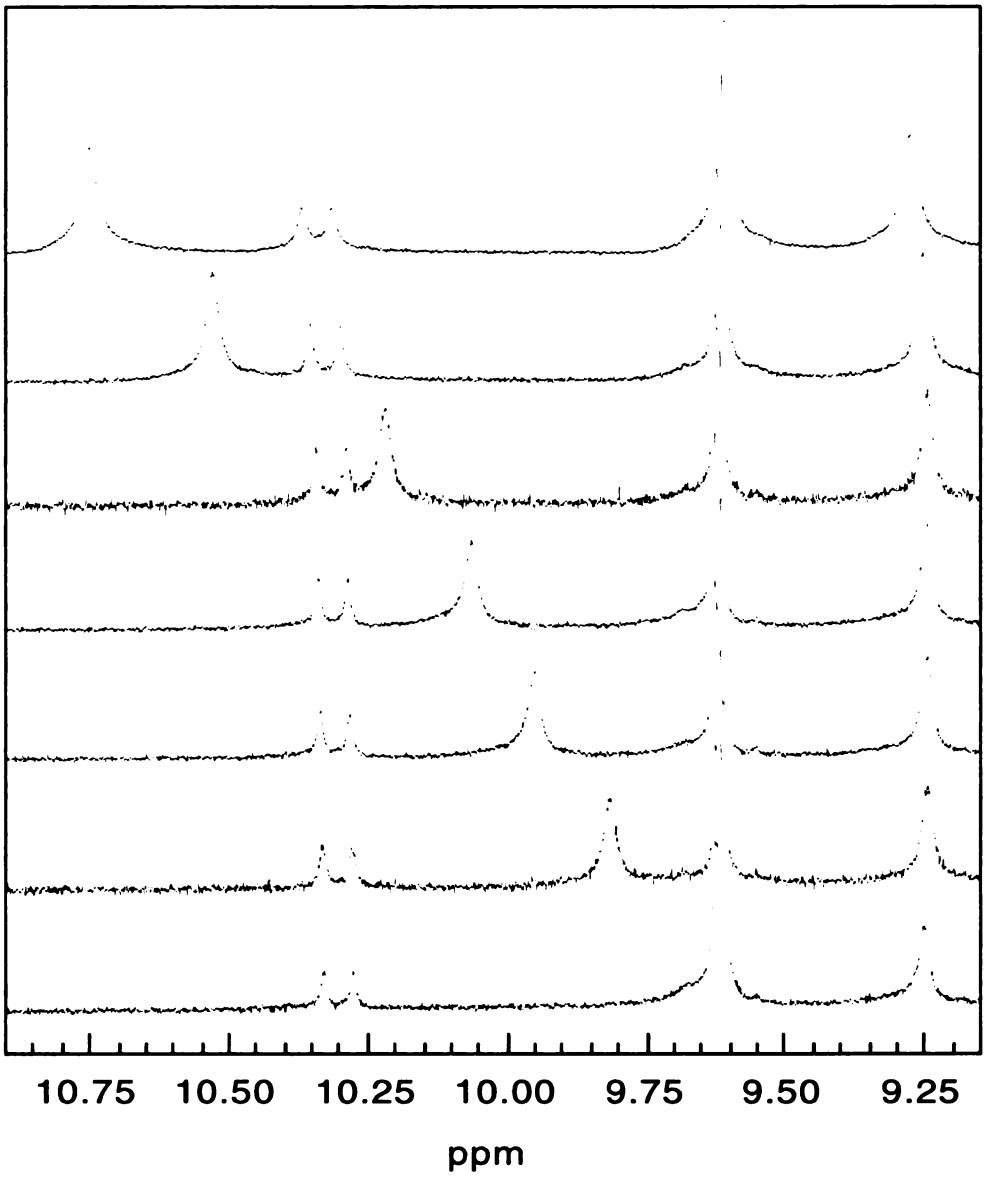

Figure 40. Selected ^{1}H NMR spectra of **12** in the presence of one equivalent of 3,4–DNBCOOH for concentrations of 1.7, 2.6, 3.5, 4.3, 6.1, 13.0 and 26.0 mM in DMSO–d_6 (bottom to top). The spectral range captures the amidinium and vinylic protons of the interface and the meso protons of the octaethyl porphyrin ring.

Figure 41 plots the chemical shift of NH_{ax} versus concentration and the non-linear least squares fit of these data[84] to Eq. 4.1 yields a binding constant (K_{assoc}) of 3500 M^{-1} in DMSO–d_6 at 23.5 °C. Titration of the chloride salt of **12** with the tetramethylammonium salt of the carboxylate yields similar overall behavior for the chemical shifts of the amidinium protons, but the overall binding constant is reduced owing to the presence of the increased ionic strength resulting from the presence of an external salt. As expected on the basis of substituent effects in the association of zwitterionic hydrogen-bonded interfaces,[85] the binding constant increases for benzoate owing to the removal of the electron withdrawing NO_2 groups from the acceptor.

The observed binding constant for the amidinium–carboxylate salt bridge is appreciable. In the context of Jorgensen's classification of hydrogen bonded interfaces,[86] the association of **12** and **13** to carboxylates is driven by two favorable secondary electrostatic interactions. However, the favorable electrostatic charge within the salt bridge also plays a significant role in its formation. Ureas bound to carboxylate also exhibit two favorable secondary electrostatic interactions, but the association constants of these systems in DMSO are reduced to ~150 M^{-1}.[87] The thirty-fold increase in binding of amidinium to carboxylate most probably reflects the stabilization imparted by the molecular recognition of the negatively charged carboxylate by the positively charged amidinium, as opposed to the neutral urea.

$$\delta_{obs} = \delta_{Am} + \Delta\delta_{max}\left[1 + \frac{1}{2[AmCa]_0 K_{assoc}} - \sqrt{\left(\frac{1}{2[AmCa]_0 K_{assoc}}\right)^2 + \left(\frac{1}{[AmCa]_0 K_{assoc}}\right)}\right] \qquad (4.1)$$

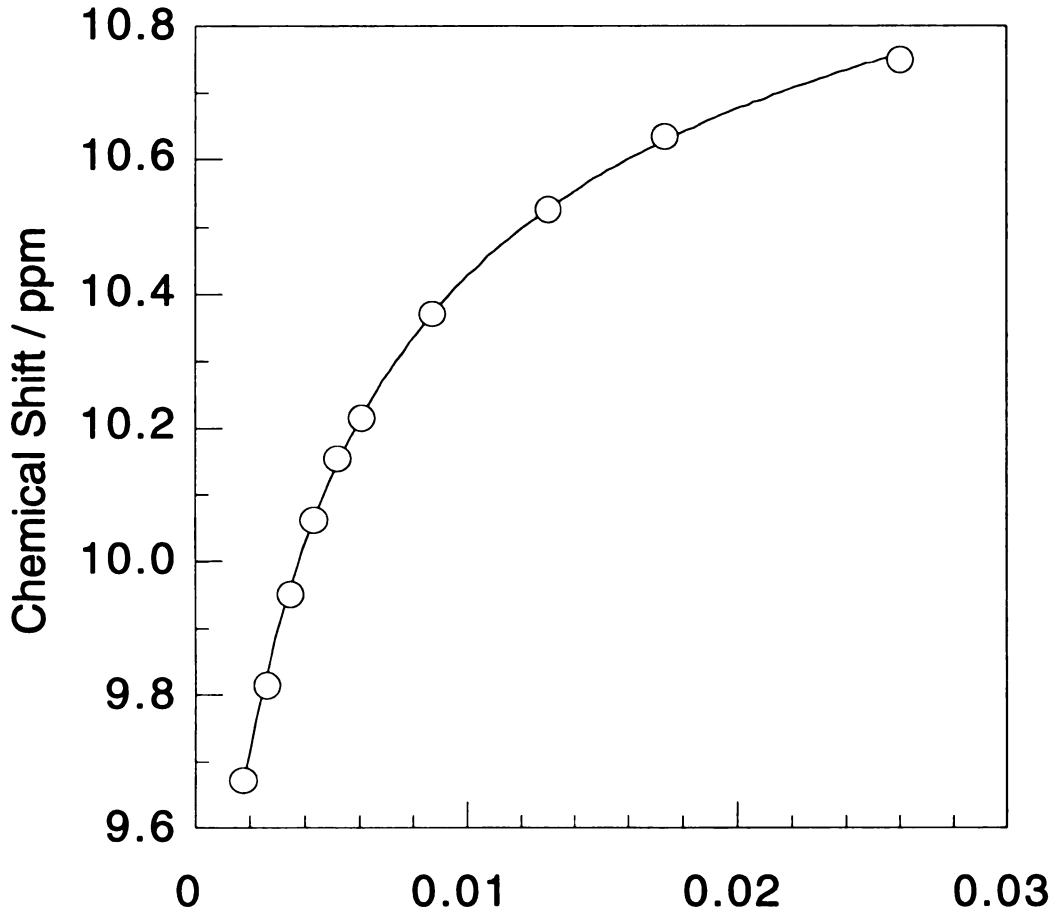

Figure 41. Plot of the chemical shift of the amidinium protons hydrogen bonded to carboxylate versus concentration of **12** and 3,4–DNBCOOH.

3. Photophysical Behavior

The singlet excited state of **13** luminesces in CH_2Cl_2 at 25 °C thereby permitting the excited state reactivity of studies.[88] The luminescence of **13** when complexed to benzoic acid decays monoexponentially with a lifetime of 434 picoseconds (λ_{exc} = 580 nm, λ_{det} = 760 nm). When benzoic acid is replaced by the well-known electron acceptor 3,4–DNBCOOH, the luminescence maximum is unchanged, however, the luminescence intensity is quenched and the excited state lifetime is diminished (τ = 327 picoseconds). This observation is consistent with electron transfer from the singlet excited state of **4** to 3,4-DNBCOOH mediated by the amidinium-carboxylate salt bridge. A unimolecular rate constant for photoinitiated PCET in **5** is 7.5×10^8 s^{-1} as calculated from the emission lifetime decay kinetics. The results reported herein show that a salt bridge can not only pre-organize a donor and an acceptor but that it can also mediate the electron transfer chemistry between the donor-acceptor pair.

C. Materials and Methods

Synthesis of Ni^{II}OEP-acrylonitrile (11). A solution of diethyl cyanomethylphosphonate (0. 2 4 g, 1.36 mmol) in freshly distilled THF (5 mL) was added dropwise through a cannula to sodium amide (0.053 g, 1.36 mmol) under an argon atmosphere. The resulting solution immediately turned a deep red color, and was stirred for an additional 4 hours, afterwhich a solution of Ni^{II}OEP aldehyde, **10**, (0.20 g, 0.32 mmol) in THF (10 mL) was added through a cannula. This reaction mixture was stirred for 24 hours under an argon atmosphere at 60 °C. The solution was then diluted with dichloromethane (100 mL) and washed with water (3 × 100 mL). The organic solvents where removed under reduced pressure, and the resulting solid was purified by silica gel column chromatography, eluting with chloroform/hexane (1:1 v/v) to yield **11** (0.11 g,

53%): MS: m/z 641.4; ^{1}H NMR ($CDCl_3$): δ 9.76 (1H, d), 9.45 (3H, s), 4.61 (1H, d), 3.81 (16H, m), 1.76 ppm (24H, m).

Synthesis of Ni^{II}OEP amidine (12). A solution of methyl aluminum(III) chloroamide in toluene (1.0 M, 5 mL, 5 mmol) was added to **11** (0.25 g, 0.39 mmol) under an argon atmosphere. This reaction mixture was stirred at 80 ℃ for 2 days under an argon atmosphere and then quenched upon addition to a chloroform/silica gel slurry (20 mL). The hydrochloride salt of **12** was collected by thoroughly rinsing the silica gel slurry with chloroform/methanol (20:1 v/v, 50 mL), and it was isolated as a crystalline solid by removing the solvent mixture under reduced pressure. Addition of 5 equivalents of NaOH to a methanol solution of the salt, and trituration with water, yielded **12** as a pink solid. This product was washed with water, and dried by rinsing with copious amounts of anhydrous ether; to yield **12** (0.23 g, 90%): MS: m/z 658.3; ^{1}H NMR (methanol-d_4): δ 10.09 (1H, d), 9.40 (1H, s), 9.38 (2H, s), 5.29 (1H, d), 3.73 (16H, m), 1.65 ppm (24H, m).

Synthesis of Zn^{II}OEP-vinyl-amidine (13). A sample of **12** was placed onto a fine frit, and concentrated sulfuric acid was added until **12** passed through the frit. Crushed ice was added to the mixture, then sodium hydroxide was added until the solution becomes basic. The free base amidine, free base porphyrin was extract into dichloromethane. A saturated solution of zinc acetate is added, and resulting solution is stirred for 30 minutes. Removal of Ni(II) and insertion of Zn(II) was accomplished with standard procedures to yield **13** quantitatively.[82] ES–MS: $[M]^{1+}$ 666.4; ^{1}H NMR (**13** with benzoic acid in CD_2Cl_2 with a trace of methanol-d_4): δ 10.52 (1H, d), 10.12 (2H, s), 10.02 (1H, s), 8.02 (2H, d), 7.45 (3H, m), 6.01 (1H, d), 4.05 (16H, m), 1.92 ppm (24H, m).

Synthesis of [Zn^{II}OEP-vinyl-amH$^+$][3,4–dinitrobenzoate] (14). An equivalent each of **13** and 3,4–dinitrobenzoic acid are placed in dichloromethane. Hexane is added until a precipitate forms. ES–MS: $[M]^{1+}$ 877.8; ^{1}H NMR (DMF–d_7): δ 10.97 (1H,

d), 10.96 (2H, s), 10.18 (2H, s), 10.15 (1H, s), 9.56 (2H, s), 8.68 (1H, s), 8.54 (1H, d), 8.39 (1H, d), 6.40 (1H, d), 4.10 (16H, m), 1.95 ppm (24H, m).

Chapter 5

PULSE RADIOLYSIS EXPERIMENTS TO PROBE PCET

A. Introduction

The pules radiolysis experiment complement photochemical methods to study ET. Pulse radiolysis experiments aimed at assessing the effects of amide hydrogen bonds on ET in D/A modified polypeptides accentuate the complexity of the amide hydrogen bond.[89] The observed kinetic behavior with respect to pulse radiolysis initiated ET reactions in D/A modified polypeptides showed multiple decay pathways. The kinetic behavior was best explained by the presence of multiple hydrogen bonded configurations of the polypeptide giving rise to statistical distribution hydrogen bonded structural motifs separating D and A, for a given D/A modified polypeptide sequence. Subsequent photoinitiated ET studies on D/A modified polypeptides in conjunction with circular dichroism experimental results showed conclusively the relation between conformation and folding and the observed ET rates. The effects of the orientation of the amide hydrogen bond in the polypeptide backbone, in particular when the polypeptide backbone is folded into an α-helix is evident in a photoinitiated ET rate measurements bonds, where the rate for ET correlates to the direction of the helix dipole created by the amide hydrogen bonds forming an α-helix. [90]

One resolution to the problem of multiple amide hydrogen bonding modes has been to make the switch to a different naturally relevant hydrogen bonding motif. To this end the hydrogen bonding interaction of the amidinium-carboxylate salt bridge has been successfully employed to structurally juxtapose D/A assemblies for ET measurements. For the amidinium-carboxylate salt bridge shows greater structural specificity in that there exists

only one major structural conformation in a two-point primary hydrogen bonding motif. Indeed, mono-phasic kinetic behavior is observed in D/salt-bridge/A system, where D is a spyrofluorene group, the hydrogen bond is the amidinium-carboxylate salt-bridge, and A is a 2-methylnaphthalene. For the first time the pulse radiolysis technique has been applied to assess the rate for an intramolecular ET reaction in a D-salt bridge-A system, as depicted schematically in Eq. 5.1.

$$D^{\bullet-1}\text{–\{salt bridge\}–}A \longrightarrow D\text{–\{salt bridge\}–}A^{\bullet-1} \qquad (5.1)$$

B. Background

1. Measurement of Equilibria Between Radical Anions

Absorption spectroscopy can be applied to measure equilibria in solutions of two different radical anions of aromatic organic molecules D and A, as shown in Eq. 5.2.[91]

$$D^{\bullet-1} + A \rightleftharpoons D + A^{\bullet-1} \qquad (5.2)$$

The equilibrium represented in Eq 5.2 consists of four components at some equilibrium concentration of D, A and their corresponding radical anions $D^{\bullet-1}$ and A^{-1}. The equilibrium constant (K_{eq}) for Eq. 5.2 is defined by Eq. 5.3, and consists of the ratios of the equilibrium concentrations of the different radical anions and neutral molecules.

$$K_{eq} = \frac{[D][A^{\bullet-1}]}{[A][D^{\bullet-1}]} \qquad (5.3)$$

The application of the absorption technique to measure K_{eq} requires that for a given detection wavelength one of the radical anions should have an appreciably greater extinction coefficient than the other, for greater sensitivity, and that the neutral molecules should have extinction coefficients near zero at a given wavelength. If these conditions are met, then Eq.

5.3 can be rewritten in terms of the absorbance intensity at a given wavelength for $D^{\bullet-1}$ ($I_{D^{\bullet-1}}$), $A^{\bullet-1}$ ($I_{A^{\bullet-1}}$) and an equilibrium mixture of the two, I_{eq}. This expression assumes that D has a greater extinction coefficient than A and that [A] >> [$A^{\bullet-1}$] and that [D] >> [$D^{\bullet-1}$].

$$K_{eq} = \frac{(I_{D^{\bullet-1}} - I_{eq})\,[A]}{(I_{eq} - I_{A^{\bullet-1}})\,[D]} \tag{5.4}$$

With K_{eq} in hand it is possible to calculate the relative free energy change ($\Delta G°$) for the equilibrium shown in Eq. 5.2 by simply substituting the calculated K_{eq} into Eq. 5.5. For equilibria measurements employing the absorption spectroscopy technique, the radical anions of interest can be generated in solution by treatment with of known concentrations of aromatics with alkali metal. For the radical anions in the presence of alkali metals there needs to be some corrections made for ion pairing.

$$\Delta G° = -RT\ln(K_{eq}) \tag{5.5}$$

Values of K_{eq} and the corresponding $\Delta G°$ determined spectrophotometrically for one such equilibria are displayed in Eq. 5.6. This technique is useful for measuring K_{eq} out to values of about 150, as dictated by how reliably the ratio of [D] to [A] can be accurately adjusted using standard volumetric techniques.

Using this technique, the equilibria for such systems allows for the determination of the relative $\Delta G°$ between a series radical anion ($D^{\bullet-1}$/A)/(D/$A^{\bullet-1}$) pairs including pyrene and anthracene. In fact, this technique is generally applicable to many organic radical anions for which the electronic absorption spectra of their corresponding radical ions are known.[92] In one system the radical anion of pyrene (Pyr) acts as a D and anthracene (Ant) is the A, as determined spectrophotometrically by comparing mixtures of solutions of their corresponding radical anions ($Pyr^{\bullet-1}$, λ_{max} = 492 nm, $\varepsilon = 10^5\ M^{-1}cm^{-1}$; $Ant^{\bullet-1}$, λ_{max} = 370

nm, $\varepsilon = 5\times10^4\ M^{-1}cm^{-1}$). Similar techniques are employed using the pulse radiolysis technique; yet in the pulse radiolysis technique there is no alkali metal to compete in side pairing reactions. The spectrophotometric technique and the pulse radiolysis technique give similar results for the biphenyl (D)/naphthalene (A) system with their corresponding radical anions $(D^{\bullet-1}/A)/(D/A^{\bullet-1})$ for which $\Delta G°$ is determined to be –43 mV.

$$Pry^{\bullet-1} + Ant \rightleftharpoons Pyr + Ant^{\bullet-1}\ (K_{eq} = 74;\ \Delta G° = -114\ mV) \qquad (5.6)$$

2. Kinetic Measurements Employing the Pulsed Radiolysis Experiment

The time resolution for kinetic measurements in the pulse radiolysis experiment stems from the ability to generated very short temporal pulses of electrons, 30 picoseconds, from the 20 MeV linear accelerator (Linac) at Argonne National Laboratories. When high energy pulses of electrons pass through media such as organic solvents, the solvent becomes ionized. This is not due to depositing electrons into the solvent from the Linac pulse, but rather due to electrons being ejected from the solvent molecules as the Linac pulse passes through the solvent. The ejected electrons rapidly become solvated or are solvated electrons represented as $(e^{\bullet-1})_{sol}$ and solvent radical cation hole, $[solvent^{\bullet+1}]$ (Eq. 5.7).

$$solvent \longrightarrow (e^{\bullet-1})_{sol} + [solvent^{\bullet+1}] \qquad (5.7)$$

The formation of solvated electron can be followed by transient absorption spectroscopy, for the $(e^{\bullet-1})_{sol}$'s absorbs light throughout the visible spectrum and into the infrared spectral region. In highly pure neat, oxygen free N-methylpyrrolidone (NMP), the NMP solvated electron, $(e^{\bullet-1})_{NMP}$, has a lifetime of about 6 microseconds. For the experiments described here $(e^{\bullet-1})_{sol}$'s are produced at a concentration of about 10 micromolar. However, operation of the Linac allows for adjustment of the size of the Linac pulse giving flexibility to the concentration of $(e^{\bullet-1})_{sol}$. Stated simply, the concentration of $(e^{\bullet-1})_{sol}$ is dose dependent.

Once $(e^{\bullet -1})_{sol}$ is produced in solution it can react through a variety of channels. Most importantly for the work described here is that it reacts as a powerful reductant and can attach itself to organic aromatic molecules to yield organic aromatic radical anions, Eq. 5.8. The rate constant for this reaction approaches the rate of diffusion in solution (10^{10} $M^{-1}s^{-1}$). Restated, whenever $(e^{\bullet -1})_{sol}$ comes in contact with an organic aromatic group in solution it attaches itself to the organic group producing an organic aromatic radical anions. The formation of aromatic radical anions is conveniently followed by transient absorption spectroscopy, as different aromatic organic radical anions are readily distinguished by their absorption spectra. The rate for the electron attachment step as illustrated in Eq. 5.8 typical aromatic around 2×10^{10} $s^{-1}M^{-1}$ as determined by transient absorption spectroscopy.

$$(e^{\bullet -1})_{sol} + \text{aromatic} \longrightarrow \text{aromatic}^{\bullet -1} \quad (5.8)$$

When a solution contains an equimolar mixture of two different aromatic molecules, a D and an A, the solvated electron, at 10 micromolar, will react without discrimination to produce a non-equilibrium mixture of $D^{\bullet -1}$ and $A^{\bullet -1}$ at a concentration of approximately 5 micromolar each on the time scale of the Linac as shown in Eq. 5.9. These radical anion species are generated on roughly the diffusional time scale, the time scale of the pulse radiolysis technique (10^{10} s^{-1}), which sets the time scale for which kinetic information can be obtained about ensuing reactions between organic aromatic molecules and radical anions.

$$(e^{\bullet -1})_{sol}\,(10\ \mu M) + D + A \longrightarrow D^{\bullet -1}\,(5\ \mu M) + A^{\bullet -1}\,(5\ \mu M) \quad (5.9)$$

The radical anions generated using the pulse radiolysis technique can go on to react or exchange electrons with other organic aromatic molecules present in solution as the solution as a hole comes to equilibrium. That is, the radical species in solution achieve a steady state. This process reveals kinetics information corresponding to electron transfer form $D^{\bullet -1}$ to A as shown in Eq. 5.10. Again, this process is also followed by transient

absorption spectroscopy, as $D^{\bullet-1}$ and $A^{\bullet-1}$ are easily distinguishable by their corresponding absorption spectra. Changes in time in the color of the solution indicate changes in electronic structure due to ET. For experiments described here the growth and decay of colored aromatic radical anion species forms the basis by which ET between different aromatic species is investigated.

$$D^{\bullet-1} + A \longrightarrow D + A^{\bullet-1} \qquad (5.10)$$

The above discussion covers the approach used to study intermolecular ET in solution or frozen glasses containing a mixture of D and A molecules. When within a single molecule there exists the presence of both D and A it is possible to assess the rate for intramolecular ET, Eq. 5.11.

$$D^{\bullet-1}\text{–spacer–}A \longrightarrow D\text{–spacer–}A^{\bullet-1} \qquad (5.11)$$

Shown in Figure 5.1 is a scheme describing the cascade of events leading from irradiation a solution of a D–spacer–A molecule to radical anions, which can then go on to participate in intra- or intermolecular ET. The ensuing ET reactions are again predicated on the fact that there exists some driving force for ET and that the initial radical anions are formed in non-equilibrium mixture. For a 10 micromolar yield of solvated electron in the presence of D–spacer–A, the initial electron attachment step yields 5 micromolar $D^{\bullet-1}$–spacer–A and 5 micromolar D–spacer–$A^{\bullet-1}$, Eq. 5.12.

$$\begin{aligned} (e^{\bullet-1})_{sol}\ (10\ \mu M) \quad &+ \quad D\text{–spacer–}A \longrightarrow \\ D^{\bullet-1}\text{–spacer–}A\ (5\ \mu M) \quad &+ \quad D\text{–spacer–}A^{\bullet-1}\ (5\ \mu M) \end{aligned} \qquad (5.12)$$

As the D–spacer–A system comes to equilibrium via electron flow, there are two major pathways that electron flow may take place between radical anions and aromatic groups, by either intermolecular ET as is the case for non covalent D/A systems, or by intramolecular ET. For the case of purely intermolecular ET, the observed rate constant,

k_{obs}, has a linear dependence in the [A] for the rate of disappearance of $D^{\bullet-1}$ or the appearance of $A^{\bullet-1}$, where the intercept is zero for the dependence of k_{obs} on the concentration of A. However in the case of the D–spacer–A systems, k_{obs} shows quite different behavior. A plot of the dependence of the concentration on k_{obs} displays a non-zero intercept as the concentration of D–spacer–A approaches zero. This is because in D–spacer–A systems, k_{obs} is the sum of inter- and intramolecular ET. In Eq. 5.13 is the rate law for electron flow in D–spacer–A systems. In fact, to determine the rate for intramolecular ET, k_{intrra} it is necessary experimental requires one to vary the concentration of D–spacer–A to determine the intercept thereby determining the rate for intramolecular electron transfer.

$$k_{obs} = k_{intra} + [D\text{–spacer–}A]\cdot k_{inter} \qquad (5.13)$$

3. Hydrogen Production in the Pulse Radiolysis Experiment

A few words are needed to address the issue of hydrogen atom production in the pulse radiolysis experiment. Indeed the solvated electron can react with protons to generate the hydrogen atom. In water, under acidic conditions (pH 1), $(e^{\bullet-1})_{sol}$, the hydrated electron, reacts with hydronium ion in a diffusion controlled reaction to produce the hydrogen atom. For the experiments presented here however, this reaction is hardly worth mentioning. This due to the competition of electron attachment reactions as described in earlier sections. If the concentration of $(e^{\bullet-1})_{sol}$ is 10 micromolar, then it follows that any proton source or strong acid from the solvent hole is limited to a concentration of 10 micromolar (pH 6). Recalling that the concentration of aromatics used for ET are typically 10 millimolar, 1000 times more than the highest possible concentration of acid, combined with the fact that the electron attachment reaction is also diffusion controlled, one can estimate that the lowest total concentration of aromatic radical anions produced will be 9.99

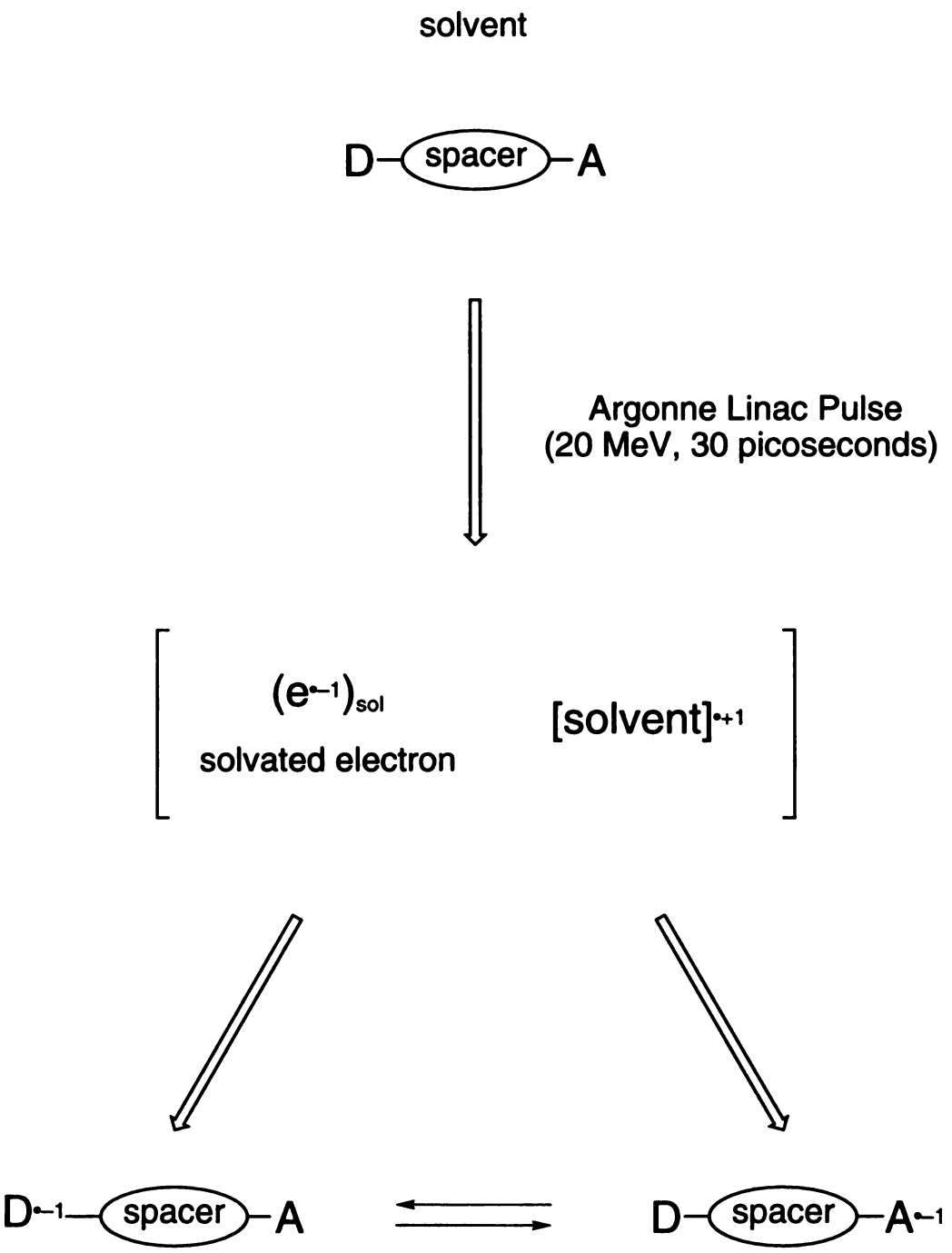

Figure 42. Electron flow in the pulse radiolysis experiment for mixed aromatic D/A compounds.

micromolar (99.9%) and that the highest possible concentration of the hydrogen atom produced will be 0.01 micromolar (00.1%). Thus, reaction of $(e^{-1})_{sol}$ to yield the hydrogen atom is negligible. Neglected in this arguement is the fact that the amidinium protons may act as a weak acid and protonate the solvated electron. If this is the case hydrogen atom production should not compete well with electron attachment. Experiments in fact show this as presented in the following section.

C. Results and Discussion

1. Synthesis

The first synthetic challenge in preparing a D–salt bridge–A assembly for pulse radiolysis was to choose appropriate groups to form a rigid structural framework from which either a Ca functional group or an Am groups might be attached. The D/A organic aromatic groups for the systems in this study are fluorene (Fl) and naphthalene (Na), which act as D and A, respectively as their absorption spectra corresponding to radical anions are known as well as the free energy change for of 62 mV. In this first study, a spyrofluorene molecule is functionalized with Ca to yield the D portion, FlCa of a D/A system, while modification of 2-methylnaphthalene with Am yields the acceptor portion AmNa. The two halves of the D/A system yield a D–salt bridge–A molecule {FlCa:AmNa} for which intramolecular salt bridge mediated electron transfer is assessed for the first time.

Displayed in Figure 43 are the synthetic steps for a series of compound for the measure of ET by the pulse radiolysis technique. The synthesis of the spyroketone was reported by Closs in his studies on triplet transfer.[93] In the work here, it was found that the yield, isolation and purification of the product 1-spyrofluorenecyclohexyl-4-ketone greatly improves with the substitution of trifluoroacetic acid for sulfuric acid in the Lewis acid catalysis intramolecular Friedel-Craft spyrocyclization step. The spyroketone is smoothly converted to the enol ether using a modified Wittig reaction. Hydrolysis of the enol ether

yields fluorospyroaldehyde. The aldehyde is converted to the nitrile, which is in turn converted to the carboxylic acid by acid hydrolysis. The salt bridge complexes {FlCa:AmCy}, {FlCa:AmNa}, and {CyCa:AmNa} where prepared by simple precipitation from aqueous solution. The ketone is converted to an enol ether through the action of the instant ylide.[94] The first challenge was to find the appropriate groups that contain a rigid carbon frame work from which either a carboxylate functional group or an amidinium functional group might be attached The fluorene functional group was chosen as the donor portion of the system described here. Conversion of the enol ether to the aldehyde proceeds efficiently with the action of acid catalysis in dichloromethane with perchloric acid. Protonation, and loss of methanol followed by rearrangement leads to the aldehyde group. Reaction of the aldehyde group with hydroxylamine hydrochloride in wet refluxing formic acid gives the carboxylic acid group. The reaction most likely proceeds through a nitrile intermediate, which is hydrolyzes under acidic conditions in the presence of water to the corresponding amide and then to the corresponding carboxylic acid.

The formation of the salt bridge complexes {FlCa:AmCy}, {FlCa:AmNa}, and {CyCa:AmNa} is quite straight forward. As described in previous section, the corresponding carboxylic acids are dissolved in a minimal amount of water by titrating in one equivalent of the strong base, DBU. Addition of a separate aqueous solution of the amidinium chloride salt produces an immediate precipitation. Upon isolation and characterization by mass spec and NMR it is shown that the precipitate is the 1:1 amidinium-carboxylate salt bridge, which can be isolated by simple filtration.

This method of preparing salt bridge complexes is applied here to a series of complexes in an attempt to form aromatic complexes linked by a the non-covalent salt bridge to probe intramolecular electron transfer. There are two classes of complexes that were prepared in this study by this method.

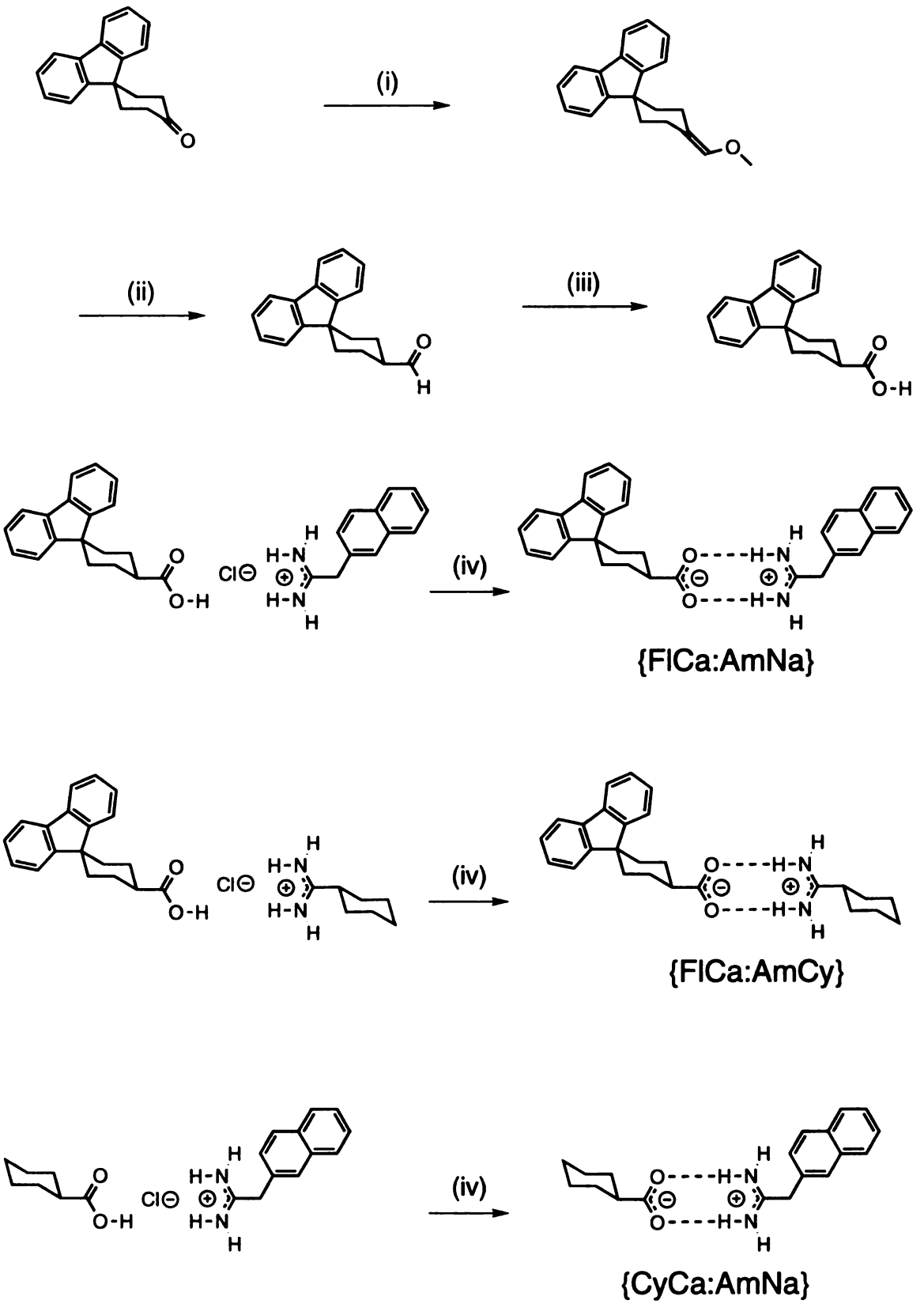

Figure 43. Synthesis of complexes for the study of electron transfer using the pulse radiolysis technique, (i) instant ylide; (ii) perchloric acid, dichloromethane; (iii) hydroxylamine hydrochloride, formic acid; and (iv) DBU, water.

2. Salt Bridge Mediated Electron Transfer

The system reported in this study display electron transfer through similar to fixed distance electron transfer through rigid covalent spacers, but incorporates a salt bridge, Figure 44. The donor for this study was the spyrofluorene molecule, used by Closs in his studies of triplet transfer reactions. The spyro fluorene groups has several advantages, it is very rigid, as seen by NMR and with respect to electron transfer, has a fewer degrees of freedom, thereby decreasing the inner reorganizational energy. The acceptor in this case was a 2-naphthylamidinium, which was reported by Garigapati.

In the pulse radiolysis experiments there are observed absorption at a given wavelenght clearly inidicative of radical species that correspond to the radical anion of the fluorene syro group. From previous studies is known that the potential for the spyro group is around -2.6 volts. The absorption spectrum of the fluorene radical anion has been reported by Shida and coworkers.

Some decay is observed for the transient at 680 nm in a 7.2 mM solution of {FlCa:AmCy} by pulse radiolysis experiment. Addition of {CyAm:Cl} to 6.8 mM appears to reduce the yield of the transient, but does not substantially increase the decay of the radical anions. However addition of phenanthrene at 4.8 mM causes a normal decay of the transient as would be expected for intrermolecular electron transfer from the {FlCa:AmCy} anion to biphenyl/phenanthrene at a potential of around (124 mV) or a driving force of This gave a normal bimolecular ET quenching rate constant of 4.2×10^9 s^{-1} M^{-1}. These results suggest the the {FlCa:AmCy} radical anion is fairly stable towards protonation by free amidinium groups and that it is a potent electron donor and may be rewritten as $\{Fl^{\bullet-}\ ^1Ca:AmCy\}$ suggesting that the initial electron attachment step yields a fluorene localized radical anion as suggested in Eq. 5.14.

$$(e^{\bullet-1})_{sol} + \{FlCa:AmCy\} \longrightarrow \{Fl^{\bullet-1}Ca:AmCy\} \quad (5.14)$$

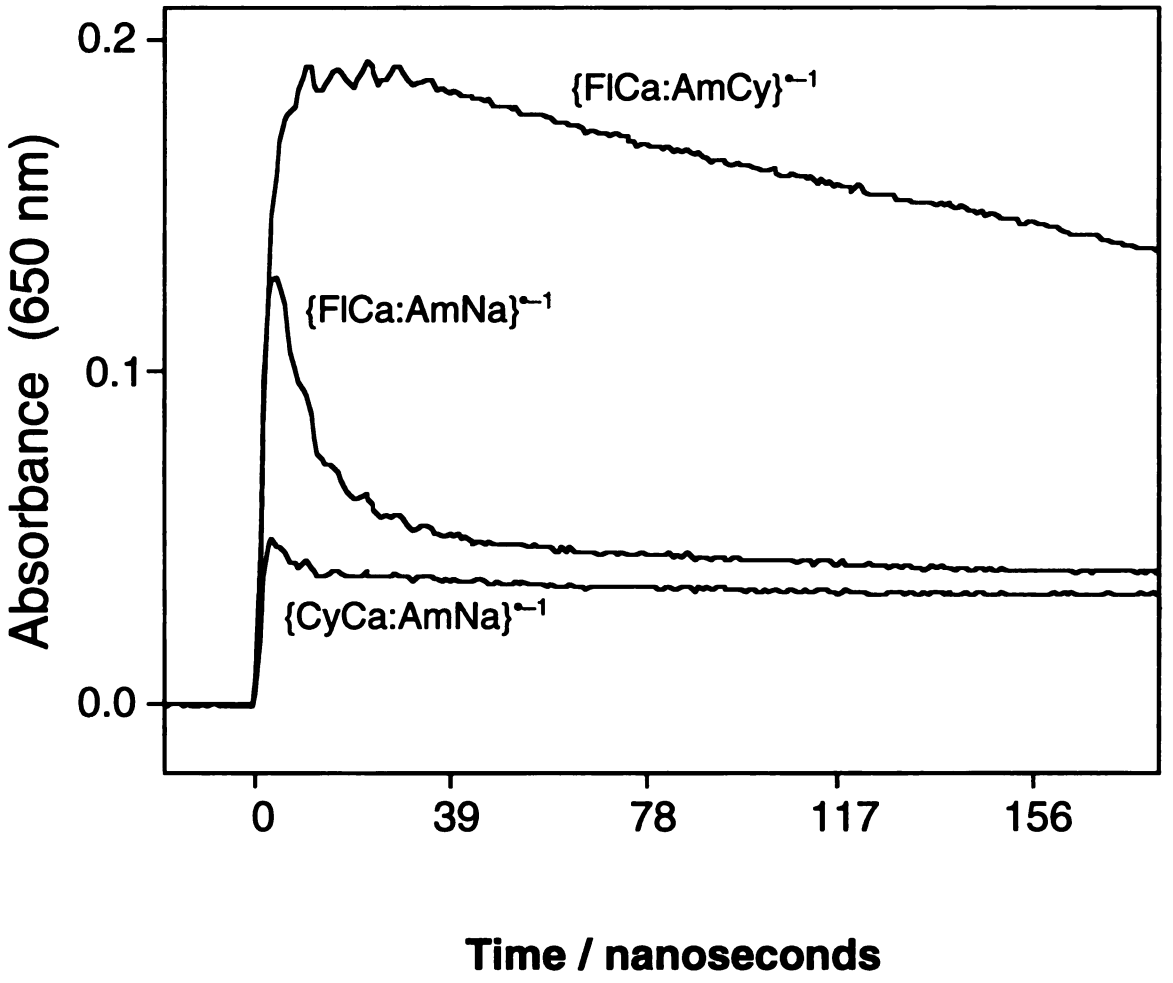

Figure 44. Typical decay profiles on the nanosecond timescale for radical anions of {FlCa:AmCy} (top), {FlCa:AmNa} (middle), and {CyCa:AmNa} (bottom) generated via the pulse radiolysis experiment in NMP and monitored at 650 nm.

In a control experiment it is shown that the the radical anion {Fl$^{\bullet-1}$Ca:AmCy} donates its electron to phenanthrene (Phen), as displayed in eq 5.15. The free energy change for this process is has been estimated to be about 100 mV. The reaction is followed by both the decay of transient {Fl$^{\bullet-1}$Ca:AmCy} species appearing at 650 nm, or by the growth of Phen$^{\bullet-1}$ with a characteristic absorbance at 1100 nm. The rate for the ET reaction has a bimolecular rate constant of $k_{inter} = 4.2 \times 10^9$ $M^{-1}s^{-1}$, Eq. 5.9. This value in line with the results of other bimolecular ET reactions. This control experiment helps to establish the reducing power of {Fl$^{\bullet-1}$Ca:AmCy}.

{Fl$^{\bullet-1}$Ca:AmCy} + Phen ⟶ {FlCa:AmCy} + Phen$^{\bullet-1}$ (5.15)

In the pulse radiolysis experiments involving {CyCa:AmNa} the concentration range studied is from 0.21 to 10.77 mM. For each concentration studied the rate for electron attachment from the solvated electron could be assessed in a global fit from the decay data. From these data an electron attachment rate of $k_{attach} = 2.0 \times 10^{10}$ for the reaction shown in equation 5.16. This rate is assessed by observing the decay of the solvated electron which absorbs in the near infra red where the absorption due to radical anions in negligible. From these data it appears that the electron attaches to the AmNa portion of the salt bridge complex, and is nearly identical to electron attachment to naphthalene.

$(e^{\bullet-1})_{sol}$ + {CyCa:AmNa} ⟶ {CyCa:AmNa$^{\bullet-1}$} (5.16)

And in the mixed aromatic salt bridge system what appears to be normal electron transfer is observed, Eq. 5.17. The ET rates, k_{obs} follow a linear dependence on the concenctration of {FlCa:AmNa}, Figure 45, from which a fit to the rate law given in Eq. 5.13 yields the intra- and intermolecular ET rates ($k_{intra} = 3(1) \times 10^7$ s^{-1}; k_{inter} 2×10^9 $M^{-1}s^{-1}$).

{Fl$^{\bullet-1}$Ca:AmNa} ⟶ {FlCa:AmNa$^{\bullet-1}$} (5.17)

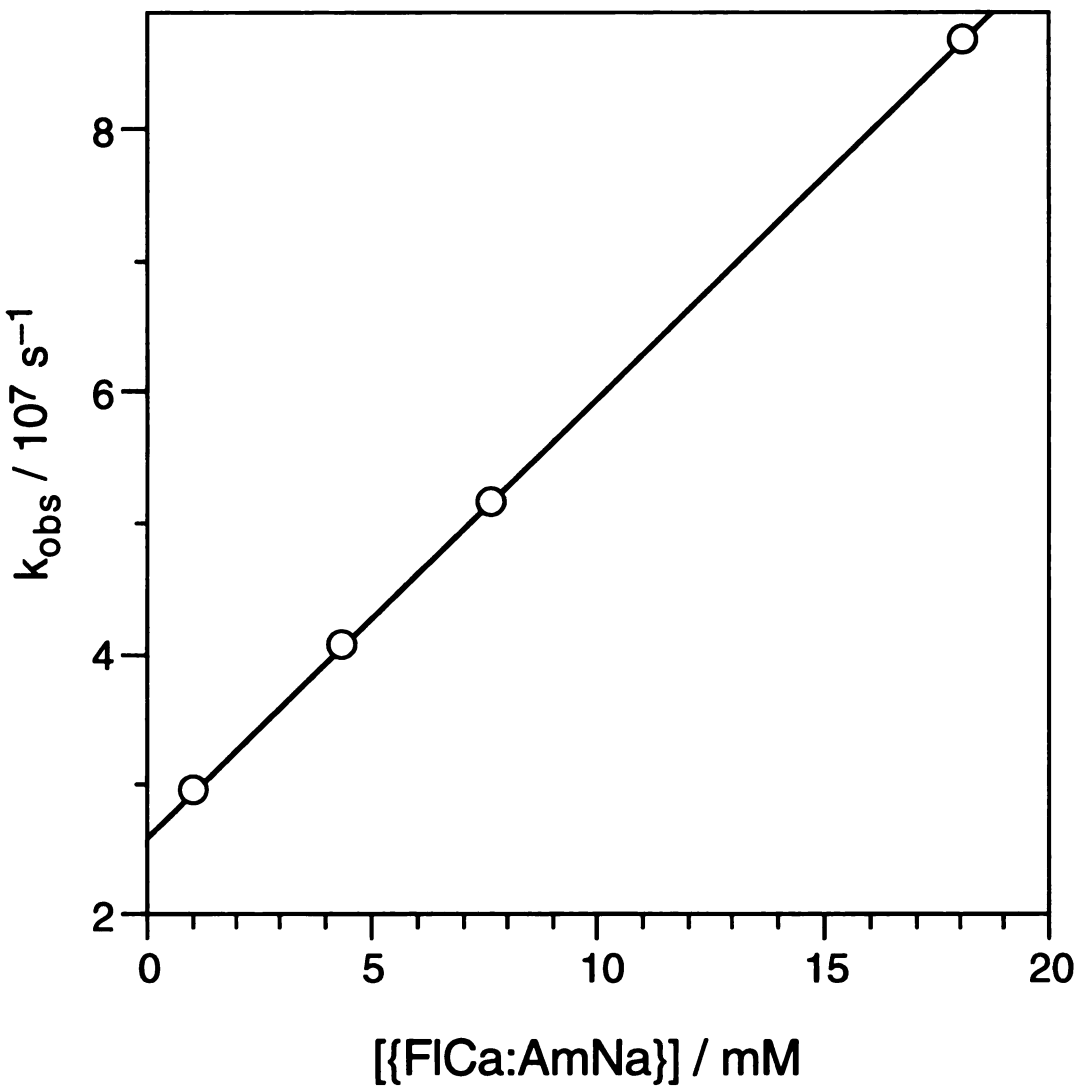

Figure 45. Observed ET rates in {FlCa:AmNa} measured at 1.1, 4.4, 7.6. and 18.1 mM.

D. Materials and Methods

Preparation of N-Methylpyrrolidone (NMP). Reagent grade NMP (500 mL) was placed in a single neck round bottom flask, and calcium hydride (50 g) was added. The solution was distilled at 30 mmHg. A 300 ml fraction was collected boiling at 40 °C, at 30mmHg. This was combined with sodium and terphenylene, and again purified in a second distillation step.

Synthesis of Fluorene-9-spyro-4-cyclohexanone. A slurry of dry trifluoroacetic acid and the protected 2-biphenyl-1-hydroxylcyclohexan-4-one are allowed the to stir at room temperature for 3 hours. Upon addition of the a Sm the solution turns a deep blue color, after 15 minutes or so the solution becomes a deep red color, with no further color change after which the reaction is quenched by careful addition to iced water. The ice water solution is neutralized with sodium carbonate, 200 mL of DCM is added and the extracts are washed with water (3 x 100 mL). The organic extracts are dried with anhydrous magnesium sulfate, filtered, and the solvent is removed under reduced pressure, yielding a colorless oil. Addition of a minimal amount of hexane initiates a dramatic crystallization of the product, which is isolated by filtration in about 60% yield.

Synthesis of Fluorene-9-spyro-4-carboxaldehyde. A solution of instant ylide (5.0 g) was generated in freshly distilled toluene under an inert atmosphere. After refluxing for 1 h, the solution was cooled to room temperature, and the ketone (1.0 g), in 20 ml of dry toluene was added through a canula. This solution was refluxed overnight. The next day it was taken to dryness, and passed through a short column of silica gel to remove phosphorus. The product was collected, the solvents were removed by rotary evaporation, and the product was taken into dichloromethane and washed with water. The product was dried with magnesium sulfate, and the solvent was removed by rotary evaporation. The product crystallizes with the addition of hexanes. The enol ether was not isolated. The product was hydrolyzed by refluxing in 50 ml of a solution of THF/H_2O/HCl

in a ratio of 5.0:1.0:0.5 for 1hr. The hydrolysis was followed by TLC, 2:1 dichloromethane/hexanes. And the product aldehyde has an Rf of 0.6, 70%. The product gave satisfactory characterized ^{1}H NMR (CDC_3): δ 9.92 (1H, s), 7.75 (2H, t), 7.67 (1H, d), 7.51 (1H, d), 7.31 (4H, m), 2.64 (1H, s), 2.05 (5H, m), 1.73 (2H, m), 1.55 ppm (1H, s).

Synthesis of Fluorene-9-spyro-4-carboxylic acid. The products from above where combined with an excess of Hydroxylaminehydrochloride and refluxed in formic acid overnight. The product was quenched with 10% sodium hydroxide, washed dichloromethane acidified with hydrochloric acid, which produced a white precipitate. This precipitate was extracted with dichloromethane. Removal of solvents under reduced pressure yielded the acid. MS: m/z 278.2; ^{1}H NMR ($CDCl_3$): δ 7.83 (1H, d), 7.72 (2H, m), 7.33 (5H, m), 2.72 (1H, m), 2.23 (4H, m), 2.01 (2H, m), 1.66 ppm (2H, d); ^{13}C NMR ($CDCl_3$): δ 182.17, 152.71, 151.41, 140.01, 139.33, 127.29, 127.17, 126.75, 125.58, 122.89, 120.07, 119.74, 49.27, 42.09, 34.33, 25.02 ppm .

Synthesis of Cyclohexylamidinuium chloride {CyAm:Cl}. This compound was prepared by the litrature procedures employing sodium methoxide in methanol. MS: m/z 126.2; ^{1}H NMR (DMSO-d_6): δ 8.98 (2H, s), 8.82 (2H, s), 2.43 (1H, t), 1.64 (7H, m), 1.22 ppm (3H, m).

Synthesis of [Cyclohexylamidinuium][fluorene-9-spyro-4-carboxylate] ({FlCa:AmCy}). The acid (0.062 g, 0.22 mmol) above was combined with DBU (0.030 g, 0.20 mmol) in water. This solution was added to an aqueous solution of cyclohexylamidinium chloride. A white precipitate formed immediately. The solution was mixed thoroughly, then filtered. The filtrate was then washed with a minimal amount of water, air dried then washed with an excess of anhydrous ether, to afford the product (0.069 g, 0.17 mmol) in 85% yield. ^{1}H NMR (DMSO-d_6): δ 11.60 (2H, br), 8.25 (2H, br), 7.82 (3H, m), 7.53 (1H, d), 7.32 (4H, m), 2.38 (2H, m), 1.90 (11H, m), 1.32 ppm (7H, m).

Synthesis of [2-Naphthylacetamidinium][fluorene-9-spyro-4-carboxylate] ({FlCa:AmNa}). The same procedure was used as for **{FlCa:AmCy}** described above. The product **{FlCa:AmNa}** was obtained in 93% yield. MS: m/z 278.2 (CaFl), 183.1 (NaAm); ^{1}H NMR (DMSO-d_6): δ 10.45 (br), 7.60 (7H, m), 7.53 (4H, m), 7.31 (4H, m), 3.84 (2H, s), 2.26 (1H, t), 1.95 (6H, m), 1.38 ppm (2H, d).

Synthesis of 2-Naphthylacetamidinuium cyclohexylcarboxylate {CyCa:AmNa}. The same procedure used for **{FlCa:AmCy}** described above is used here. The product **{CyCa:AmNa}** was obtained in 20% yield. ^{1}H NMR (DMSO-d_6): δ 10.25 (br), 7.90 (4H, m), 7.51 (3H, m), 3.84 (2H, s), 1.60 (6H, m), 1.18 ppm (5H, m).

List of References

1. Lehn, J. -M. *Supramolecular Chemisty*, VCH, Weinheim, **1995.**
2. (a) Pranata, J.; Wierschke, S. G.; Jorgensen, W. L. *J. Am. Chem. Soc.* **1991**, *113*, 2810. (b) Jorgensen, W. L.; Pranata, J. *J. Am. Chem. Soc.* **1990**, *112*, 2008.
3. (a) Honig, B.; Nicholls, A. *Science* **1995**, *268*, 1144; (b) Gunner, M. R.; Nicholls, A.; Honig, B. *J. Phys. Chem.* **1996**, *100*, 4277.
4. (a) Russell V. A.; Etter, M. C.; Ward, M. E. *J. Am. Chem. Soc.* **1994**, *116*, 1941. (b) Russell V. A.; Etter, M. C.; Ward, M. E. *Chem. Mater.* **1994**, *6*, 1206; (c) Russell V. A.; Ward, M. E. *Chem. Mater.* **1996**, *8*, 1654; (a) Russell, V. A.; Evans, C. C.; Li, W.; Ward, M. D. *Science* **1997**, *276*, 579.
5. Pavletich, N. P.; Pabo, C. O. *Science* **1991**, *252*, 809.
6. (a) Puglisi, J. D.; Chen, L.; Frankel, A. D.; Williamson, J. R. *Proc. Natl. Acad. Sci. USA* **1993**, *90*, 3680-3684; (b) Puglisi, J. D.; Tan, R.; Calnan, B. J.; Frankel, A. D.; Williamson, J. R. *Science* **1992**, *257*, 76.
7. (a) Ganem, B *Angew. Chem. Int. Ed. Engl.* **1996**, *35*, 937; (b) Lee, A. Y.; Karplus, P. A.; Ganem, B.; Clardy, J. *J. Am. Chem. Soc.* **1995**, *117*, 3627.
8. (a) Chook, Y. M.; Ke, H.; Lipscomb, W. N. *Proc. Natl. Acad. Sci. USA* **1993**, *90*, 8600; (b) Chook, Y. M.; Gray, J. V.; Ke, H.; Lipscomb, W. N. *J. Mol. Biol.*

1994, *240*, 476.

9. Albert, J. S.; Goodman, M. S.; Hamilton, A. D. *J. Am. Chem. Soc.* **1995**, *117*, 1143.
10. Göbel, M. W.; Bats, J. W.; Düner, G. *Angew. Chem. Int. Ed. Engl.* **1992**, *31*, 207.
11. Terfort, A.; Kiedrowski, G. von *Angew. Chem. Int. Ed. Engl.* **1992**, *35*, 654.
12. (a) Closs, G. L.; Calcaterra, L. T.; Green, N. J.; Penfield, K. W.; Miller, J. R. *J. Phys. Chem.* **1986**, *90*, 3673; (b) Closs, G. L.; Miller, J. R. *Science* **1988**, *240*, 440.
13. Miller, J. R.; Beitz, J. V.; Huddleston, R. K. *J. Am. Chem. Soc.* **1984**, *106*, 5057.
14. Liang, N.; Miller, J. R.; Closs, G. L. *J. Am. Chem. Soc.* **1990**, *112*, 5354.
15. Miller, J. R.; Paulson, B. P.; Bal. R.; Closs, G. L. *J. Phys. Chem.* **1995**, *99*, 6923.
16. Wasielewski, M. R.; Niemczyk, M. P. *J. Am. Chem. Soc.* **1984**, *106*, 5043.
17. (a) Wasielewski, M. R.; Gaines III, G. L.; O'Neil, M. P.; Svec, W. A.; Niemczyk, M. P. *J. Am. Chem. Soc.* **1990**, *112*, 4559; (b) Wasielewski, M. R.; Gaines III, G. L.; O'Neil, M. P.; Svec, W. A.; Niemczyk, M. P. *Mol. Cryst. Liq. Cryst.* **1991**, *194*, 201.
18. Opperman, K. A.; Mecklenburg, S. L.; Meyer, T. J. *Inorg. Chem.* **1994**, *33*, 5295.
19. Ramirez, B. E.; Malmström, B. G.; Winkler, J. R.; Gray, H. B. *Proc. Natl. Acad. Sci. USA* **1995**, *92*, 11949.
20. Brzezinski, P. *Biochemistry* **1996**, *35*, 5611.
21. (a) Graige, M. S.; Paddock, M. L.; Bruce, J. M.; Feher, G.; Okamura, M. Y. *J.*

Am. Chem. Soc. **1996**, *118*, 9005. (b) Okamura, M. Y.; Feher, G. *Annu. Rev. Biochem.* **1992**, *61*, 861.

22. Takahashi, E.; Maroti, P.; Wraight, C. In *Electron and Proton Transfer in Chemistry and Biology*; Müller, A., Ratajczaks, H., Junge, W., Diemann, E., Eds.; Elsevier: Amsterdam, 1992; p 219.
23. Babcock, G. T.; Barry, B. A.; Debus, R. J.; Hoganson, C. W.; Atamian, M.; McIntosh, L.; Sithole, I.; Yocum, C. F. *Biochemistry* **1989**, *28*, 9557.
24. Burgess, B. K.; Lowe, D. J. *Chem. Rev.* **1996**, *96*, 2983.
25. (a) Pilato, R. S.; Stiefel, E. I. In *Bioinorganic Catalysis*; Reedijk, J., Ed.; Dekker: New York, 1993, p 131. (b) Stiefel, E. I. In *Molybdenum Enzymes, Cofactors, and Model Systems*; ACS Symposium Series 535; Stiefel, E. I., Coucouvanis, D., Newton, W. E., Eds.; American Chemical Society: Washington, DC, 1993, p 1. (c) Stiefel, E. I. *Proc. Natl. Acad. Sci. USA* **1973**, *70*, 988.
26. Feig, A. L.; Lippard, S. J. *Chem. Rev.* **1994**, *94*, 759.
27. Wallar, B. J.; Lipscomb, J. D. *Chem. Rev.* **1996**, *96*, 2625.
28. Solomon, E. I.; Sundaram, U. M.; Machonkin, T. E. Chem. Rev. 1996, 96, 2563.
29. (a) Uhlin, U.; Eklund, H. *Nature* **1994**, *370*, 533. (b) Nordlund, P.; Eklund, H. *J. Mol. Biol.* **1993**, *232*, 123.
30. Ekberg, M.; Sahlin, M.; Eriksson, M.; Sjoberg, B.-M. *J. Biol. Chem.* **1996**, *271*, 20655.
31. Averill, B. A. *Chem. Rev.* **1996**, *96*, 2951.
32. (a) Winkler, J. R.; Nocera, D. G.; Yocom, K. M.; Bordignon, E.; Gray, H. B. *J. Am. Chem. Soc.* **1982**, *104*, 5798; (b) Isied, S.S.; Worosila, G.; Atherton, S. J. *J. Am. Chem. Soc.* **1982**, *104*, 7659.

33. (a) Galoppini, E.; Fox, M. A. *J. Am. Chem. Soc.* **1996**, *118*, 2299; (b) Fox, M. A.; Galoppini, E. *J. Am. Chem. Soc.* **1997**, *119*, 5277.

34. Crane, B. R.; Siegel, L. M.; Getzoff, E. D. *Science* **1995**, *270*, 59.

35. Turró, C.; Chang, C. K.; Leroi, G. E.; Cukier, R. I.; Nocera, D. G. *J. Am. Chem. Soc.* **1992**, *114*, 4013.

36. Rege, P. J. F. de; Williams, S. A.; Therien, M. J. *Science* **1995**, *269*, 1409.

37. Sessler, J. L.; Wang, B.; Harriman, A. *J. Am. Chem. Soc.* **1993**, *115*, 10418.

38 Pinner, A. *Die Imidoäther und ihre Derivate.* Oppenheim, Berlin **1892**.

39 Krechl, J.; Smrckova, S.; Kuthan, J. *Collect. Czech. Chem. Commun.* **1990**, *55*, 460.

40. Kemp, D. S.; Cox, D. D.; Paul, K. G. *J. Am. Chem. Soc.* **1975**, 97, 7312.

41. Desiraju, G. R. *Angew. Chem., Int. Ed. Engl.* **1995**, *34*, 2311.

42. (a) Whitesides, G. M.; Mathias, J. P.; Seto, C. T. *Science* **1991**, *254*, 1312. (b) MacDonald, J. C.; Whitesides, G. M. *Chem. Rev.* **1994**, *94*, 2383.

43. (a) Fagan, P. J.; Ward, M. O.; Calabrese, J. C. *J. Am. Chem. Soc.* **1989**, *111*, 1698; (b) Ward, M. O.; Fagan, P. J.; Calabrese, J. C.; Johnson, D. C. *J. Am. Chem. Soc.* **1989**, *111*, 1719.

44. (a) Russell V. A.; Etter, M. C.; Ward, M. E. *J. Am. Chem. Soc.* **1994**, *116*, 1941. (b) Russell V. A.; Etter, M. C.; Ward, M. E. *Chem. Mater.* **1994**, *6*, 1206. (c) Russell V. A.; Ward, M. E. *Chem. Mater.* **1996**, *8*, 1654.

45. Hosseini, M. W.; Ruppert, R.; Schaeffer, P.; Cian, A. De C.; Kyrisakas, N.; Fischer, J. *J. Chem. Soc., Chem. Commun.* **1994**, 2135.

46. (a) Aakeröy, C. B.; Hughes, D. P.; Nieuwenhuyzen, M. *J. Am. Chem. Soc.* **1996**, *118*, 10134. (b) Aakeröy, C. B.; Hitchcock, P. B.; Moyle, B. D.; Seddon, K. R. *J. Chem. Soc., Chem. Commun.* **1992**, 553.

47. Schwiebert, K. E.; Chin, D. N.; MacDonald, J. C.; Whitesides, G. M. *J. Am. Chem. Soc.* **1996**, *118*, 4018.

48. The benzoate of the previously known 3–amidinium chloride benzoic acid (Wagner, G.; Vieweg, H.; Kuehmstedt, H. *Pharmazie*, **1973**, *28*, 288) was prepared in one-step synthesis as described in supporting information.

49. A Rigaku diffractometer with Mo Kα radiation (λ = 0.71073 Å) was used to collect data to a maximum of 2θ = 50° from crystals of 0.65 × 0.40 × 0.20 mm dimensions at 293 K. A total of 1397 independent reflections were collected, of which 1288 reflections were considered observed ($I > 2\sigma(I)$) after Lp and absorption correction (correction was based on ψ scans of a few suitable reflections with χ values close to 90°). Crystallographic data were as follows: $C_8H_8N_2O_2$, MW = 164.16, monoclinic, space group $P2_1/n$ (14), a = 7.253(2) Å, b = 6.934(3) Å, c = 14.602(2) Å, β = 93.64(2)°, V = 733.0(4) Å^3, Z = 4, ρ_{calc} = 1.488 g cm^{-3}. The structure was solved by using direct methods (SHELXS) and refined by using full-matrix least-squares procedures based on F^2 (SHELXL-93) with R1 = 0.0398 and wR2 = 0.1242.

50. (a) Pranata, J.; Wierschke, S. G.; Jorgensen, W. L. *J. Am. Chem. Soc.* **1991**, *113*, 2810. (b) Jorgensen, W. L.; Pranata, J. *J. Am. Chem. Soc.* **1990**, *112*, 2008.

51. (a) Kirby, J. P.; Dantzig, N. A. van; Chang, C. K.; Nocera, D. G. *Tetrahedron Lett.* **1995**, *36*, 3477. (b) Roberts, J. A.; Kirby, J. P.; Nocera, D. G. *J. Am. Chem. Soc.* **1995**, *117*, 8051.

52. Derissen, J. L. *Acta Cryst.* **1974**, *B30*, 2764.

53. (a) Kratochvíl, B.; Ondráč ek, J.; Malý , K.; Csordás, L. *Collect. Czech. Chem. Commun.* **1988**, *53*, 294. (b) Kratochvíl, B.; Ondráč ek, J.; Krechl, J.; Haš ek, J.

Acta Cryst. **1987**, *C43*, 2182.

54. Olah, G. A.; Keumi, T. *Synthesis* **1979**, 112.

55. Garigipati, R. A. *Tetrahedron Lett.* **1990**, 31, 1969.

56. Schaefer, F. C.; Peters, G. A. *J. Org. Chem.* **1961**, *26*, 412.

57. Sullivan, B. P.; Salmon, D. J.; Meyer, T. J. *Inorg. Chem.* **1978**, *12*, 3334.

58. Müller, G.; Riede, J.; Schmidtchen, P. Angew. Chem., Int. Ed. Engl. 1988, *27*, 1516.

59. Wilcox, C. S. In *Frontiers in Supramolecular Organic Chemistry and Photochemistry*; Schneider, H.-J., Durr, H., Eds.; VCH: Weinheim, 1991; p 123.

60. Albert, J. S.; Goodman, M. S.; Hamilton, A. D. *J. Am. Chem. Soc.* **1995**, *117*, 1143.

61. Hupp, J. T.; Neyhart, G. A.; Meyer, T. J.; Kober, E. M. *J. Phys. Chem.* **1992**, *96*, 10820

62. Balzani, V.; Scandola, F. *Supramolecular Photochemistry*; Ellis Horwood: New York, 1991; Ch. 2.7.2.

63. Bock, C. R.; Connor, J. A.; Gutierrez, A. R.; Meyer, T. J.; Whitten, D. G.; Sullivan, B. P.; Nagle, J. K. *J. Am. Chem. Soc.* **1979**, *101*, 4815.

64. Assuming a diffusion-controlled on rate of 10^9 M^{-1} s^{-1} for these systems, from the measured equilibrium constants for **1** and **2**, off rates of 2×10^3 M and 10^2 s^{-1}, respectively, are expected for these systems. Of course, the pertinent equilibrium is with electronically excited Ru(II) complex and not the ground state complex, as measured by absorption spectroscopy. Notwithstanding, the largest ΔpK_a changes for Ru(II) polypyridyl complexes between ground and excited states are 3; for instance, bpy's directly appended with carboxylic acids exhibit ΔpK_as of 2.5. Hence the observed intramolecular electron transfer decay rates well

exceed equilibration rates, and intramolecular electron transfer occurs for a static complex. This is not the case for **3**, however, where the off rates are expected to be commensurate with the electron transfer kinetics. For this system, the interpretation of the observed PCET rate constant reported in Table 1 is complicated by a dynamic equilibrium between acceptor and donor.

65. Galoppini, E.; Fox, M. A. *J. Am. Chem. Soc.* **1996,** *118*, 2299.

66. Stanley, R. J.; King, B.; Boxer, S. G. *J. Phys. Chem.* **1996,** *100*, 12052.

67. Heller, B. A.; Holten, D.; Kirmaier, C. *Science* **1995,** *269*, 940.

68. Scherer, T.; van Stokkum, I. M. H.; Brouwer, A. M.; Verhoeven, J. W. *J. Phys. Chem.* **1994,** *98*, 10539.

69. Gray, H. B.; Winkler, J. R. *Annu. Rev. Biochem.* **1996,** *65*, 537.

70. (a) J. Pranata, S. G. Wierschke and W. L. Jorgensen, *J. Am. Chem. Soc.*, *113* (1991) 2810. b) W. L. Jorgensen and J. Pranata, *J. Am. Chem. Soc.*, *112* (1990) 2008.

71. E. Galoppini and M. A. Fox, *J. Am. Chem. Soc.*, *118* (1996) 2299.

72. B. A. Heller, D. Holten and C. Kirmaier, *Science*, *269* (1995) 940.

73. Peek, B. M.; Ross, G. T.; Edwards, S. W.; Meyer, G. J.; Meyer, T. J.; Erickson, B. W. *Int. J. Peptide Protein Res.* **1991,** *38*, 114.

74. Opperman, K. A.; Mecklenburg, S. L.; Meyer. T. J. *Inorg. Chem.* **1994,** *33*, 5295.

75. Creary, X. *J. Org. Chem.* **1993,** *58*, 7700.

76. B. M. Peek, G. T. Ross, S. W. Edwards, G. J. Meyer, T. J. Meyer and B. W. Erickson, *Int. J.* Peptide *Protein Res.*, *38* (1991) 114.

77. Garigipati, R. A. *Tetrahedron Lett.* **1990,** *31*, 1969.

78. Kalyanasundaram, K. *Photochemistry of Polypyridine and Porphyrin Complexes*; Academic Press: London, **1992.**

79. Levin, J. I.; Turos, E.; Weinreb, S. M. *Synth. Comm.* **1982**, *12*, 989.

80. Morgan, A. R.; Tertel, N. C. *J. Org. Chem.* **1986**, *51*, 1347.

81. Grigg, R.; Shelton, G.; Sweeney, A.; Johnson, A. W. *J. Chem. Soc., Perkin Trans. 1* **1972**, 1789.

82. Falk, J. E. *Porphyrins and Metalloporphyrins*; Elsevier: New York, **1964**, pg. 129.

83. Göbel, M. W.; Bats, J. W.; Dürner, G. *Angew. Chem. Int. Ed. Engl.* **1992**, *31*, 207.

84. Wilcox, C. S. In *Frontiers in Supramolecular Organic Chemistry and Photochemistry*; Schneider, H.-J. Durr, H. Eds.; VCH: Weinheim, **1991**; pp. 123-143.

85. Wilcox, C. S.; Kim, E.-i.; Romano, D.; Kuo, L. H.; Burt, A. L.; Curran, D. P. *Tetrahedron* **1995**, *51*, 621.

86. Kelly, T. R.; Kim, M. H. *J. Am. Chem. Soc.* **1994**, *116*, 7072.

87. (a) Jorgensen, W. L.; Pranata, J. *J. Am. Chem. Soc.* **1990**, *112*, 2008. (b) Pranata, J.; Wierschke, S. G.; Jorgensen, W. L. *J. Am. Chem. Soc.* **1991**, *113*, 2810.

88. Zaleski, J. M.; Chang, C. K.; Nocera, D. G. *J. Phys. Chem.* **1993**, *97*, 13206.

89. Meier, M. S.; Fox, M. A.; Miller, J. R. *J. Org. Chem.* **1991**, *56*, 5380.

90. Refer to the discusion on this topic presented in Chapter 1 of this theis.

91. Slates, R. V.; Szwarc, M. *J. Phys. Chem.* **1965**, *69*, 4124.

92. Shida, T. *Electronic Absorpiton Spectra of Radical Ions*, Elsevier, **1988**.

93. Sigman, M. E; Closs, G. L. *J. Phys. Chem.* **1991**, *95*, 5012.

94. Petrzilka, M.; Germann, A. *Mol. Cryst. Liq. Cryst.* **1985**, *131*, 327.